NTNU

Norwegian University of
Science and Technology

Model of Single-Phase Synchronous Generator for Rotary Frequency Converter

Gaute Molland Solberg

Master of Energy and Environmental Engineering
Submission date: June 2018
Supervisor: Trond Toftevaag, IEL

Norwegian University of Science and Technology
Department of Electric Power Engineering

PROBLEM DESCRIPTION

The standard for the Norwegian traction power system is single-phase AC voltage at 15 kV and $16^2/_3$ Hz. This single-phase system is fed from the three-phase public power grid through several converter stations. Most of these converter stations are made up of synchronous-synchronous rotary frequency converters. This Master's Thesis continues the work carried out fall 2017 and presented in the specialization project "Model of Single-Phase Synchronous Generators for Rotary Frequency Converters". The Master's Thesis will describe different approaches for modeling single-phase synchronous generators for rotary frequency converters.

The thesis will cover the following tasks:

- Carry out further literature study. Focus on instantaneous time-domain modeling of synchronous machines and possible material newly published regarding single-phase synchronous machines and rotary frequency converters.
- Clarify the parameter adjustments presented in the specialization project "Model of Single-Phase Synchronous Generators for Rotary Frequency Converters" from autumn 2017. These parameter adjustments are necessary when modeling single-phase synchronous machines as asymmetrical loaded three-phase synchronous machines.
- Develop equations for an instantaneous time-domain model of a single-phase synchronous machine. Apply two rotating MMF distributions for describing the behavior of the single-phase pulsating armature MMF distribution of the machine.
- Develop alternative modeling methods to the ones presented above for describing the single-phase synchronous machine. Explore the possibility of applying the phase equations directly without transforming the machine quantities to a common rotor direct- and quadrature axis reference frame.
- Implement and test the developed equations and adjusted parameters presented above in a suitable simulation tool (e.g., MATLAB® /Simulink).

Project start: January 15th, 2018
Supervisor: Trond Toftevaag

ABSTRACT

Synchronous-synchronous rotary frequency converters are in the Norwegian traction power system applied for converting three-phase AC voltage at 50 Hz to single-phase AC voltage at $16^2/_3$ Hz. The converters consist of a three-phase synchronous motor and a single-phase synchronous generator combined on a common shaft. The three-phase motor is fed from the public grid and drives the single-phase generator. The motor-to-generator number of pole ratio is three-to-one, enabling the single-phase generator to generate the voltage at a frequency one-third of that applied to the three-phase motor.

This Master's Thesis describes three approaches for modeling single-phase synchronous generators in rotary frequency converters.

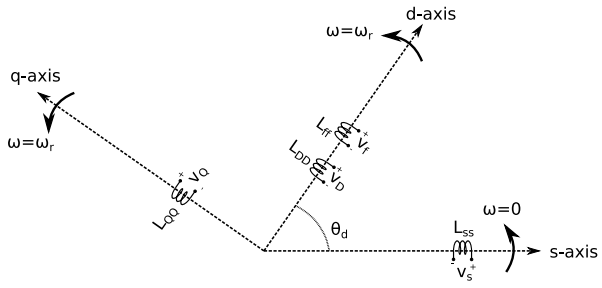

(a) Model 1

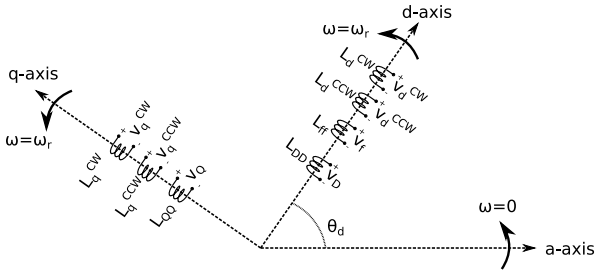

(b) Model 2

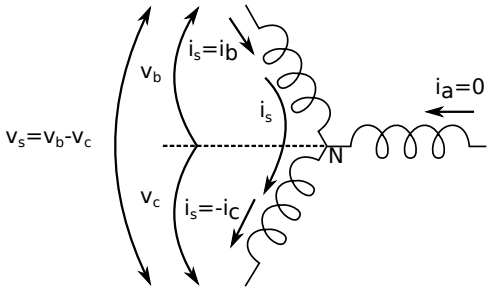

(c) Model 3

Model 1 is developed by applying one armature winding combined with rotor windings identical to the three-phase machine's rotor configuration. The equations are used directly, and not transformed to a common reference frame. Test results obtained from the implemented model present a rotary converter model experiencing initial conditions that are destabilizing the converter.

Model 2 views the behavior of the armature single-phase winding's pulsating MMF distribution as the result of two fictitious three-phase machines. Each machine induces a rotating MMF distribution. Equations are developed for each machine individually. They are decoupled from each other but interacts with their common rotor circuits. Successful model implementation has not been obtained,

due to the simulation not converging to final solutions.

Model 3 applies a three-phase synchronous machine with one open-circuited phase and necessary parameter adjustments for obtaining the behavior of the single-phase machine. Test results present the converter model behaving as expected during the loaded steady-state performance. The rate of decay of symmetrical fault current is faster than for sets of parameter adjustments carried out in the literature.

SAMMENDRAG

Det elektriske norske jernbanenettet bruker roterende frekvensomformere for å konvertere 50 Hz trefase vekselspenning til $16^2/_3$ Hz enfase vekselspenning. Disse omformerne består av to synkronmaskiner, en trefasenmotor mekanisk koblet til en enfasegenerator via en rotoraksling. Trefasemotoren er forsynt av regionalnettet og driver enfasegeneratoren. Frekvensforholdet mellom trefasenettet og enfasenettet er et resultat av polforholdet mellom motor og generator.

Denne masteroppgaven beskriver tre alternative metoder for å modellere enfase synkrongeneratorer brukt i roterende frekvensomformere.

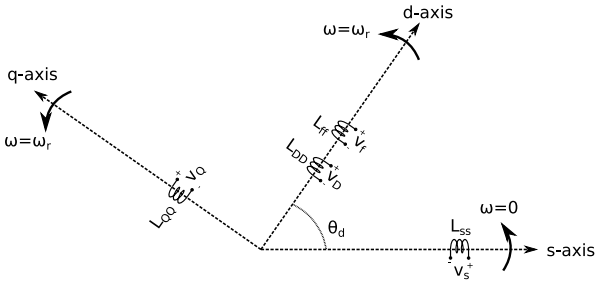

(a) Model 1

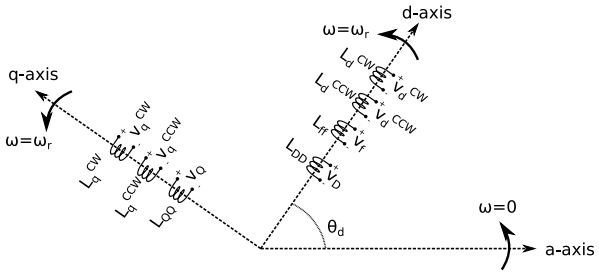

(b) Model 2

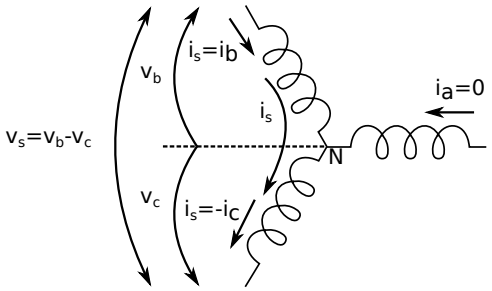

(c) Model 3

Modell 1 tar i bruk en fase-vikling i stator, kombinert med rotorviklinger identiske de som blir brukt for trefasemaskiner. Likningene er implementert direkte, uten å transformere variablene til et felles referansesystem. Resultater fra den implementerte modellen presenterer en omformer med initielle verdier som destabiliserer modellen.

Model 2 presenterer enfasemaskinens oppførsel som et resultat av to fiktive trefasemaskiner. Hver maskin induserer en distribuert MMF. Individuelle likningssett er utviklet for hver maskin. Maskinene er magnetisk dekoblet fra hverandre, men arbeider sammen med felles elektriske rotorkretser. Grunnet manglende konverging av løsninger under simulering er ikke vellykkede testresultater hentet fra modellen

Modell 3 tar i bruk en synkron trefasemaskin med en åpen fase og nødvendige parameterjusteringer

for a oppnå oppførselen til den synkrone enfasemaskinen. Testresultater presenterer en frekvensomformer som oppfører seg som forventet under stajonær opptreden. Reduksjonshastigheten til symmetrisk kortslutningsstrøm er raskere enn ved bruk av parameterjusteringer behandlet i alternative kilder.

PREFACE

This Master's Thesis concludes my Master of Science degree in Energy and Environmental Engineering with the Department of Electric Power Engineering at the Norwegian University of Science and Technology. The thesis was initiated by Bane NOR and represents a follow-up of the specialization project "Modeling Single-Phase Synchronous Generators for Rotary Frequency Converters" from autumn 2017. The thesis' objective is to describe different approaches for modeling single-phase synchronous generators for rotary frequency converters in the Norwegian traction power system.

The work presented in this Master's Thesis has been challenging, and I owe my gratitude to several people. I would like to thank my main supervisor Trond Toftevaag for his never-ending enthusiasm regarding the topics of this thesis. His knowledge, combined with his patience and ability to reassure me during "dark days" has been crucial for completing the thesis. I would also like to express my appreciation to Øyvind Stensby and my co-supervisor Steinar Danielsen from Bane NOR. They have always made time for my questions and provided me with helpful guidance. I also wish to show my appreciation to Abel Assegid Taffese. He has spent numerous hours guiding me with my rotary converter models, and his effort has been invaluable. Last, but not least, I would like to thank my fellow students at the MSc program Energy and Environmental Engineering.

Trondheim, June 11, 2018

Gaute Molland Solberg

Contents

Nomenclature

α	Mechanical angle from a stationary winding's magnetic axis
β_f	Angle between the counterclockwise rotating armature MMF distribution and the d-axis rotor MMF distribution
$\boldsymbol{\psi_R}$	Rotor flux linkages
$\boldsymbol{\psi_S}$	Armature flux linkages
$\boldsymbol{\psi}$	Machine flux linkages
$\boldsymbol{i_R}$	Rotor currents
$\boldsymbol{i_S}$	Armature currents
$\boldsymbol{i}$	Machine currents
$\boldsymbol{L_{RS}}$	Mutual inductance rotor to stator matrix
$\boldsymbol{L_R}$	Rotor inductance matrix
$\boldsymbol{L_{SR}}$	Mutual inductance stator to rotor matrix
$\boldsymbol{L_S}$	Armature inductance matrix
$\boldsymbol{L}$	Machine inductance matrix
δ	Electrical rotor angle with respect to a synchronously rotating frame of reference
δ_m	Mechanical rotor angle with respect to a synchronously rotating frame of reference
γ	Angle between the rotating armature MMF distributions and the armature magnetic axis of reference
$\mathscr{F}_{3ph(1)}$	Fundamental component of the MMF distribution for three phase-windings
$\mathscr{F}_{max}$	MMF distribution amplitude for a single phase-winding
$\mathscr{F}_{Res,d}$	Resultant d-axis MMF distribution component
$\mathscr{F}_{Res}$	Resultant MMF distribution
$\mathscr{F}_{S(1)}$	fundamental component of the MMF distribution for a single phase-winding
$\mathscr{F}_{S(1)}^{CCW}$	Counterclockwise rotating MMF distribution
$\mathscr{F}_{S(1)}^{CW}$	Clockwise rotating MMF distribution
$\mathscr{R}_d$	d-axis reluctance
$\mathscr{R}_{ss0}$	Average reluctance for a machine with a salient-pole rotor
$\mathscr{R}_{ssP}$	Peak reluctance variation for a machine with a salient-pole rotor

$\mathscr{R}_S$	Reluctance for a machine with a salient-pole rotor
ω_m	Mechanical rotational velocity in rad/s
ω_r	Rotor electrical rotational velocity in rad/s
ω_{sm}	Synchronous mechanical angular velocity in rad/s
ω_s	Synchronous angular velocity in rad/s
ϕ	Flux
ψ_0	Zero sequence flux linkage
ψ_a	Armature phase-a flux linkage
ψ_b	Armature phase-b flux linkage
ψ_c	Armature phase-c flux linkage
ψ_D	d-axis damper winding flux linkage
ψ_d	d-axis armature flux linkage
ψ_f	Field flux linkage
ψ_Q	q-axis damper winding flux linkage
ψ_q	q-axis armature flux linkage
ψ_s	Flux linkage for a single armature phase-winding
θ_d	Electrical rotor angle with respect to a stationary frame of reference
θ_m	Mechanical rotor angle with respect to a stationary frame of reference
ζ	Location of armature windings
D	Damping coefficient
D_d	Damping torque coefficient
f_s	Synchronous electrical frequency
H	Inertia constant
i_0	Zero sequence current
i_a	Armature phase-a current
i_b	Armature phase-b current
i_c	Armature phase-c current
i_D	d-axis damper current
i_d	d-axis armature current
i_f	Field current
i_Q	q-axis damper current
i_q	q-axis armature current
i_S	Armature current for a single phase-winding
J_{tot}	Total moment of inertia
k_w	Winding factor

L_0	Zero sequence inductance
L_{aD}	Mutual inductance between armature- and d-axis damper winding
L_{aQ}	Mutual inductance between armature- and q-axis damper winding
L_d	d-axis synchronous inductance
L_{ii}	Self inductance for phase-a-, phase-b-, phase-c-, field-, d-axis damper- and q-axis damper winding
L_{ij}	Mutual inductance for phase-a-, phase-b-, phase-c-, field-, d-axis damper- and q-axis damper winding
L_{lD}	Leakage inductance for the d-axis damper winding
L_{lf}	Leakage inductance for the field winding
L_{lQ}	Leakage inductance for the q-axis damper winding
L_{ls}	Leakage inductance for an armature winding
L_{md}	d-axis magnetizing inductance
L_{mq}	q-axis magnetizing inductance
L_q	q-axis synchronous inductance
L_{s1s2}	Constant term of the mutual inductance between two armature windings
L_{sDP}	Peak mutual inductance between armature- and d-axis damper winding
L_{SfP}	Peak mutual inductance between armature- and field winding
L_{sQP}	Peak mutual inductance between armature- and d-axis damper winding
L_{ss0}	Constant term of the self-inductance
L_{ssP}	Varying term of the self-inductance
L_{ss}	Self-inductance for an armature winding
n_{ms}	Synchronous mechanical angular velocity in rot./min
N_S	Number of winding turns
P	Number of machine poles
P_{em}	Electromagnetic power
P_t	Terminal power
R_D	d-axis damper winding resistance
R_f	Field winding resistance
R_Q	q-axis damper winding resistance
R_S	Armature winding resistance
T''_{d0}	d-axis sub-transient open-circuit time constant
T'_{d0}	d-axis transient open-circuit time constant
T_{em}	Electromagnetic torque
T_m	Mechanical torque

T''_{q0}	q-axis sub-transient open-circuit time constant
v_0	Zero sequence voltage
v_a	Armature phase-a voltage
v_b	Armature phase-b voltage
v_c	Armature phase-c voltage
v_D	d-axis damper terminal voltage (=0)
v_d	d-axis armature voltage
v_f	Field terminal voltage
v_Q	q-axis damper terminal voltage (=0)
v_q	q-axis armature voltage

Chapter 1

Introduction

1.1 Background

Electrified railways are the most energy and emission-efficient major mode of land-based transport [1]. The most efficient way of electrifying railways is through overhead contact lines located alongside the railway tracks [2]. Environmental considerations are a priority for future investments in the national infrastructure. Since electrified railway is a low CO_2-emission mode of travel, investments in the national railway infrastructure is essential for both infrastructural and environmental reasons [3].

The Norwegian electric traction power system standard is single-phase AC voltage at 15 kV and $16^2/_3$ Hz, and was introduced by a committee formed by the Norwegian parliament in 1916 [4]. System standard assessments were carried out by the Norwegian State Railway, NSB, in 1995 regarding transitioning the standard to 25 kV and 50 Hz. The transitioning was viewed financially not feasible, and the original 15 kV and $16^2/_3$ Hz standard were decided to be used for the future traction power systems [4].

The $16^2/_3$ Hz single-phase electric traction system is fed from the three-phase 50 Hz public system. Frequency converters are applied for coupling the two frequency systems [5]. A converter is a device that changes forms of the electricity. For the specific railway case in Norway, this changing of electricity is from three-phase 50 Hz AC to single-phase $16^2/_3$ Hz AC. These converters are in the Norwegian traction power system designed in two main ways, either electromechanical based or power electronic based. The electromechanical based converters are known as rotary frequency converters, and consist of a motor-generator set connected mechanically to a common shaft. Power electronic based converters use power electronic solutions and are known as static frequency converters [2].

The majority of frequency converters applied in the Norwegian traction power system are rotary

converters. These converters consist of a three-phase synchronous motor mechanically coupled to a single-phase synchronous generator through a shaft. The behavior of the three-phase machine is well-documented, and a variety of predefined models are applied for power system stability studies. The single-phase synchronous machine is on the other hand not as widely used as the three-phase machine. The single-phase machine's time-domain related behavior is not documented in the same manner as the three-phase machine's. Because of it's single-phase armature winding the machine's behavior differs from that of the three-phase machine, not enabling the same modeling techniques to be applied.

1.2 OBJECTIVE

The overall objective of this Master's Thesis is to obtain knowledge of the instantaneous time-domain related behavior of the single-phase synchronous generator applied for synchronous-synchronous rotary frequency converters. It is desired to develop sets of equations describing the single-phase machine by using the classical modeling equations for electrical machines, combined with theories presenting single-phase machine behavior.

1.3 LITERATURE SURVEY

A literature survey has been carried out for obtaining necessary knowledge regarding possible modeling methods that can are used for single-phase synchronous machines. The literature dealing with modeling methods for single-phase synchronous machines is limited, and a variety of alternative sources have been viewed. The major sources applied for the different modeling techniques developed during the work of the Master's Thesis is presented below.

- [6], [7], [8], [9], [10], [11] and [12] present the single-phase synchronous machine applied in rotary converters. Modeling the single-phase machine as a asymmetrical loaded three-phase synchronous machine are mentioned in a majority of these sources.
- [13] and [14] describe the armature MMF distribution's pulsating behaviour in the single-phase synchronous machine by applying two armature MMF distributions rotating in opposite directions.
- [15], [16], [17], [18], [19], [20] and [21] present dynamic modeling of single-phase induction motors. The articles has been a important for understanding the behaviour of single-phase machines, even though the sources are not directly applied in this Master's Thesis.

- [22], [23], [13], [24], [25], [26], [27], [28], [29], [30], [31], [32], [33], [34], [35], [36], [37], [38], [39], [40], [41] and [42] present both general and detail information regarding behavior and modeling techniques for three-phase synchronous machines. The foundation of the work presented in this Master's Thesis is based on these sources.

1.4 SCOPE OF WORK

Based on the background information presented above, the literature survey carried out and the Master's Thesis objective the following scope of works have been established:

- Carry out further literature study. Focus on material newly published regarding single-phase synchronous machines and rotary frequency converters.
- Clarify the parameter adjustments necessary when applying asymmetrical loaded three-phase machines as single-phase machines. Apply new obtained parameters and compare new test results with test results obtained for parameter adjustments carried out in the literature.
- Develop new single-phase synchronous machine equations based on the machine's phase quantities. Apply the quantities directly, without transforming quantities to a common reference frame.
- Develop new single-phase synchronous machine equations based on the doubling revolving field theory. View the single armature phase-winding's pulsating MMF distribution as the result of two fictitious three-phase machines.
- Implement and test the developed single-phase machine equations.

1.5 LIMITATIONS

The work presented in this Master's Thesis is to be carried out focusing on developing sets of equations describing single-phase synchronous machine's behavior. The main simplifications of this thesis are:

- Machine saturation has not been taken into account.
- The machine is modeled with constant applied field voltage, and AVR systems have not been an issue for the work presented.

- The focus has been on the single-phase synchronous machine, and the remaining traction power system components have been greatly simplified.

1.6 SOFTWARE

The rotary frequency converter models presented in this Master's Thesis have been implemented and tested in MATLAB®/Simulink. MATLAB®/Simulink is a high-level language used for computationally intensive tasks and is a product of MathWorks. Simulink blocks, defining mathematical relationships between its inputs and outputs, and the Simscape language, with predefined mathematical systems, have both been applied.

1.7 OUTLINE OF THE THESIS

The outline of the thesis is as follows:

- Chapter 1 introduces this thesis. Thesis objective and scopes of work are established based on the literature study carried out and the background introduction presented.
- Chapter 2 introduces the Norwegian traction power system, and briefly presents the rotary frequency converters.
- Chapter 3 gives an introduction to the equations applied when modeling three-phase synchronous machines. The sub-transient-, transient- and steady state time regime are presented briefly.
- Chapter 5 develops system equations and necessary parameter adjustments for implementing three models of single-phase synchronous machines. The equation of motion for a rotary converter is introduced.
- Chapter 6 presents test results from implementing three rotary converters applying the three single-phase machine models presented in Chapter 5. The chapter includes an overview and a discussion comparing test results with established single-phase theory.

Chapter 2

The Norwegian Traction Power System

2.1 The Norwegian Traction Power System

The Norwegian railway infrastructural system consists of 4208 km of railway lines, whereas 2456 km are electrified [43]. The electrified $16^2/_3$ Hz traction power system contains power generation-, power conversion- and power transmission equipment, in addition to the traction power system loads [44]. The conversion equipment presents 33 converter stations, located at intervals alongside the traction power line, and is feeding power from the public- to the traction power grid [45]. These intervals are commonly 20-90 km in the Norwegian traction power system [44]. This feeding method is commonly referred to as decentralized feeding. Fig. 2.1 presents such a system, where a 66 kV three-phase 50 Hz AC system is feeding power to a 16.5 kV $16^2/_3$ Hz single-phase AC system through two rotary- and one static converter.

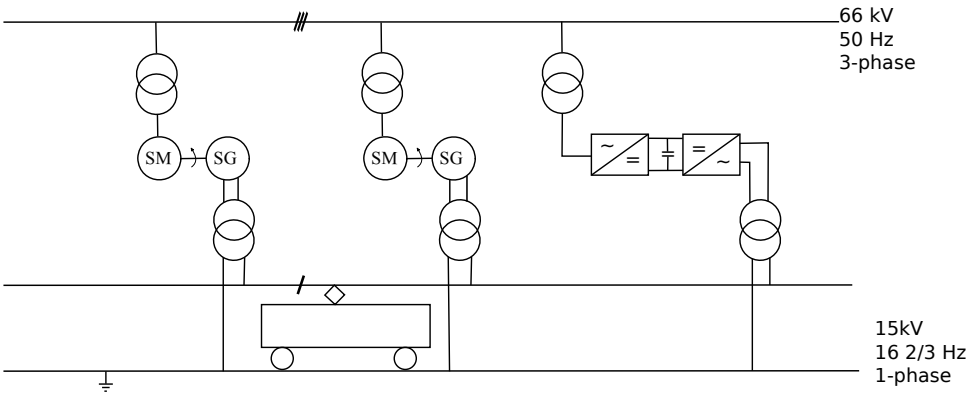

Figure 2.1: Decentralized feeding of the traction power system[1]

[1] Based on [46]

The low frequency of the Norwegian traction power system is a result of the limited commutating ability of the available propulsion motors during the early 20th-century [47]. The German Länderbahnen signed in 1912 an "Agreement on the execution of electrical railway transport". This agreement sat the standard of traction power system to single-phase AC voltage at 15 kV and 16⅔ Hz [5]. These standards are today applied in Germany, Austria, Sweden, Switzerland and Norway [48].

2.2 ROTARY FREQUENCY CONVERTER

The decentralized Norwegian feeding of the traction power system is carried out by applying, in addition to static converters, fixed-frequency synchronous-synchronous rotary frequency converters. These converters consist of a three-phase synchronous motor and a single-phase synchronous generator combined on a common shaft. The two machines feature the same mechanical frequency [49]. Since the motor has a triple number of poles compared to the generator, the electrical frequency on the generator side is always one-third of the applied frequency on the motor side [50]. The three-to-one relation between the motor's and generator's rotor poles is presented in Fig. 2.2. The motor and generator are here constructed with 12 and four poles, respectively.

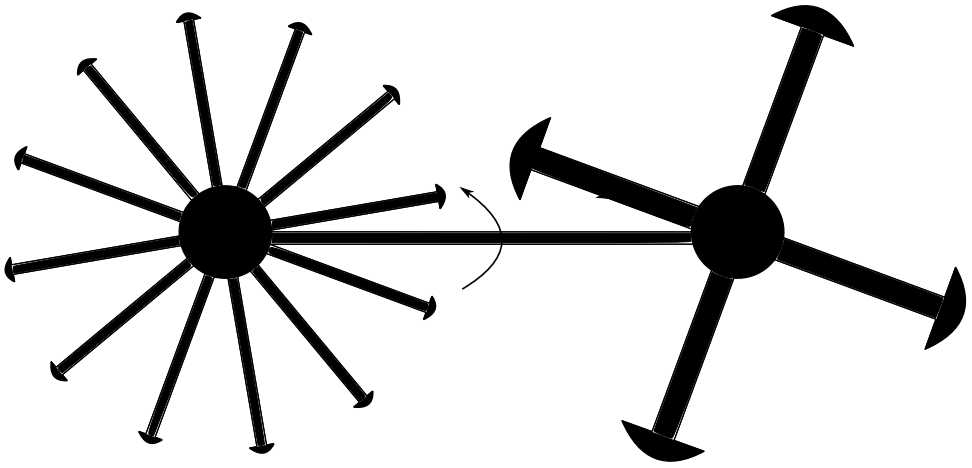

Figure 2.2: 12-poled synchronous motor mechanically coupled to a 4-poled synchronous generator[2]

The three-phase motor is supplied from the 50 Hz public grid. The common mechanical coupling between the generator and motor results in shared mechanical frequency, and based on (2.1) a 16⅔ Hz electrical generation is achieved at the generator side [26].

$$n_m P = 120 f_s \tag{2.1}$$

[2]Based on [7]

Loads of the traction power system, being the traction locomotives, varies heavily to time as the locomotives accelerate and decelerate along the railway line. The active power these loads require is fed from the three-phase grid through a step-down transformer and via the mechanical shaft of the converter [51]. The power is further on supplied to the traction power grid through a single-phase step-up transformer at 16.5 kV. The voltage delivered by the converters to the traction power system is 1.5 kV higher than the traction system's nominal voltage. The high voltage compensates for large voltage drops occurring between the converter and the railway locomotives [3]. The transformers enable the converters to be galvanic isolated from the two electrical systems at the same time as the nominal voltage of the converter components can be decreased.

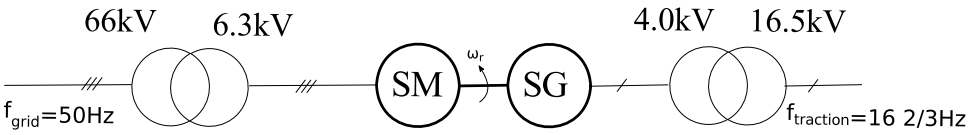

Figure 2.3: A three-phase public grid and a single-phase traction grid connected through a rotary converter

The rating of the rotary converters varies from 5.8-10 MVA [45]. As an example, the rotary converter type ASEA Q38 has a 4.4 MVA rated motor and a 4.0 MVA rated generator [52]. The converter has a total of 5.8 MVA rating, which is possible due to increased cooling of the machines. The ASEA Q38 converters are mounted on dedicated railway carriages and are equipped with automatic voltage regulators on both the motor and the generator side [53].

Chapter 3

The Three-Phase Synchronous Machine

Almost all energy from primary energy sources that are consumed by various loads in an electric power system is converted to electrical energy by synchronous machines. The largest portion of these are three-phase synchronous machines, and it is of high importance to develop usable and realistic models of these machines when dealing with dynamic phenomena in electric power systems [39]. In the following chapter a general mathematical description of a salient-poled three-phase synchronous machine with damper bars will be obtained.

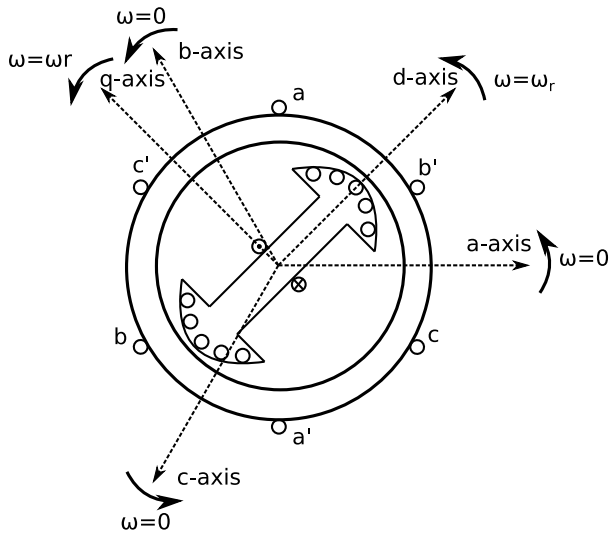

Figure 3.1: Three-phase synchronous machine with armature- and field windings and damper bars located on the rotor poles[1]

[1] Based on [32]

3.1 MMF DISTRIBUTION FOR A SINGLE PHASE-WINDING

The MMF distribution induced by one single-phase armature winding is sinusoidal and stationary, pulsating back and forth along the winding's magnetic axis.

The fundamental component of air-gap MMF for a distributed multi-pole winding with N_S turns is presented in (3.1).

$$\mathscr{F}_{S(1)} = \frac{4}{\pi}(\frac{k_w N_S}{P}) i_S \cos(\alpha) \tag{3.1}$$

$\frac{4}{\pi}$ arises from the Fourier series fundamental component of a rectangular MMF distribution, k_w is the machine's winding factor, $k_w N_S$ is the effective series turns for the single-phase winding, P is the number of machine poles and α is the angle measured from the winding's magnetic reference axis. The term $\cos(\alpha)$ is indicating that the MMF is sinusoidally distributed in space [28]. If in addition assuming a sinusoidally shaped phase-current in the armature winding, the MMF distribution is given as presented in (3.2).

$$\mathscr{F}_{S(1)} = \mathscr{F}_{max} \cos(\alpha) \cos(\omega_s t) \tag{3.2}$$

The peak amplitude of the MMF, $\mathscr{F}_{max}$, equals $\frac{4}{\pi}\frac{k_w N_{ph}}{P} I_s$ and $\cos(\omega_e t)$ implies that the MMF's amplitude is varying sinusoidally in time at frequency ω_e at given angular position α [28]. The MMF distribution is rewritten by applying the trigonometric relationship presented in (3.3).

$$\cos(a)\cos(b) = \frac{1}{2}(\cos(a+b) + \cos(a-b)) \tag{3.3}$$

The resulting MMF distribution of a single-phase winding can finally be viewed as the sum of two sinusoidally distributed MMFs rotating in counterclockwise/synchronous and clockwise/counter-synchronous direction [14]. The amplitude of the two rotating MMFs are equal, but half of the pulsating armature MMF's amplitude [54].

$$\mathscr{F}_{S(1)} = \underbrace{\frac{1}{2}\mathscr{F}_{max}\cos(\alpha - \omega_s t)}_{\mathscr{F}^{CCW}_{S(1)}} + \underbrace{\frac{1}{2}\mathscr{F}_{max}\cos(\alpha + \omega_s t)}_{\mathscr{F}^{CW}_{S(1)}} \tag{3.4}$$

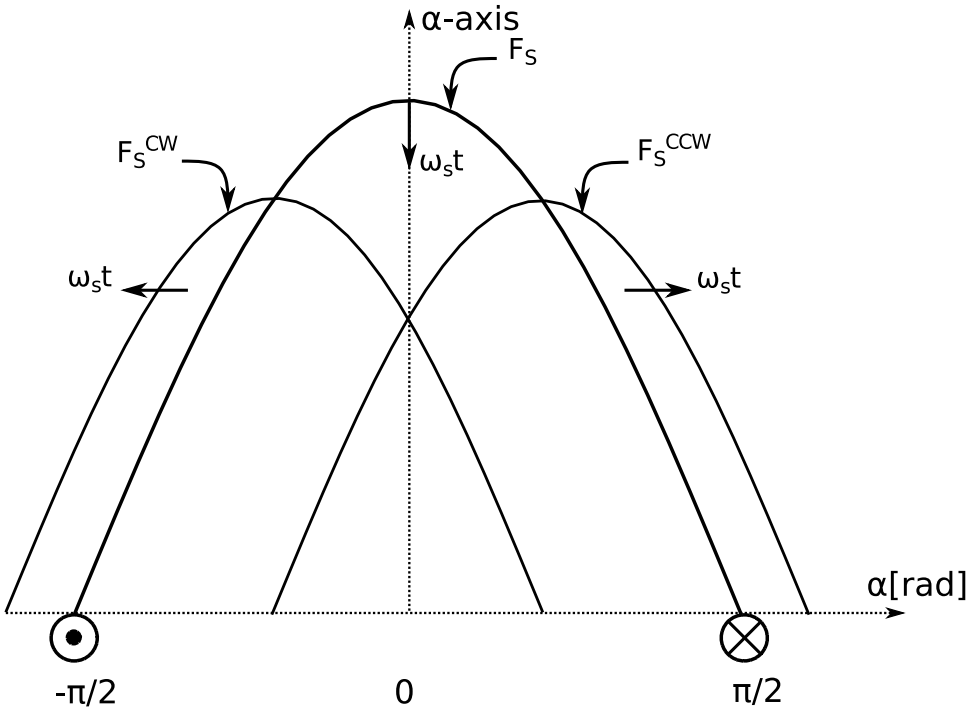

Figure 3.2: A pulsating sinusoidally distributed armature field, viewed as two rotating sinusoidally distributed fields[2]

Both MMF distributions in (3.4) are presented as space vectors rotating in counterclockwise and clockwise direction, respectively [13].

3.2 MMF DISTRIBUTION FOR THREE PHASE-WINDINGS

For a three-phase machine, every winding will induce the same MMF distribution as presented for a single-phase machine. The combined MMF for the entire machine is the sum of the MMF contributions from each individual winding. The windings of the individual phases are displaced 120 degrees in space and the instantaneous armature currents are shifted 120 electrical degrees in time. The result is the space vector MMF presented in (3.5), rotating in counterclockwise direction with constant amplitude $^3/_2$ times larger that of the the maximum peak of a single phase-winding's MMF [24].

$$\mathscr{F}_{3ph(1)} = \frac{3}{2}\mathscr{F}_{max}\cos(\alpha - \omega_s t) = \frac{3}{2}\mathscr{F}_{S(1)}^{CCW} \tag{3.5}$$

[2] Based on [54, 24, 13]

3.3 REFERENCE FRAMES

The rotor field winding of a synchronous machine has a DC excitation, inducing a MMF distribution stationary to the rotor. The rotor is revolving due to a primary energy source and the rotor MMF is therefore rotating at the same speed as the rotor. The three phase-currents flowing in the armature windings located on the stator are inducing a MMF distribution in the air-gap rotating at synchronous speed in counterclockwise direction. The three-phase synchronous machine will produce steady torque when the rotor- and stator MMFs are rotating at the same velocity [35].

Based on the symmetry of the rotor field-poles a magnetic reference axis referred to as the direct-axis is introduced, aligned with the rotating DC-current induced rotor MMF distribution [32]. The quadrature axis is located midway between two poles, 90 electrical degrees on the direct-axis. These axes, commonly referred to as the d- and q-axis, form the rotor reference frame. The armature windings of the stator have individual stationary magnetic axes. The armature- and rotor reference frames are observed in Fig. 3.1. A rotor angle, θ_d, is commonly introduced as the angle between the stationary magnetic axis of phase-a winding and the direct axis of the rotor. It is assumed that these axes are aligned at time equals zero [37].

3.4 INDUCTANCE

Salient-pole rotors are normally applied for synchronous machines operating at low speeds. The air-gap between the salient-poled rotor and the cylindrical shaped stator is non-uniform, and the machine's magnetic coupling will be influenced by the rotation of the rotor [32]. When the rotor's magnetic axis, the d-axis, is aligned with an armature winding's magnetic axis, the air-gap length between the stator- and rotor cores is at it's minimum. If the rotor rotates 90 electrical degrees the q-axis will be aligned with the armature winding's magnetic axis and the air gap will be at it's maximum. Since the main reluctance of the flux in the machine is offered by the air-gap length the reluctance will have a permanent value in addition to a periodically changing term [35]. This is presented in (3.6).

$$\mathscr{R}_S = \mathscr{R}_{ss0} + \mathscr{R}_{ssP}\cos(2\theta_d) \tag{3.6}$$

The self-inductance of a winding is the ratio of the flux linking a winding to the current flowing in the winding when no other currents are flowing. The inductance is proportional to the inverse of the machine's reluctance and can be derived based on the winding's MMF distributed along the d-

and q-axis. The result is an inductance with a second harmonic variation with respect to the rotor's rotation, as presented in (3.7). L_{ss0} is the constant term of the self inductance, and L_{ls} is the leakage inductance representing the winding's leakage flux.

$$L_{ss} = L_{ls} + L_{ss0} - L_{ssP}\cos(2\theta_d) \tag{3.7}$$

The mutual inductance between two windings is the ratio of flux linked by one winding due to the current flowing in the second winding when all other winding currents are zero [30]. The mutual inductance will be at it's peak value when the q-axis is aligned with one of the windings. The rotor's magnetic axis is then located midway between the two windings. In the same manner as deriving the self-inductance of an armature winding, the mutual inductance between two armature windings located ζ electrical degrees apart can be derived. The result is presented in (3.8) for a phase-a and phase-b winding in a three-phase machine. ζ is here equal to $\frac{2\pi}{3}$. The constant term L_{s1s2} of the mututal inductance equals half of the constatn term of a winding's self inductance.

$$L_{ab} = -L_{s1s2} - L_{ssP}\cos(2\theta_d - \zeta) = -\frac{L_{ss0}}{2} - L_{ssP}\cos(2\theta_d - \zeta) \tag{3.8}$$

The mutual inductance between rotor- and stator windings do not contain any constant terms since the air gap for d- and q-axis windings are fixed. The maximum mutual inductance between the armature winding and d- or q-axis windings will occur when the d- or q-axis are aligned with the armature winding's magnetic axis respectively. This is presented in (3.9a) for the mutual inductance between phase-a winding and d-axis damper winding, and and (3.9b) for the mutual inductance between phase-a winding and the q-axis damper winding [37] .

$$L_{aD} = L_{sDP}\cos(\theta_d) \tag{3.9a}$$

$$L_{aQ} = L_{sQP}\cos(\theta_d + \frac{\pi}{2}) = -L_{sQP}\sin(\theta_d) \tag{3.9b}$$

The self- and mutual inductances for the rotor windings do not dependent upon the rotor angle θ_d due to the cylindrical structure of the stator [32]. The windings on the d-axis and the q-axis are located 90 electrical degrees apart, and there will be no mutual coupling between these windings [37].

3.5 MAGNETIC COUPLING

The armature- and field windings and damper bars located in a three-phase synchronous machine are magnetically coupled to each other. This means that the flux in each winding depends on the current in all the other windings and bars. This is represented by the flux-linkage in (3.10) [34].

$$\boldsymbol{\psi} = \boldsymbol{L} \cdot \boldsymbol{i} \tag{3.10}$$

A general description of coupling between the machine windings and bars are presented in (3.11).

$$\begin{bmatrix} \boldsymbol{\psi_S} \\ \boldsymbol{\psi_R} \end{bmatrix} = \begin{bmatrix} \boldsymbol{L_S} & \boldsymbol{L_{SR}} \\ \boldsymbol{L_{RS}} & \boldsymbol{L_R} \end{bmatrix} \cdot \begin{bmatrix} -\boldsymbol{i_S} \\ \boldsymbol{i_R} \end{bmatrix} \tag{3.11}$$

The stator inductance matrix $\boldsymbol{L_S}$ in the inductance matrix $\boldsymbol{L}$ contains self- and mutual inductances for the armature windings. The inductance matrix $\boldsymbol{L_{SR}}$ presents the mutual inductances between the armature stator windings and the rotor windings. This matrix is identical to the transposed matrix of mutual inductances between the rotor and stator $\boldsymbol{L_{RS}}$. All elements in these three matrices are rotor angle dependent. The rotor inductance matrix $\boldsymbol{L_R}$ contains the self- and mutual inductances for the rotor windings. All inductance elements in this matrix are constant due to the rotor configuration and the applied DC quantities to the field circuit. Mutual inductances between the d- and q-axis are zero. The minus sign observed for the phase currents in (3.11) is a result of the current- and flux linkage reference direction.

For a three-phase synchronous machine with one additional damper winding in the d- and q-axis, (3.11) is expanded to (3.12).

$$\begin{bmatrix} \psi_a \\ \psi_b \\ \psi_c \\ \psi_f \\ \psi_D \\ \psi_Q \end{bmatrix} = \begin{bmatrix} L_{aa} & L_{ab} & L_{ac} & L_{af} & L_{aD} & L_{aQ} \\ L_{ab} & L_{bb} & L_{bc} & L_{bf} & L_{bD} & L_{bQ} \\ L_{ac} & L_{bc} & L_{cc} & L_{cf} & L_{cD} & L_{cQ} \\ L_{af} & L_{bf} & L_{cf} & L_{ff} & L_{fD} & 0 \\ L_{aD} & L_{bD} & L_{cD} & L_{fD} & L_{DD} & 0 \\ L_{aQ} & L_{bQ} & L_{cQ} & 0 & 0 & L_{QQ} \end{bmatrix} \cdot \begin{bmatrix} -i_a \\ -i_b \\ -i_c \\ i_f \\ i_D \\ i_Q \end{bmatrix} \tag{3.12}$$

3.6 VOLTAGES

The voltages, currents and flux linkages of the armature electrical circuits are related by applying Kirchoff's voltage law, as presented in (3.13).

$$\begin{aligned} v_a &= \frac{d}{dt}\psi_a - R_S i_a \\ v_b &= \frac{d}{dt}\psi_b - R_S i_b \\ v_c &= \frac{d}{dt}\psi_c - R_S i_c \end{aligned} \tag{3.13}$$

Similar relationships are experienced in the rotor electrical circuits, as presented in (3.14).

$$\begin{aligned} v_f &= \frac{d}{dt}\psi_f + R_f i_f \\ v_D &= \frac{d}{dt}\psi_D - R_D i_D = 0 \\ v_Q &= \frac{d}{dt}\psi_Q - R_Q i_Q = 0 \end{aligned} \tag{3.14}$$

The damper bars are shorted at their terminals and the terminal voltages of both d- and q-axis damper circuit are equal to zero. The system for the three-phase synchronous machine is presented in Fig. 3.3.

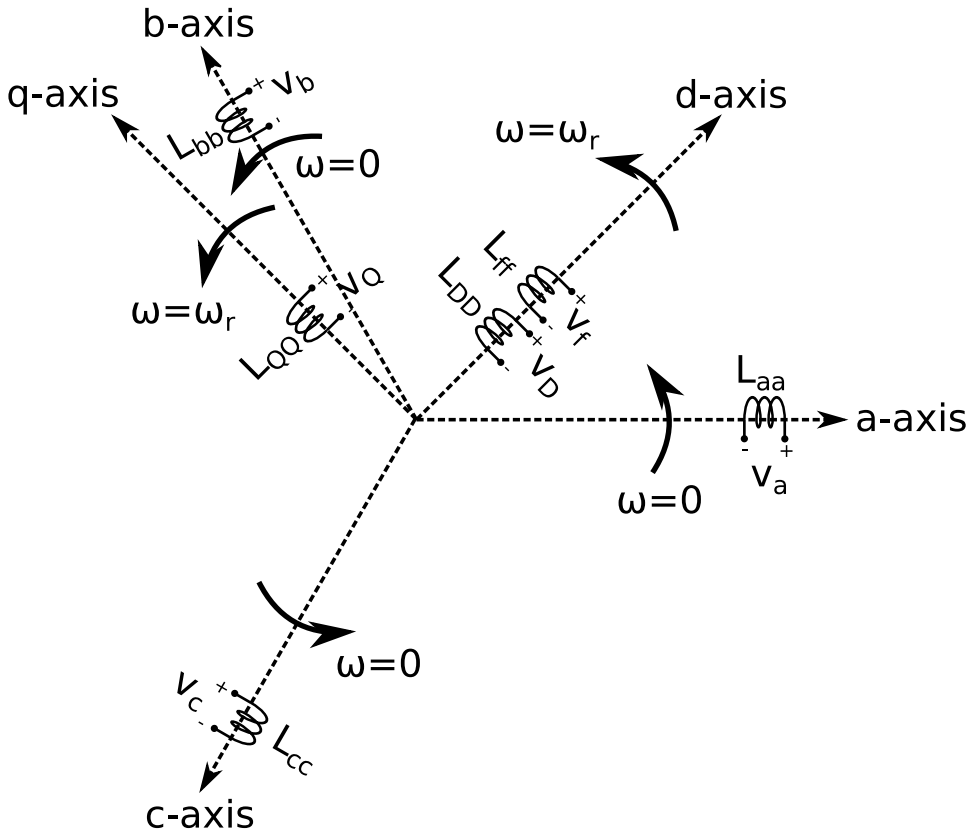

Figure 3.3: Synchronous machine with three armature windings, one field winding and one d- and one q-axis damper winding with associated self inductances[3]

3.7 FROM STATOR- TO ROTOR REFERENCE FRAME

As earlier presented, all the self- and mutual inductances of the armature windings and the mutual inductances between the field- and armature windings are angle dependent. This gives presence to a complicated time-varying coefficient in the machine's equations. When observing the flux-linkages of a three-phase synchronous machine in (3.12), it is noted that the solution of the voltage equations (3.13) and (3.14) are highly formidable. For a machine with one additional damper winding in d- and one in q-axis, the voltage equations leads to a set of six coupled differential equations with time-varying coefficients [37].

The time-varying set of differential equations in (3.13) can be greatly simplified by transforming the phase quantities of the stator to a new set of variables related to an orthogonal reference frame rotating at rotor speed [37], commonly known as the $d-q$-reference frame. This transformation is called the

[3] Based on [37]

Park's transformation and was introduced by R. H. Park in 1929 [42]. Park's voltage invariant matrix is presented in (3.15).

$$\boldsymbol{P} = \frac{2}{3}\begin{bmatrix} \cos(\theta) & \cos(\theta - \frac{2\pi}{3}) & \cos(\theta - \frac{4\pi}{3}) \\ -\sin(\theta) & -\sin(\theta - \frac{2\pi}{3}) & -\sin(\theta - \frac{4\pi}{3}) \\ \frac{1}{2} & \frac{1}{2} & \frac{1}{2} \end{bmatrix} \tag{3.15}$$

$$\boldsymbol{P^{-1}} = \begin{bmatrix} \cos(\theta) & -\sin(\theta) & 1 \\ \cos(\theta - \frac{2\pi}{3}) & -\sin(\theta - \frac{2\pi}{3}) & 1 \\ \cos(\theta - \frac{4\pi}{3}) & -\sin(\theta - \frac{4\pi}{3}) & 1 \end{bmatrix} \tag{3.16}$$

The quantities in the rotating reference frame are obtained by multiplying the three-phase quantities with Park's matrix. The transformation is presented in (3.17) for a phase variable x, representing the armature quantities of flux linkage, phase-voltage and phase-current.

$$\begin{bmatrix} x_d \\ x_q \\ x_0 \end{bmatrix} = \boldsymbol{P}\begin{bmatrix} x_a \\ x_b \\ x_c \end{bmatrix} \tag{3.17}$$

The original phase quantities are obtained by multiplying the transformed quantities with the inverse of the Park's matrix, presented in (3.16). The calculation is presented in (3.18).

$$\begin{bmatrix} x_a \\ x_b \\ x_c \end{bmatrix} = \boldsymbol{P^{-1}}\begin{bmatrix} x_d \\ x_q \\ x_0 \end{bmatrix} \tag{3.18}$$

By multiplying the variables with Park's matrix, $\boldsymbol{P}$, the armature quantities are transformed into a reference system with a stationary rotor. This implies that the new $d-q$-reference system rotates at rotor speed. Two new fictitious armature windings are identified, the armature d- and q-axis winding. The magnetic axis of the d-axis winding is aligned with the rotor d-axis rotor magnetic axis, while the magnetic q-axis winding is located 90 electrical degrees ahead of the d-axis. The new reference frame is therefore rotor referenced. The resultant rotating MMF distribution produced by the phase currents i_a, i_b and i_c can be resolved into a d- and q-axis component. The currents i_d and i_q produces a MMF along their respective magnetic axes equal the d- and q-component of the resultant rotating MMF produced by the phase currents. Since the axes are rotating, this current is constant for balanced conditions [22]. The zero-component presented in (3.17) and (3.18) are zero for balanced conditions.

The current i_0 is identical to the zero sequence phase current known from symmetrical component theory.

The factor $^2/_3$ observed in (3.15) is a result of keeping the transformation voltage and current invariant. The peak values of dq- currents and voltages are equal to the peak values of phase-currents and phase-voltages [40].

The transformed $d-q$-variables are applied in the set of voltage balance equations (3.13) and a new set of equations in a rotating reference frame are obtained. The voltage equations are rewritten, as presented in detail in Appendix A, and the final voltage equations for the armature electrical circuits are obtained. The resulting set of voltage balance equations are presented in (3.19).

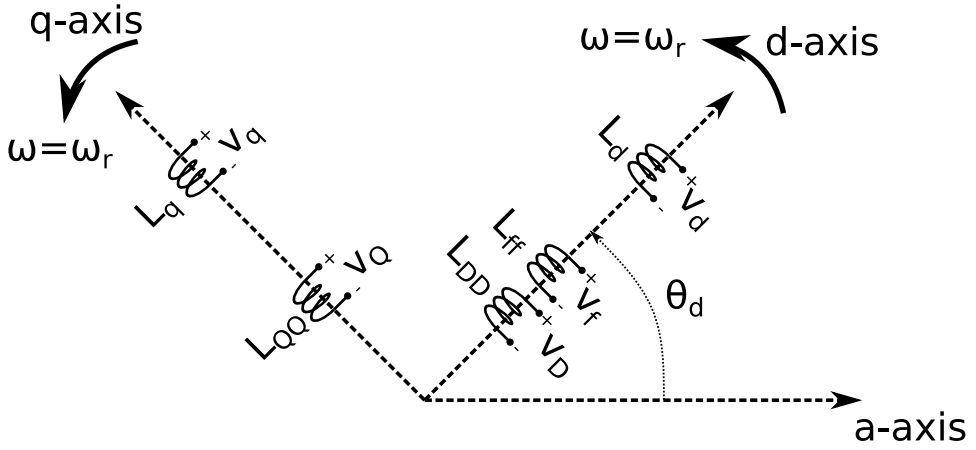

Figure 3.4: Three-phase synchronous machine with two armature windings, one field winding and one d-and-one q-axis damper winding with associated synchronous- and self inducances[4]

$$v_d = -R_S i_d + \frac{d}{dt}\psi_d - \omega_r \psi_q \tag{3.19a}$$

$$v_q = -R_S i_q + \frac{d}{dt}\psi_q + \omega_r \psi_d \tag{3.19b}$$

$$v_0 = -R_S i_0 + \frac{d}{dt}\psi_0 \tag{3.19c}$$

$$v_f = R_f i_f + \frac{d}{dt}\psi_f \tag{3.19d}$$

$$0 = R_D i_D + \frac{d}{dt}\psi_D \tag{3.19e}$$

$$0 = R_Q i_Q + \frac{d}{dt}\psi_Q \tag{3.19f}$$

[4] Based on [37]

When comparing the sets of voltage equations in (3.13) and (3.19) two additional terms are observed, $\omega_r\psi_q$ and $\omega_r\psi_d$ for the d- and q-axis voltages, respectively. These terms are known as speed voltages, and present the induced voltages in the stationary armature coils due to a an armature MMF distribution rotating at synchronous speed. The terms $\frac{d}{dt}\psi_d$ and $\frac{d}{dt}\psi_q$ are commonly referred to as the transformer voltages and are a result of the rate of change of flux linkage. During steady state machine performance the transformer voltages are zero and the speed voltages will be the dominant component of the armature voltages [32].

The rotor referenced flux linkages are obtained based on (3.10) when applying the equations of transformation as presented in (3.17) and (3.18). The calculations are presented in detail in Appendix B. The result is an associated inductance matrix that are independent of the rotor angle. The resulting flux linkages are presented in (3.20).

$$\psi_d = -L_d i_d + L_{SfP} i_f + L_{SDP} i_D \tag{3.20a}$$

$$\psi_q = -L_q i_q + L_{SQP} i_Q \tag{3.20b}$$

$$\psi_0 = -L_0 i_0 \tag{3.20c}$$

$$\psi_f = -\frac{3}{2} L_{sfP} i_d + L_{ff} i_f + L_{fD} i_D \tag{3.20d}$$

$$\psi_D = -\frac{3}{2} L_{sDP} i_d + L_{fD} i_f + L_{DD} i_D \tag{3.20e}$$

$$\psi_Q = -\frac{3}{2} L_{sQP} i_q + L_{QQ} i_Q \tag{3.20f}$$

L_d and L_q is referred to as the d- and q-axis synchronous inductance, and is based on the inductances presented in (3.12). When converting this flux-linkage equation to a reference frame, the stator inductance matrix $\boldsymbol{L_S}$ is converted into a diagonal 3x3-matrix with elements equal to the axes' synchronous inductances. The inductance matrix is presented in (B.5) of Appendix B. The magnetizing inductances of each axis are defined as viewed in (3.21a) and (3.21b) where the synchronous d-and q-axis inductances are presented.

$$L_d = L_{ls} + \underbrace{\frac{3}{2}(L_{ss0} + L_{ssP})}_{L_{md}} \tag{3.21a}$$

$$L_q = L_{ls} + \underbrace{\frac{3}{2}(L_{ss0} - L_{ssP})}_{L_{mq}} \tag{3.21b}$$

These synchronous inductances also have a practical understanding and can be measured. The d-axis synchronous inductance is the ratio of armature flux linkage to the armature current when the rotating MMF distribution of the armature is aligned with the MMF distribution of the field. Similarly, the q-axis synchronous inductance is the same ratio when the rotating MMF distribution of the armature is aligned with the q-axis [29].

The armature phase windings have N_{ph} turns, while the field winding and d- and q-axis damper bars have N_f, N_D and N_Q turns respectively. The rotor voltages, -currents and -flux linkages are substituted with stator referred variables by multiplying the rotor referred field winding and damper bars variables with N_f/N_{ph}, N_D/N_{ph} and N_Q/N_{ph} respectively. If in addition multiplying the stator referred rotor currents with a factor $2/3$ the magnetizing inductances for the all d- and q-axis windings becomes L_{md} and L_{mq} respectively [30, 41]. The flux linkages are rewritten and presented in (3.22). The subscript $'$ indicates that the rotor currents are stator referenced.

$$\psi_d = -L_d i_d + L_{md} i_f^{'} + L_{md} i_D^{'} \tag{3.22a}$$

$$\psi_q = -L_q i_q + L_{mq} i_Q^{'} \tag{3.22b}$$

$$\psi_0 = -L_0 i_0 \tag{3.22c}$$

$$\psi_f = -L_{md} i_d + L_{ff} i_f^{'} + L_{md} i_D^{'} \tag{3.22d}$$

$$\psi_D = -L_{md} i_d + L_{md} i_f^{'} + L_{DD} i_D^{'} \tag{3.22e}$$

$$\psi_Q = -L_{mq} i_q + L_{QQ} i_Q^{'} \tag{3.22f}$$

The equations presented in (3.19) and (3.22) are known as Park's equations, and are applied when modeling three-phase synchronous machines [37].

3.8 PARAMETERS OF THE THREE-PHASE SYNCHRONOUS MACHINE

The fundamental transient characteristic of a three-phase synchronous machine are examined by applying a bolted three-phase short-circuit fault at the machine's terminals [36]. The fault current has two distinct components, a symmetrical component with fundamental frequency and a DC offset

component. The symmetrical component will decay at a changing rate, fast for the first few cycles, than slower until the component reaches it's steady state value. The DC offset component will decrease exponentially. The decay of the fault circuit is observed in the Fig. 3.5 together with the decay of damper- and field currents [32].

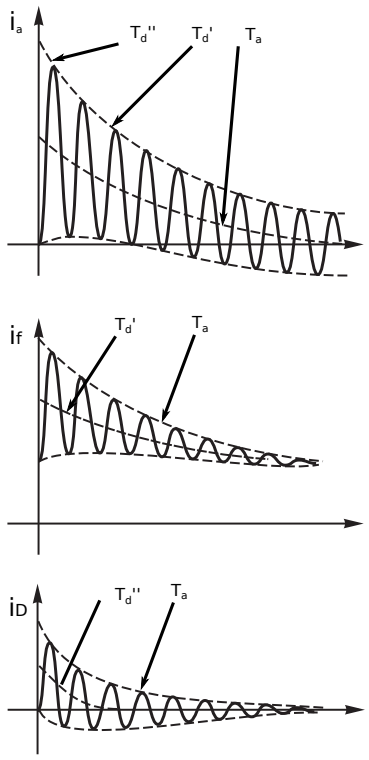

Figure 3.5: Armature-, field and damper currents during a three-phase short circuit fault [34]

The rate of decay of the symmetrical short-circuit component is explained by observing Fig. 3.6. A three-phase synchronous machine with a salient-poled rotor experiences here a three-phase short-circuit at the armature terminals. The short-circuit causes the armature currents to increase instantaneously, but flux linking a closed conducting path cannot change instantaneously [25].

$$\psi(t = 0^-) = \psi(t = 0^+) \tag{3.23}$$

As the fault current increases, the armature flux linking the other electrical circuit in the machine increases with the current. As a result, currents with symmetrical- and DC offset components are induced in the damper bars and field winding to prevent the armature flux to enter the rotor circuit [34]. The fastest decay of symmetrical fault current is related to the damper bars, while the slower decay is related to the field winding. The induced currents will therefore decrease faster in the damper

bars than in the field winding [29]. This is a result of the damper bars' resistances normally being larger than that of the field winding. The decay period where the damper bars are most active is referred to as the sub-transient state. The armature flux' path is observed in Fig. 3.6a. When the damper currents have decreased significantly the field winding's induced current will continue to decrease until it reaches it steady state value. This decrease is referred to as the transient state and the flux' path is observed in Fig. 3.6b. The armature flux is finally allowed to enter all the machines circuits, and the fault current reaches it's steady state value. The flux path is observed in Fig. 3.6c.

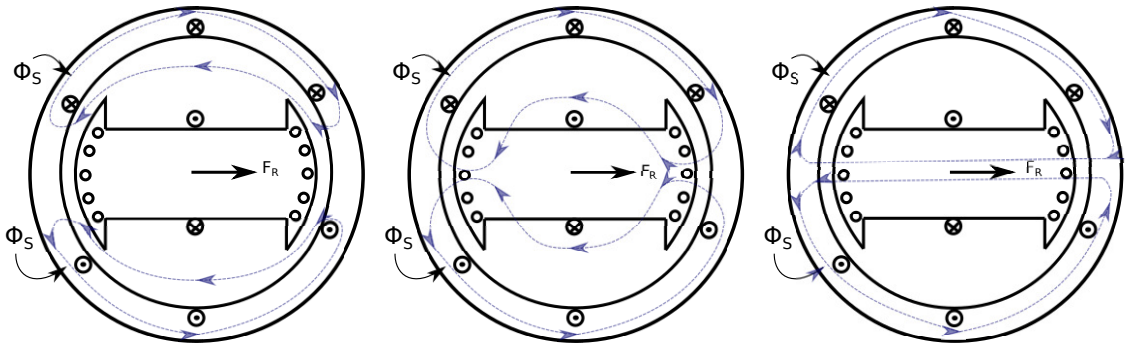

(a) The sub-transient state **(b)** The transient state **(c)** The steady-state

Figure 3.6: Rotor screening during a disturbance event[5]

The dynamics of a synchronous machine is often analyzed separately in the sub-transient-, transient- and steady state. This is carried out by assigning the states with different equivalent circuits. As mentioned earlier, the different rotor circuits are damped differently. Different rotor circuits are therefore interacting together with the armature during the three different states [29].

The change of armature d- and q-axis flux linkage in synchronous operation are defined as the change of all d- and q-axis currents multiplied with their respective inductances, as presented in (3.24a) and (3.24b), respectively. Δ indicates here the deviation from synchronous operation for flux linkages and currents.

$$\Delta\psi_d = L_d\Delta i_d + L_{md}\Delta i_f + L_{md}\Delta i_D \tag{3.24a}$$

$$\Delta\psi_q = L_q\Delta i_q + L_{mq}\Delta i_Q \tag{3.24b}$$

For the sub-transient period the induced rotor currents will keep the flux linkage for every rotor circuit initially constant, as presented in (3.23). The change in field- and damper flux linkage are therefore

[5]Based on [34, 29]

zero for the d- and q-axis, as presented in (3.25a) and (3.25b), respectively.

$$\begin{aligned} \Delta\psi_f &= L_{md}\Delta i_d + L_{ff}\Delta i_f + L_{md}\Delta i_D = 0 \\ \Delta\psi_D &= L_{md}\Delta i_d + L_{md}\Delta i_f + L_{DD}\Delta i_D = 0 \end{aligned} \tag{3.25a}$$

$$\Delta\psi_Q = L_{mq}\Delta i_q + L_{QQ}\Delta i_Q = 0 \tag{3.25b}$$

As inductance is defined as the ratio between flux linkage and current, the sub-transient d- and q-axis synchronous inductance are derived by solving the equations in (3.25a) and (3.25b) with respect to Δi_f, Δi_D and Δi_Q. By inserting these equations into (3.24a) and (3.24b) the relationship between change of d- and q-axis flux linkage and change of d- and q-axis armature current are obtained as presented in (3.26a) and (3.26b), respectively.

$$\Delta\psi_d = \underbrace{(L_d - \frac{L_{md}^2(L_{lf}+L_{lD})}{L_{ff}L_{DD}-L_{md}^2})}_{L_d''}\Delta i_d \tag{3.26a}$$

$$\Delta\psi_q = \underbrace{(L_q - \frac{L_{mq}^2}{L_{QQ}})}_{L_q''}\Delta i_q \tag{3.26b}$$

For the transient period there are no induced currents in the damper bars. The change of armature d- and q-axis flux linkage is therefore as given in (3.27a) and (3.27b).

$$\Delta\psi_d = L_d\Delta i_d + L_{md}\Delta i_f \tag{3.27a}$$

$$\Delta\psi_q = L_q\Delta i_q \tag{3.27b}$$

The field flux linkage is still zero, but not depending upon the change of damper currents. The damper currents effect are therefore removed and the field flux linkage is given as in (3.25a), except for the damper current contribution from Δi_D is removed. The relationship between change of d- and q-axis flux linkage, and change of d- and q-axis armature current are obtained as presented in (3.28a) and

(3.28b), respectively.

$$\Delta\psi_d = \underbrace{(L_d - \frac{L_{md}^2}{L_{ff}})}_{L_d^{'}} \Delta i_d \tag{3.28a}$$

$$\Delta\psi_q = \underbrace{L_q}_{L_q^{'}} \Delta i_q \tag{3.28b}$$

It is observed that since the q-axis doesn't contain any field winding, the transient- and steady state synchronous q-axis inductance are the same.

The inductances presented in (3.26a), (3.26b), (3.28a) and (3.28b) are rewritten by appreciating that the magnetizing inductances in d- and q-axis are identical for all d- and q-axis windings. The result is presented in (3.29).

$$\begin{aligned}
L_d &= L_{ls} + L_{md} \\
L_q &= L_{ls} + L_{mq} \\
L_d^{'} &= L_{ls} + \frac{L_{md}L_{lf}}{L_{md} + L_{lf}} \\
L_q^{'} &= L_{Ls} + L_{mq} \\
L_d^{''} &= L_{ls} + \frac{L_{md}\frac{L_{lD}L_{lf}}{L_{lD}+L_{lf}}}{L_{md} + \frac{L_{lD}L_{lf}}{L_{lD}+L_{lf}}} \\
L_q^{''} &= L_{ls} + \frac{L_{mq}L_{lQ}}{L_{mq} + L_{lQ}}
\end{aligned} \tag{3.29}$$

L_d, L_q, $L_d^{'}$, $L_q^{'}$, $L_d^{''}$, $L_q^{''}$ are recognized as the armature leakage inductance in series with the parallel connection of the involved electric circuits' leakage inductances. The result is presented in Fig. 3.7.

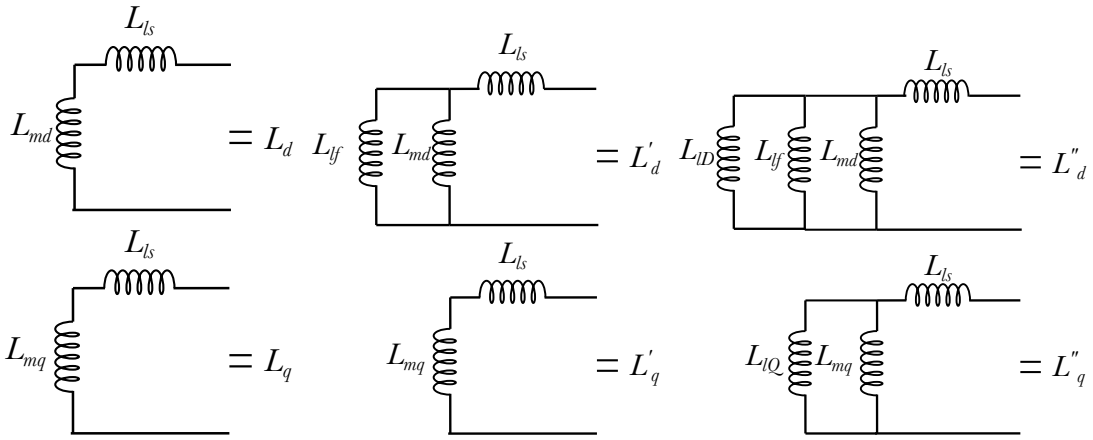

(a) The d- and q-axis synchronous inductance **(b)** The d- and q-axis transient synchronous inductance **(c)** The d- and q-axis sub-transient synchronous inductance

Figure 3.7: Synchronous inductances for the sub-transient-, transient- and steady state [6]

The symmetrical component of the short-circuit fault current will contain exponential factors in which the rate of decrement is given by time constants. It is usually convenient to express the characteristic of synchronous machines in terms of these time constants [36]. The magnetic energy in an electric circuit with an inductance and resistance will dissipate over a given time, and the circuit's current will decrease exponentially to zero with a time constant equal to (3.30) [35].

$$T = \frac{L}{R} \tag{3.30}$$

The time constants applied when describing the decay of the symmetrical component are the short-circuit time constants T'_d, T''_d and T''_q. These time constants, together with the armature time constant T_a, is observed in Fig. 3.5 during the decay of damper-, field- and armature current. The commonly applied open-circuit time constant, T'_{d0}, T''_{d0} and T''_{q0} are calculated by inserting the damper- or field resistance into the damper- or field branch presented in Fig. 3.7. The time constants are presented in (3.31).

$$T'_{d0} = \frac{L_{ff}}{R_f} = \frac{L_{lf} + L_{md}}{R_f} \tag{3.31a}$$

$$T''_{d0} = \frac{L_{lD} + \frac{L_{md} L_{lf}}{l_{lf} + L_{md}}}{R_D} \tag{3.31b}$$

$$T''_{q0} = \frac{L_{QQ}}{R_Q} = \frac{L_{lQ} + L_{mq}}{R_Q} \tag{3.31c}$$

[6] Based on [32]

3.9 ELECTROMAGNETIC POWER

The terminal power output of a three-phase synchronous machine is the product of armature phase voltages and phase currents, as presented in (3.32) [41].

$$P_t = v_a i_a + v_b i_b + v_c i_c \tag{3.32}$$

The phase quantities are eliminated in terms of rotor referenced quantities by applying the transformation presented in (3.17). The rotor referenced armature voltages, v_d and v_q, from (3.19) can further on be substituted into the power equation of (3.32), and the resulting power output is presented in (3.33) [37].

$$P_t = \frac{3}{2}(\underbrace{(i_d \frac{d}{dt}\psi_d + i_q \frac{d}{dt}\psi_q + 2i_0 \frac{d}{dt}\psi_0)}_{\textbf{Armature magnetic power}} + \underbrace{\frac{2}{P}\omega_r(\psi_d i_q - \psi_q i_d)}_{\textbf{Air-gap power}} - \underbrace{(i_d^2 + i_q^2 + 2i_0^2)R_s)}_{\textbf{Ohmic losses}} \tag{3.33}$$

The power transferred across the air gap is here denoted as the electromagnetic power output of the machine, and is defined as the terminal machine power in addition to the ohmic losses of the machine. By assuming steady state machine performance, the magnetic power term goes to zero, and the electromagnetic power is defined as presented in 3.34 [32].

$$P_{em} = \frac{3}{2}\frac{2}{P}\omega_r(\psi_d i_q - \psi_q i_d) \tag{3.34}$$

3.10 EQUATION OF MOTION

The rotational inertia equations are of great importance when describing the effect of unbalance between generated electromagnetic torque and applied mechanical torque for electric machines. The motion of the machine's rotor is determined by Newton's second law of motion, given by (3.35) [32].

$$J_{tot}\frac{d^2}{dt^2}\theta_m(t) = T_m(t) - T_{em}(t) - D_d\omega_m(t) \tag{3.35}$$

The total moment of inertia of all rotating parts is presented as J_{tot}, θ_m is the mechanical rotor angle with respect to a stationary reference, T_m and T_{em} are the applied mechanical torque and the generated electromagnetic torque and $D_d\omega$ is the damping toque, here expressed by the damping torque coefficient, D_d, and the mechanical rotational velocity of the rotor, ω_m [37], [34].

For convenience, the equation of motion are rewritten on a synchronously rotating reference frame with rotor electrical angles. The rotor angle is measured with respect to a synchronously rotating reference, $\omega_{sm}t$, as presented in (3.36). The rotor angle is further transformed to electrical degrees by multiplying the mechanical angle with the number of machine pole pairs.

$$\delta_m = \theta_m - \omega_{sm}t \tag{3.36}$$

$$\delta = \frac{P}{2}\delta_m \tag{3.37}$$

It is furthermore appreciated that the product of torque and mechanical rotational velocity is power. (3.35) is then rewritten in terms of unbalance of power, and the equation is normalized in terms of rated power. The resulting equation of motion is presented in (3.38).

$$\frac{2H}{\omega_s}\frac{d^2}{dt^2}\delta + D\frac{d}{dt}\delta = p_{m,pu} - p_{em,pu} \tag{3.38}$$

The inertia constant, here presented as H, is the machine's stored kinetic energy at synchronous speed divided by the it's rated apparent power. H is one of the most important parameters of the machine, and directly affects the stability of the power system [37]. ω_s is the nominal electrical rotational velocity, D is the damping coefficient related to the damping power, and $p_{m,pu}$ and $p_{em,pu}$ are the normalized applied mechanical power and generated electromagnetic power, respectively [37]. (3.38) can further rewritten by appreciating the calculations presented in (3.39), where δ_{pu} is the per unit rotor angle.

$$\frac{1}{\omega_s}\frac{d^2}{dt^2}\delta = \frac{d^2}{dt^2}\delta_{pu} \tag{3.39}$$

The equation of motion, commonly referred to as the swing equation, is presented in (3.40).

$$2H\frac{d^2}{dt^2}\delta_{pu} + D\frac{d}{dt}\delta_{pu} = p_{m,pu} - p_{em,pu} \tag{3.40}$$

Chapter 4

The Single-Phase Synchronous Machine

An electric synchronous machine constructed with one armature winding is commonly referred to as a single-phase synchronous machine. The machine contains the same magnetic components as the traditional three-phase synchronous machine, a rotor, and a stator. The fundamental construction of the machine is presented in Fig. 4.1.

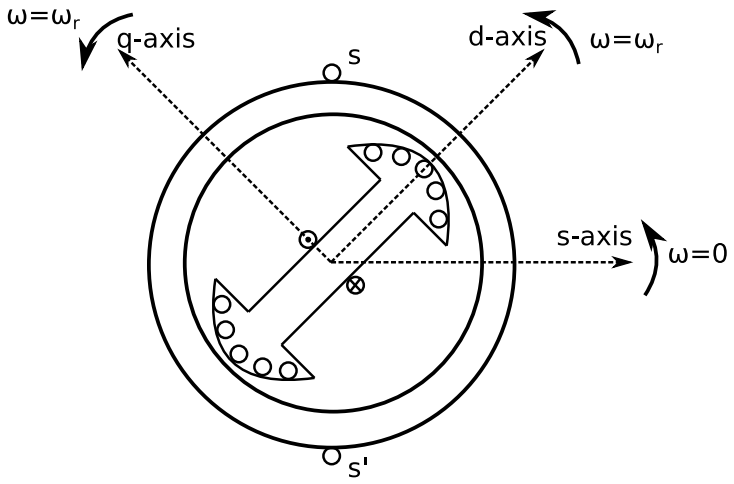

Figure 4.1: Single-phase synchronous machine

The machine's rotor is similar to that of the three-phase machine's. The poles have a salient shaped construction due to the low-frequency operation and contain short-circuited damper bars [12]. The rotor also includes the field winding, responsible for inducing the machine's rotor MMF distribution. The stator is constructed with one armature winding, generating power to a single-phase electric

system. Since there is not provided symmetrical three-phase windings in the stator, traditional methods for modeling three-phase synchronous machines cannot be applied when analyzing single-phase machines [49]. A three-phase machine can induce constant electromagnetic power during steady state machine performance. Currents are only induced in the damper bars for producing damping power during electromechanical transients [25]. When only one armature winding is loaded, which is the case for a single-phase machines, the induced electromagnetic power pulsates at double AC frequency [55]. The pulsation causes rotor currents to be induced in the rotor circuits at double AC frequency [12], also during steady-state machine operation. Currents will flow continuously in these windings, and the damper bars for the single-phase machine are therefore constructed larger than those of the three-phase machine [10].

4.1 SINGLE ARMATURE PHASE-WINDING

The MMF distribution of a loaded single-phase winding was presented in (3.1). By applying trigonometric relationships, the pulsating MMF distribution was presented as two MMF distribution rotating in a counterclockwise- and clockwise direction at synchronous speed. This was presented in (3.4) and was observed in Fig. 3.2. The peak MMF distributions of the armature are viewed in Fig. 4.2. It is here observed how the counterclockwise- and clockwise rotating MMF distributions, $\mathscr{F}_S^{CCW}$ and $\mathscr{F}_S^{CW}$, recreates the behavior of the pulsating armature MMF distribution, $\mathscr{F}_S$.

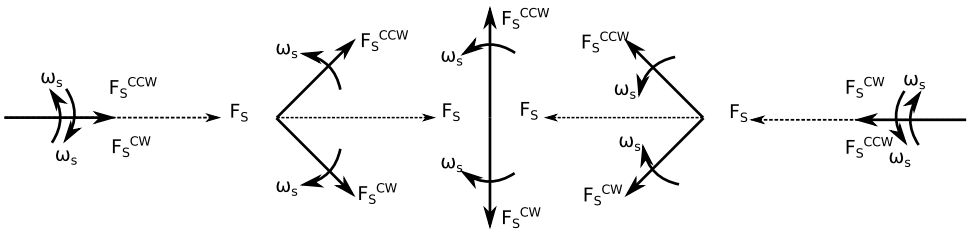

Figure 4.2: Two fields rotating in opposite directions, resulting in a stationary pulsating field [1]

The counterclockwise-rotating MMF distribution rotates at synchronous speed and locks onto the rotor MMF distribution. The clockwise MMF distribution rotates in a clockwise direction at double speed compared to the rotor MMF distribution [13]. The MMF distribution rotating in a counterclockwise direction is responsible for the desired electromagnetic torque induced by the machine converting from mechanical- to electrical energy. The effect of the clockwise rotating field is damped out by Eddy currents in the rotor [54] and second harmonic currents induced in the short-circuited damper bars and field winding of the rotor [12]. If the rotor core is laminated the effect of Eddy

[1] Based on [54]

currents are nonexistent [14]. The second harmonic currents induced in the rotor circuits are a direct result of the relative rotational speed between the clockwise rotating MMF distribution and the rotor MMF distribution. The induced currents cause a MMF distribution oscillating at second fundamental frequency along the machine's rotating d-axis. The double fundamental frequency MMF can be viewed as two MMFs rotating at three times the fundamental frequency in a counterclockwise direction and at the fundamental frequency in a clockwise direction, respectively [13]. The two MMF distributions are presented in Fig. 4.3.

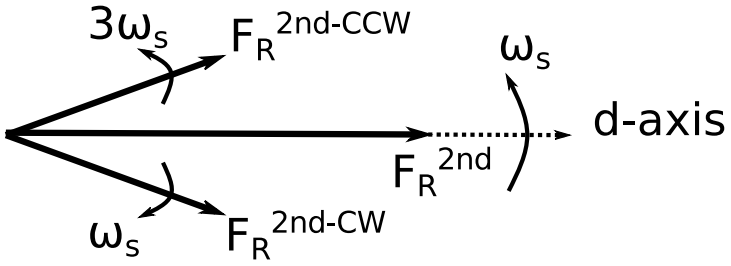

Figure 4.3: Rotor MMF oscillating along the d-axis, viewed as two MMFs rotating at $2\omega_s$ counterclockwise and ω_s clockwise

The resultant MMF distribution of the machine is the sum of the MMF distribution from the armature and the MMF distribution from the rotor field.

$$\overrightarrow{\mathscr{F}_{Res}} = \overrightarrow{\mathscr{F}_S} + \overrightarrow{\mathscr{F}_R} \tag{4.1}$$

The resultant flux of the machine is therefore equal to the resultant MMF distribution divided by the air-gap reluctance. This relationship is presented in (4.2) and the stator and rotor fluxes can be observed in Fig. 4.4.

$$\phi = \frac{\mathscr{F}_{Res}}{\mathscr{R}} \tag{4.2}$$

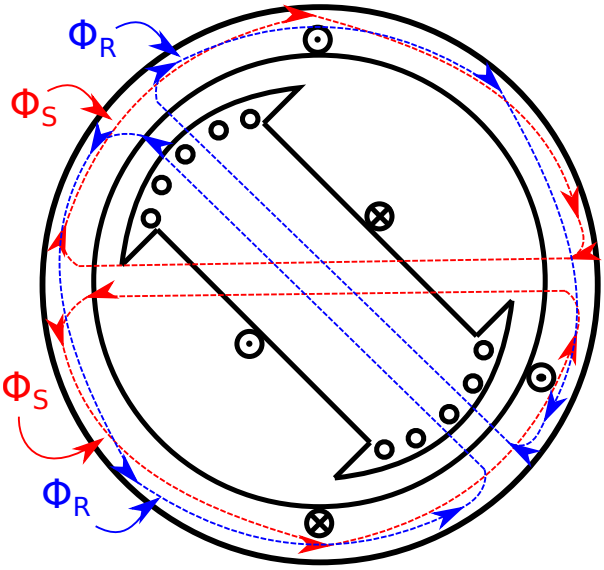

Figure 4.4: Fluxes from the rotor and armature in flux lines blue and red, respectively

Since the single-phase synchronous machine dealt with has salient poles, the magnetic circuit will have larger magnetic resistance in the q-axis then in the d-axis. Since $\mathscr{R}_d < \mathscr{R}_q$, the q-axis flux are neglected due to the d-axis flux being larger than the q-axis flux. This dramatically simplifies the analyzes of the machine behavior [13], [14].

The total flux produced is assumed only dependent upon the d-axis component of the resultant MMF and the reluctance of that exact axis, as presented in (4.3).

$$\phi \approx \frac{\mathscr{F}_{Res,d}}{\mathscr{R}_d} \tag{4.3}$$

In the following calculation, it is assumed that the d-axis is aligned with the armature's magnetic axis at $t = 0$.

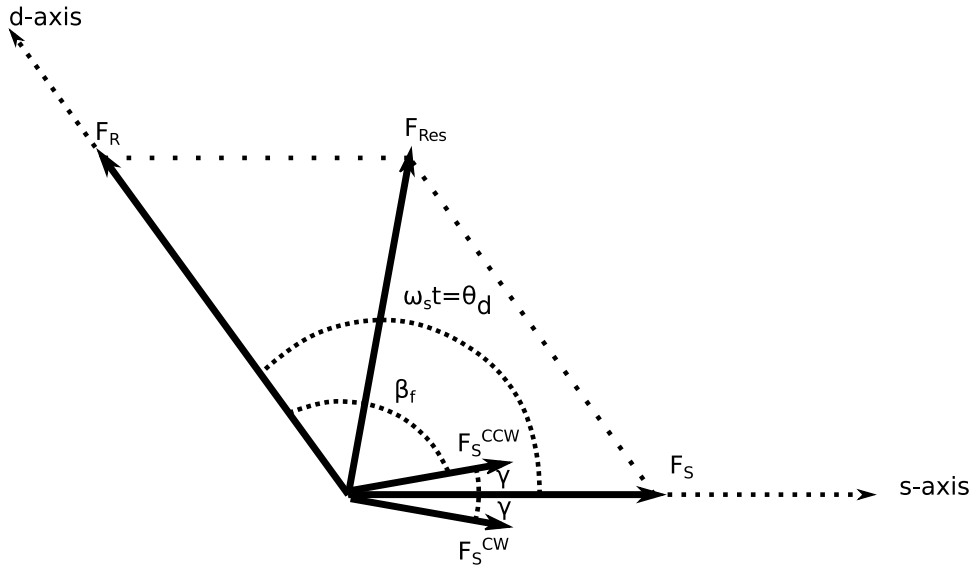

Figure 4.5: Resultant MMF in the single-phase machine[2]

Since the counterclockwise MMF distribution and the rotor d- axis is in synchronism the angle β_f is constant. γ presents the angle between the pulsating armature MMF distribution aligned with stationary s-axis and the counterclockwise and clockwise MMFs that together presents the behavior of the pulsating MMF distribution. The angle is presented in (4.4). It is observed that γ will change by following the rotation of the rotor.

$$\gamma = \omega_s t - \beta_f \tag{4.4}$$

The d-axis component of the resultant MMF is calculated by determining the d-axis components of the rotor MMF, the counterclockwise armature MMF and the clockwise armature MMF.

$$\begin{aligned} \mathscr{F}_{Res,d} &= \mathscr{F}_R + \mathscr{F}_{S,d} \\ &= \mathscr{F}_R + \mathscr{F}_S^{CCW}\cos(\beta_f) + \mathscr{F}_S^{CW}\cos(2\omega_s t - \beta_f) \end{aligned} \tag{4.5}$$

In accordance with (4.3), the machine's flux is presented as in (4.6).

$$\phi_{tot} = \frac{1}{\mathscr{R}_d}(\mathscr{F}_R + \mathscr{F}_S^{CCW}\cos(\beta_f) + \mathscr{F}_S^{CW}\cos(2\omega_s t - \beta_f)) \tag{4.6}$$

[2]Based on [14]

The total flux is rotating at speed ω_s. Since the armature winding is stationary, the total flux is passing this winding at ω_s. The armature winding's flux linkage is therefore equal to (4.7).

$$\begin{aligned}\psi_S &= \sqrt{2}k_w N_S \phi_{Tot}\cos(\omega_s t) \\ &= \frac{\sqrt{2}k_w N_S}{\mathscr{R}_d}(\mathscr{F}_R\cos(\omega_s t) + \mathscr{F}_S^{CCW}\cos(\beta_f)\cos(\omega_s t)... \\ &...+\frac{1}{2}\mathscr{F}_S^{CW}\cos(3\omega_s t-\beta_f)+\frac{1}{2}\mathscr{F}_S^{CW}\cos(\omega_s t-\beta_f)\end{aligned} \tag{4.7}$$

By Faraday's law, the induced voltage in the armature winding is the rate of change of the flux linkage of that exact winding. The induced armature voltage is presented in (4.8).

$$\begin{aligned}e_S &= -\frac{d}{dt}\psi_S \\ &= \frac{\sqrt{2}k_w N_S\omega_s}{\mathscr{R}_d}(\mathscr{F}_R\sin(\omega_s t) + \mathscr{F}_S^{CCW}\cos(\beta_f)\sin(\omega_s t)... \\ &...+\frac{3}{2}\mathscr{F}_S^{CW}\sin(3\omega_s t-\beta_f)+\frac{1}{2}\mathscr{F}_S^{CW}\sin(\omega_s t-\beta_f)) \\ &= E_{e(1)}\sin(\omega_s t) + E_{(1)}^{CCW}\sin(\omega_s t) + E_{(1)}^{CW}\sin(\omega_s t-\beta_f) + E_{(3)}^{CW}\sin(3\omega_s t-\beta_f)\end{aligned} \tag{4.8}$$

It is here observed that the induced voltage in the armature winding will contain both fundamental and third harmonic terms. The third harmonic term is a result of the counterclockwise rotating armature MMF distribution, $\mathscr{F}_S^{CCW}$, that induces second harmonic currents in the field winding and the damper bars. The induced currents cause an oscillating rotor MMF aligned with the rotor's d-axis that is rotating at a fundamental frequency, ω_s. The pulsating MMF is viewed as a counterclockwise and clockwise MMF rotating at $3\omega_s$ and $-\omega_s$. The counterclockwise-rotating MMF and field MMF will induce fundamental frequency voltage in the armature winding, while the clockwise rotating MMF will induce fundamental- and third harmonic voltages in the same winding. The peak values of the voltage are equal to $E_{(1)}^{CW}$, $E_{e(1)}$, E_1^{CW} and $E_{(3)}^{CW}$, respectively [13].

Chapter 5

Modeling Single-Phase Synchronous Machine

Theory and modeling principles of the three-phase synchronous machine were presented in Chapter 3. Three-phase AC quantities are transformed into a rotor reference frame and converted into two-phase DC quantities. When the transformation is carried out for the three-phase inductance matrix, the dependent rotor angle self-inductances of the armature windings and the rotor angle dependent mutual inductances between the armature- and rotor windings becomes rotor angle invariant. This was one of the primary motivations when developing the transformation presented by R. H. Park.

Theory and behavior of the single-phase synchronous machine were presented in Chapter 4. This machine seems identical to the three-phase machine except for the number of armature phase-windings, but its behavior is fundamentally different. The rotating MMF distribution of the three-phase machine is induced by three phase-currents shifted 120 electrical degrees in time flowing in three phase-windings located 120 degrees in space. The MMF distribution of the single-phase machine is induced by a single phase-current flowing in a single phase-winding. The MMF distribution of the single phase-winding will pulsate along with the magnetic axis of the armature winding. This causes several difficulties when trying to analyze the instantaneous behavior of the single-phase machine.

Since the single-phase synchronous machine is not provided with balanced three-phase windings in the stator, the traditional Park equations introduced in Chapter 3 cannot be applied directly. Three different methods have therefore been developed for modeling a single-phase synchronous machine in a synchronous-synchronous rotary frequency converter.

5.1 MODEL 1: ONE ARMATURE WINDING

The following section presents a mathematical model for determining the instantaneous time-domain related behavior of a single-phase synchronous machine applying one armature phase-winding, together with one field winding and one d- and one q-axis damper winding. The phase quantities for the single-phase machine's armature winding are applied directly, without any attempts to transform any quantities to another frame of reference. The machine consists of two reference frames. The stationary reference frame along the magnetic axis of the single armature phase-winding and the rotor $d-q$-reference. The rotor circuits are identical to the ones presented for the three-phase synchronous machine presented in Chapter 3. The single-phase synchronous machine is presented in 5.1. The damper bars are located on the rotor poles, and the field winding is presented in the center of the rotor.

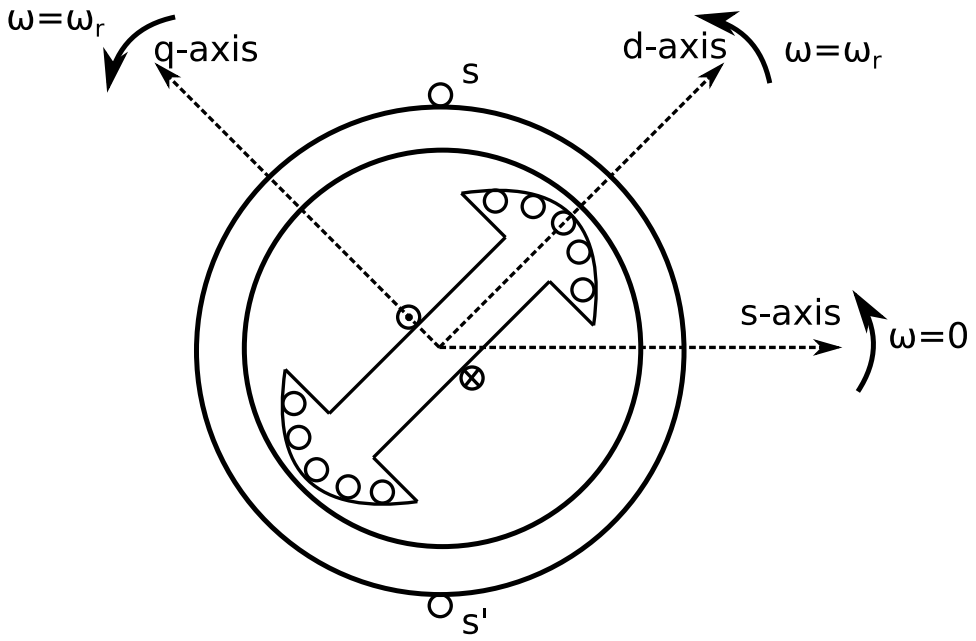

Figure 5.1: Single-phase synchronous machine

The two reference frames of the machine in Fig. 5.1 are presented in Fig. 5.2.

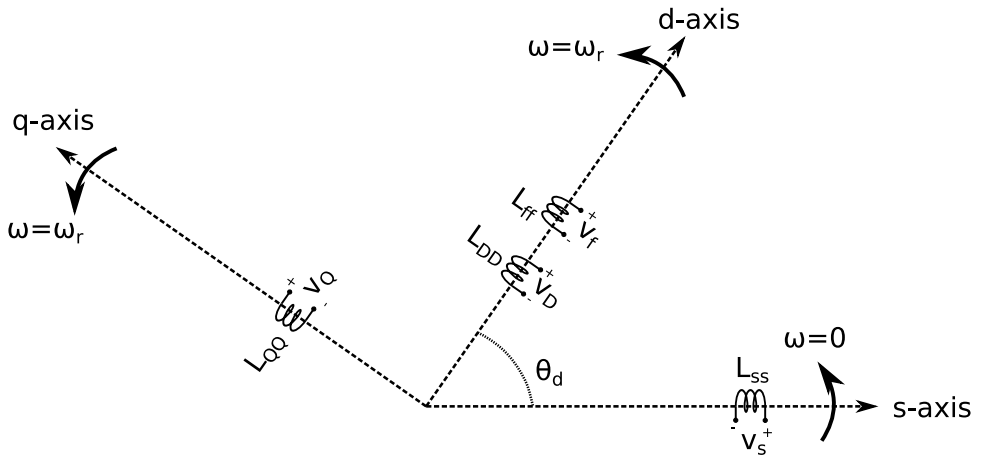

Figure 5.2: Single-phase synchronous machine with two systems of reference

The windings presented on each axis in Fig. 5.2 demonstrates the necessary number of voltage balance equations. The rotor circuits are magnetically coupled to the armature circuit, and the field and d-axis damper circuit are magnetically coupled to each other. The circuits on the rotor d-axis and the damper circuit of the q-axis are decoupled.

5.1.1 Inductance

The armature inductance matrix of a three-phase synchronous machine, $\boldsymbol{L_S}$, was presented in Chapter 3. The armature inductance matrix for the single-phase machine contains only one armature winding. No mutual inductances between other armature windings occur, and the armature inductance matrix has only the self-inductance of the single armature winding. The inductance is presented in (5.1).

$$\boldsymbol{L_S} = L_{ss} = L_{ls} + L_{ss0} + L_{ssP}\cos(2\theta_d) \tag{5.1}$$

The self-inductance contains a leakage inductance and a fixed inductance term, $L_{ls} + L_{ss0}$, together with a second harmonic term due to the salient-pole rotor configuration. The second harmonic term will oscillate periodically along the fixed term with an amplitude equal to L_{ssP}.

The single-phase machine's rotor is identical to the standard three-phase machine's. There are mutual inductances between the armature winding, the field winding and the damper bars of the rotor due to magnetic coupling. The mutual inductance matrix between the armature to rotor windings are identical to the transposed mutual inductance matrix between the rotor to armature windings, as presented in (5.2).

$$\boldsymbol{L_{SR}} = \boldsymbol{L_{RS}^T} = \begin{bmatrix} L_{sfP}\cos(\theta_d) & L_{sDP}\cos(\theta_d) & -L_{sQP}\sin(\theta_d) \end{bmatrix} \tag{5.2}$$

The rotor windings contain self-inductances and mutual inductances between windings located on the same rotor reference axis. There are no mutual inductances between the windings located on the d-and on the q-axis.

$$\boldsymbol{L_R} = \begin{bmatrix} L_{ff} & L_{fD} & 0 \\ L_{fD} & L_{DD} & 0 \\ 0 & 0 & L_{QQ} \end{bmatrix} \tag{5.3}$$

The single-phase synchronous machine's inductance matrix is presented in (5.4).

$$\boldsymbol{L} = \begin{bmatrix} L_{ss}(\theta_d) & L_{sf}(\theta_d) & L_{sD}(\theta_d) & L_{sQ}(\theta_d) \\ L_{sf}(\theta_d) & L_{ff} & L_{fD} & L_{fQ} \\ L_{sD}(\theta_d) & L_{fD} & L_{DD} & L_{DQ} \\ L_{sQ}(\theta_d) & L_{fQ} & L_{DQ} & L_{QQ} \end{bmatrix} \tag{5.4}$$

The inductances involving the armature winding are dependent upon the rotor position.

5.1.2 Magnetic Coupling

The magnetic coupling of the machine is presented by the machine's flux linkages, as presented in (5.5).

$$\begin{bmatrix} \psi_s \\ \psi_f \\ \psi_D \\ \psi_Q \end{bmatrix} = \begin{bmatrix} -L_{ss}(\theta_d) & L_{sf}(\theta_d) & L_{sD}(\theta_d) & L_{sQ}(\theta_d) \\ -L_{sf}(\theta_d) & L_{ff} & L_{fD} & 0 \\ -L_{sD}(\theta_d) & L_{fD} & L_{DD} & 0 \\ -L_{sQ}(\theta_d) & 0 & 0 & L_{QQ} \end{bmatrix} \cdot \begin{bmatrix} i_s \\ i_f \\ i_D \\ i_Q \end{bmatrix} \tag{5.5}$$

It is observed that the armature flux linkage, ψ_s, is dependent upon the coupling between all machine windings. The circuits located on the d- and q-axis are decoupled.

5.1.3 Voltage Balance

By appreciating that induced voltage is the rate of change of flux linkage, the voltage balances for each electric circuit in the machine presented in Fig 5.2 are obtained. It is observed that the damper bars are short-circuited, leaving their terminal voltages equal to zero. The voltage balances for the single-phase synchronous machine are presented in (5.6).

$$\begin{aligned} v_s &= -R_S i_S + \frac{d}{dt}\psi_s \\ v_f &= R_f i_f + \frac{d}{dt}\psi_f \\ v_D &= R_D i_D + \frac{d}{dt}\psi_D = 0 \\ v_Q &= R_Q i_Q + \frac{d}{dt}\psi_Q = 0 \end{aligned} \tag{5.6}$$

5.1.4 Currents

The machine's currents are obtained by appreciating the relationship between flux linkages and currents, presented in (3.10). The inverse inductance matrix is calculated and presented in Appendix E. The machine's flux linkages are multiplied by the inverse inductance matrix, as presented in (5.7).

$$\begin{bmatrix} i_s \\ i_f \\ i_D \\ i_Q \end{bmatrix} = \underbrace{\begin{bmatrix} -L_s(\theta_d) & L_{sf}(\theta_d) & L_{sD}(\theta_d) & L_{sQ}(\theta_d) \\ -L_{sf}(\theta_d) & L_{ff} & L_{fD} & 0 \\ -L_{sD}(\theta_d) & L_{fD} & L_{DD} & 0 \\ -L_{sQ}(\theta_d) & 0 & 0 & L_{QQ} \end{bmatrix}^{-1}}_{\boldsymbol{L}^{-1}} \cdot \begin{bmatrix} \psi_S \\ \psi_f \\ \psi_D \\ \psi_Q \end{bmatrix} \tag{5.7}$$

The inductances L_{ss}, L_{sf}, L_{sD}, L_{sQ} are dependent upon the rotor angle, θ_d. This results in the matrix elements of the inverse inductance matrix to be extensive, each depending on θ_d. The inverse inductance matrix is presented in Appendix E. The first element in this matrix, here referred to as a_{11} is presented in (5.8) for illustrating the rotor angle dependency of the inverse inductance matrix elements.

$$a_{11} = \frac{A_{11} + B_{11}\cos(\theta_d) + C_{11}\cos(2\theta_d) + D_{11}\cos(3\theta_d) + ... + K_{11}\cos(10\theta_d)}{L_{11} + M_{11}\cos(2\theta_d) + N_{11}\cos(4\theta_d) + O_{11}\cos(6\theta_d) + P_{11}\cos(8\theta_d) + Q_{11}\cos(10\theta_d)} \tag{5.8}$$

A_{11}, B_{11}, C_{11}, D_{11}, E_{11}, F_{11}, G_{11}, H_{11}, I_{11}, J_{11}, K_{11}, L_{11}, M_{11}, N_{11}, O_{11}, P_{11} and Q_{11} are constants made up of the constant inductance terms presented in the inductance matrix of (5.4).

The equations for calculating the machine currents are rewritten from (5.7) and presented in (5.9). a_{nm} presents the elements of $\boldsymbol{L^{-1}}$, where n and m denotes the row and column of the elements, respectively. These elements are presented in Appendix E.

$$\begin{aligned} i_S &= a_{11}\psi_S + a_{12}\psi_f + a_{13}\psi_D + a_{14}\psi_Q \\ i_f &= a_{21}\psi_S + a_{22}\psi_f + a_{23}\psi_D + a_{24}\psi_Q \\ i_D &= a_{31}\psi_S + a_{32}\psi_f + a_{33}\psi_D + a_{34}\psi_Q \\ i_Q &= a_{41}\psi_S + a_{42}\psi_f + a_{43}\psi_D + a_{44}\psi_Q \end{aligned} \tag{5.9}$$

5.1.5 Electromagnetic Power

The electromagnetic power induced by the single-phase synchronous machine is presented in (5.10). The expression is based on that of the three-phase synchronous machine's electromagnetic power, presented in Section 3.9.

$$P_{em} = v_s i_s - R_s i_s^2 \tag{5.10}$$

5.1.6 Model 1 - Overview

A simplified overview of an implemented rotary frequency converter model is viewed in Fig. 5.3. The three-phase synchronous motor is applying the Park equations for a three-phase machine, while the single-phase synchronous machine applies the single-phase machine equations for a machine viewed in phase quantities with one armature phase-winding.

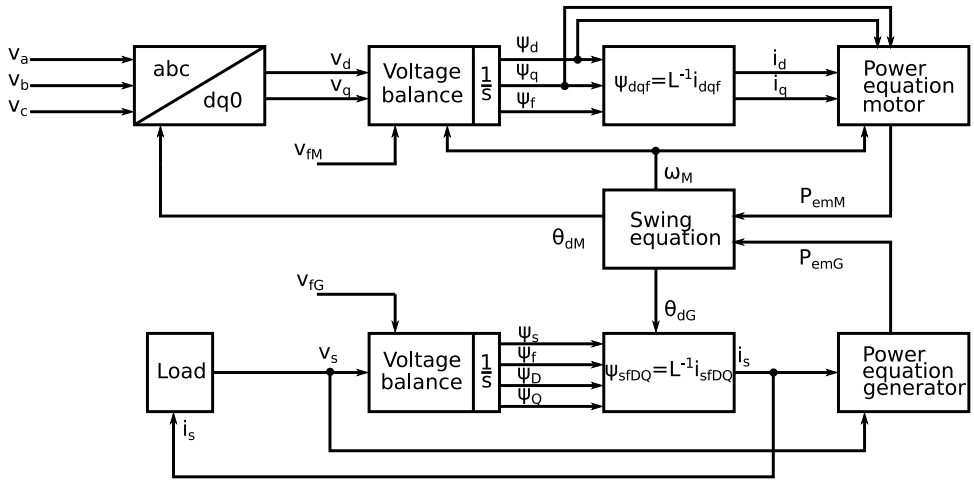

Figure 5.3: Rotary frequency converter with Model 1 of the single-phase machine implemented

Three phase-voltages are applied to the three-phase synchronous motor's terminals. Park transformation is carried out with respect to the motor's rotor angle, as presented in (3.15), and DC voltages are obtained. The DC voltages are applied for calculating the motor's flux linkages based on voltage balance, as presented in (3.19). The motor's currents are calculated by multiplying the flux linkages, in Fig. 5.3 presented as ψ_{dqf}, with the inverse motor's rotor angle invariant inductance matrix. The motor's electromagnetic power, P_{emM}, is obtained by applying (3.34). The motor power drives the generator, and electromagnetic power is induced. Based on the equation of motion provided for a motor-generator-set, presented in Section 5.4, the speed, and rotor angle for both the motor and generator are obtained. The motor speed is used for calculating electromagnetic motor power, while the motor's rotor angle is applied for transforming the three-phase motor quantities to DC quantities in a rotor reference frame. The generator rotor angle is used for calculating the elements of the inverse inductance matrix presented in (5.7). The terminal voltage of the single-phase machine is obtained by multiplying the single-phase current with a load.

5.2 MODEL 2: TWO ROTATING FIELDS

The following section presents a developed set of equations presenting the instantaneous time-domain related behavior of the single-phase synchronous machine viewing the pulsating armature MMF distribution behavior as two rotating MMF distributions. A pulsating MMF distribution is commonly viewed as two MMF distributions with constant amplitudes rotating at the same rotational velocity but in opposite directions. These MMF distributions are in this section referred to as the counterclockwise- and clockwise rotating MMF distributions. The theory behind the pulsating behavior of the armature MMF is presented in Chapter 4.

The following implementation of a developed set of equations attempts to apply the two-MMF distribution theory for simulating the single-phase synchronous machine's behavior. Each rotating MMF distribution is viewed as the result of three phase-currents flowing in the armature windings of a three-phase machine. By changing the order of two phase-windings for a three-phase machine, the MMF distribution will rotate in either counterclockwise- or clockwise direction. If the phase-a, phase-b and phase-c currents always flow in their respective phase windings, the MMF distribution of the machine will rotate in a counterclockwise direction. If phase winding b and -c changes position, the resulting MMF distribution will rotate in clockwise direction. The approach is presented in Fig. 5.4 as two stator configurations. The counterclockwise- and clockwise MMF distributions, $\mathscr{F}_s^{CCW}$ and $\mathscr{F}_s^{CW}$, are observed in the left- and rightmost machine stator in Fig. 5.4, respectively.

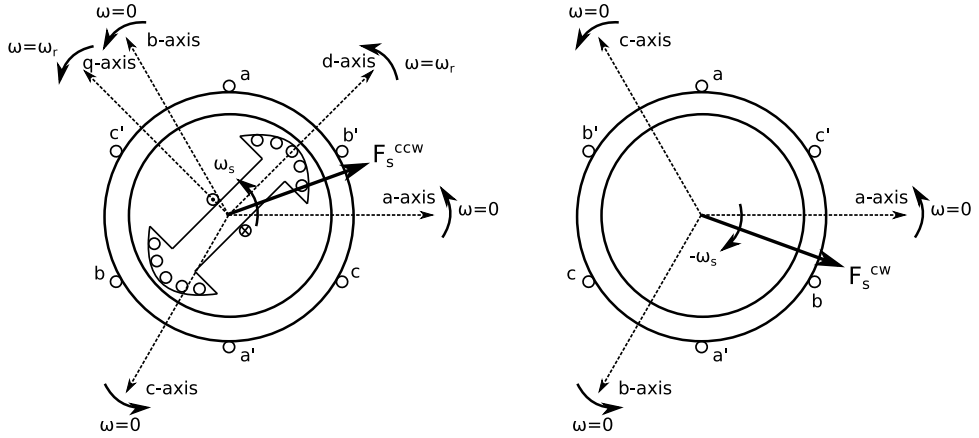

Figure 5.4: Two fictitious machines inducing two MMF distributions

The single-phase machine is therefore viewed as two fictitious three-phase synchronous machines with three armature phase-windings each, as presented in Fig. 5.4. Phase-a of both machines are connected in series, while phase-b and phase-c of the first machine are connected in series with phase-c and phase-b of the second machine, respectively. The rotor of the single-phase machine,

together with its d- and q-axis reference frame, is only depicted in the first fictitious three-phase machine. Depicting the pulsating armature MMF distribution's behavior is the reason for the two stator configurations. The two fictitious machines are "laid on top" of each other. Both machines are magnetically coupled to the rotor, but not with each other.

5.2.1 Counterclockwise Rotating MMF Distribution

The counterclockwise-rotating MMF distribution is locked to the rotor's MMF distribution. The armature counterclockwise- and rotor MMF distribution are therefore rotating at synchronism and behaving exactly like a regular three-phase synchronous machine.

The self- and mutual inductances for the armature phase-windings are presented in (5.11).

$$\boldsymbol{L_S^{CCW}} = \begin{bmatrix} L_{ss0} + L_{ssP}\cos(2\theta_d) & -\frac{L_{ss0}}{2} - L_{ssP}\cos(2(\theta_d + \frac{\pi}{6})) & -\frac{L_{ss0}}{2} - L_{ssP}\cos(2(\theta_d + \frac{5\pi}{6})) \\ -\frac{L_{ss0}}{2} - L_{ssP}\cos(2(\theta_d + \frac{\pi}{6})) & L_{ss0} + L_{ssP}\cos(2(\theta_d - \frac{2\pi}{3})) & -\frac{L_{ss0}}{2} - L_{ssP}\cos(2(\theta_d - \frac{\pi}{2})) \\ -\frac{L_{ss0}}{2} - L_{ssP}\cos(2(\theta_d + \frac{5\pi}{6})) & -\frac{L_{ss0}}{2} - L_{ssP}\cos(2(\theta_d - \frac{\pi}{2})) & L_{ss0} + L_{ssP}\cos(2(\theta_d - \frac{4\pi}{3})) \end{bmatrix} \tag{5.11}$$

The mutual inductances between the armature phase windings and the rotor windings are presented in (5.12).

$$\boldsymbol{L_{SR}^{CCW}} = \begin{bmatrix} L_{sfP}\cos(\theta_d) & L_{sDP}\cos(\theta_d) & -L_{sQP}\sin(\theta_d) \\ L_{sfP}\cos(\theta_d - \frac{2\pi}{3}) & L_{sDP}\cos(\theta_d - \frac{2\pi}{3}) & -L_{sQP}\sin(\theta_d - \frac{2\pi}{3}) \\ L_{sfP}\cos(\theta_d - \frac{4\pi}{3}) & L_{sDP}\cos(\theta_d - \frac{4\pi}{3}) & -L_{sQP}\sin(\theta_d - \frac{4\pi}{3}) \end{bmatrix} \tag{5.12}$$

5.2.2 Clockwise Rotating MMF Distribution

The clockwise rotating MMF distribution rotates in opposite direction of the single-phase machine's rotor. During steady-state the rotor is rotating at synchronous velocity and the clockwise rotating MMF distribution is rotating at double synchronous speed compared to the rotor.

The self- and mutual inductances for the armature phase-windings are presented in (5.13). It is observed that the location of the phase-b and phase-c inductances have been changed compared to those presented in (5.11), allowing the MMF distribution of the armature to rotate in the opposite direction compared to the rotor.

$$\boldsymbol{L_S^{CW}} = \begin{bmatrix} L_{ss0} + L_{ssP}\cos(2\theta_d) & -\frac{L_{ss0}}{2} - L_{ssP}\cos(2(\theta_d + \frac{5\pi}{6})) & -\frac{L_{ss0}}{2} - L_{ssP}\cos(2(\theta_d + \frac{\pi}{6})) \\ -\frac{L_{ss0}}{2} - L_{ssP}\cos(2(\theta_d + \frac{5\pi}{6})) & L_{ss0} + L_{ssP}\cos(2(\theta_d - \frac{4\pi}{3})) & -\frac{L_{ss0}}{2} - L_{ssP}\cos(2(\theta_d - \frac{\pi}{2})) \\ -\frac{L_{ss0}}{2} - L_{ssP}\cos(2(\theta_d + \frac{\pi}{6})) & -\frac{L_{ss0}}{2} - L_{ssP}\cos(2(\theta_d - \frac{\pi}{2})) & L_{ss0} + L_{ssP}\cos(2(\theta_d - \frac{4\pi}{3})) \end{bmatrix} \tag{5.13}$$

The mutual inductances between the armature phase windings and the rotor windings are presented in (5.14). The same change of phase-winding location is observed compared to (5.12).

$$\boldsymbol{L_{SR}^{CCW}} = \begin{bmatrix} L_{sfP}\cos(\theta) & L_{sDP}\cos(\theta) & L_{sQP}\sin(\theta) \\ L_{sfP}\cos(\theta - \frac{4\pi}{3}) & L_{sDP}\cos(\theta - \frac{4\pi}{3}) & L_{sQP}\sin(\theta - \frac{4\pi}{3}) \\ L_{sfP}\cos(\theta - \frac{2\pi}{3}) & L_{sDP}\cos(\theta - \frac{2\pi}{3}) & L_{sQP}\sin(\theta - \frac{2\pi}{3}) \end{bmatrix} \tag{5.14}$$

5.2.3 Two Reference Frames

The method of transforming the quantities of the stationary three-phase armature windings to the rotor frame of reference was presented in Chapter 3 for a three-phase synchronous machine. The method is identical when dealing with the two fictitious machines with different configurations. Park's matrix was presented in (3.15) and is for simplicity renamed and rewritten in (5.15).

$$\boldsymbol{P^{CCW}} = \frac{2}{3}\begin{bmatrix} \cos(\theta) & \cos(\theta - \frac{2\pi}{3}) & \cos(\theta - \frac{4\pi}{3}) \\ -\sin(\theta) & -\sin(\theta - \frac{2\pi}{3}) & -\sin(\theta - \frac{4\pi}{3}) \\ \frac{1}{2} & \frac{1}{2} & \frac{1}{2} \end{bmatrix} \tag{5.15}$$

For the counterclockwise rotating MMF distribution induced by the currents from the first fictitious machine, the three-phase quantities for the armature are transformed by appreciating the relationships presented in (3.17) and (3.18).

The resulting inductance matrices for the counterclockwise fictitious machine after when referenced to the rotor is presented in (5.16) and (5.17).

$$\begin{aligned}\boldsymbol{P^{CCW}L_S^{CCW}(P^{CCW})^{-1}} &= \begin{bmatrix} L_{ls}+\frac{3}{2}(L_{ss0}+L_{ssP}) & 0 & 0 \\ 0 & L_{ls}+\frac{3}{2}(L_{ss0}-L_{ssP}) & 0 \\ 0 & 0 & L_{ls}+L_{ss0}-2L_{ssP} \end{bmatrix} \\ &= \begin{bmatrix} L_d^{CCW} & 0 & 0 \\ 0 & L_q^{CCW} & 0 \\ 0 & 0 & L_0^{CCW} \end{bmatrix}\end{aligned} \tag{5.16}$$

$$\boldsymbol{P^{CCW}L_{SR}^{CCW}} = \begin{bmatrix} L_{sfP} & L_{sDP} & 0 \\ 0 & 0 & L_{sQP} \\ 0 & 0 & 0 \end{bmatrix} \tag{5.17}$$

For the clockwise rotating MMF distribution induced by the currents from the second fictitious machine, the three-phase quantities can be transformed to an orthogonal reference frame identical to the rotor's reference, but rotating in a clockwise direction. The Park's matrix in (5.15) is reformulated for a clockwise rotating reference frame and presented in (5.18).

$$\boldsymbol{P^{CW}} = \frac{2}{3}\begin{bmatrix} \cos(\theta) & \cos(\theta-\frac{4\pi}{3}) & \cos(\theta-\frac{2\pi}{3}) \\ -\sin(\theta) & -\sin(\theta-\frac{4\pi}{3}) & -\sin(\theta-\frac{2\pi}{3}) \\ \frac{1}{2} & \frac{1}{2} & \frac{1}{2} \end{bmatrix} \tag{5.18}$$

The resulting inductance matrices for the clockwise fictitious machine after referenced to the clockwise rotating reference is presented in (5.19) and (5.20).

$$\begin{aligned}\boldsymbol{P^{CW}L_S^{CW}(P^{CW})^{-1}} &= \begin{bmatrix} L_{ls}+\frac{3}{2}(L_{ss0}+L_{ssP}) & 0 & 0 \\ 0 & L_{ls}+\frac{3}{2}(L_{ss0}-L_{ssP}) & 0 \\ 0 & 0 & L_{ls}+L_{ss0}-2L_{ssP} \end{bmatrix} \\ &= \begin{bmatrix} L_d^{CCW} & 0 & 0 \\ 0 & L_q^{CCW} & 0 \\ 0 & 0 & L_0^{CCW} \end{bmatrix}\end{aligned} \tag{5.19}$$

$$\boldsymbol{P^{CW}L_{SR}^{CW}} = \begin{bmatrix} L_{sfP} & L_{sDP} & 0 \\ 0 & 0 & L_{sQP} \\ 0 & 0 & 0 \end{bmatrix} \tag{5.20}$$

The two reference frames are presented in Fig. 5.5.

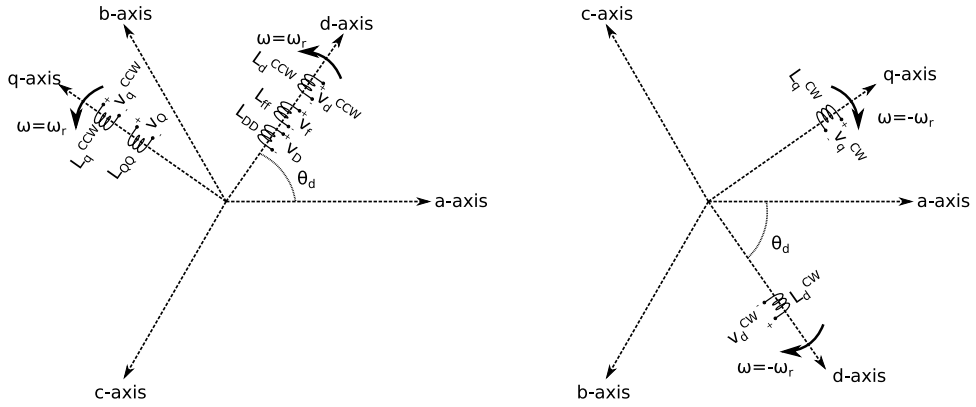

Figure 5.5: Counterclockwise- and clockwise rotating reference frame with their stationary magnetic axes

Self-inductance of the d- and q-axis for the armature windings are observed. Also, there will be mutual inductances between the armature windings of each axis and the field and damper bars on the respective axis.

5.2.4 One Reference Frame

For a three-phase synchronous machine, the transformation from a three-phase stationary reference frame and a two-phase rotating reference frame to a rotating two-phase reference frame is carried out for several reasons. One of the major reasons is the fact that the inductance matrices, and therefore also the voltage balance equations and the currents from flux linkages equations, becomes rotor angle invariant. Hence, the differential equations become less complicated to solve.

For the single-phase machine, viewed as two fictitious machines, the same situation as that of the three-phase machine is observed. It is easier to deal with the machines equations if both machines are referenced to the same reference frame. Since the rotor is rotating in a counterclockwise direction, it is useful to reference both fictitious machines to a counterclockwise rotating rotor $d-q$-reference frame. For the two machines, this is carried out by applying the Park's matrix that was presented for the first fictitious machine in (5.15). The transformation is carried out for both machines. The inductances for the counterclockwise machine is here rewritten for clarity, together with the transformed inductance matrices for the clockwise rotating machine.

$$
\begin{aligned}
(\boldsymbol{P^{CCW}})\boldsymbol{L_S^{CCW}}(\boldsymbol{P^{CCW}})^{-1} &= \begin{bmatrix} L_{ls} + \frac{3}{2}(L_{ss0} + L_{ssP}) & 0 & 0 \\ 0 & L_{ls} + \frac{3}{2}(L_{ss0} - L_{ssP}) & 0 \\ 0 & 0 & L_{ls} + L_{ss0} - 2L_{ssP} \end{bmatrix} \\
&= \begin{bmatrix} L_d^{CCW} & 0 & 0 \\ 0 & L_q^{CCW} & 0 \\ 0 & 0 & L_0^{CCW} \end{bmatrix}
\end{aligned} \tag{5.21}
$$

$$
\boldsymbol{P^{CCW}}\boldsymbol{L_{SR}^{CCW}} = \begin{bmatrix} L_{sfP} & L_{sDP} & 0 \\ 0 & 0 & L_{sQP} \\ 0 & 0 & 0 \end{bmatrix} \tag{5.22}
$$

$$
\begin{aligned}
(\boldsymbol{P^{CCW}})\boldsymbol{L_S^{CW}}(\boldsymbol{P^{CCW}})^{-1} &= \begin{bmatrix} L_{ls} + \frac{3}{2}(L_{ss0} + L_{ssP}\cos(4\theta_d)) & -\frac{3}{2}L_{ssP}\sin(4\theta_d) & 0 \\ -\frac{3}{2}L_{ssP}\sin(4\theta_d) & L_{ls} + \frac{3}{2}(L_{ss0} - L_{ssP}\cos(4\theta_d)) & 0 \\ 0 & 0 & L_{ls} \end{bmatrix} \\
&= \begin{bmatrix} L_d^{CW} & L_{dq}^{CW} & 0 \\ L_{dq}^{CW} & L_q^{CW} & 0 \\ 0 & 0 & L_0^{CW} \end{bmatrix}
\end{aligned} \tag{5.23}
$$

$$
\boldsymbol{P^{CW}}\boldsymbol{L_{SR}^{CW}} = \begin{bmatrix} L_{sfP}\cos(2\theta_d) & L_{sDP}\cos(2\theta_d) & -L_{sQP}\sin(2\theta_d) \\ -L_{sfP}\sin(2\theta_d) & -L_{sDP}\sin(2\theta_d) & -L_{sQP}\cos(2\theta_d) \\ 0 & 0 & 0 \end{bmatrix} \tag{5.24}
$$

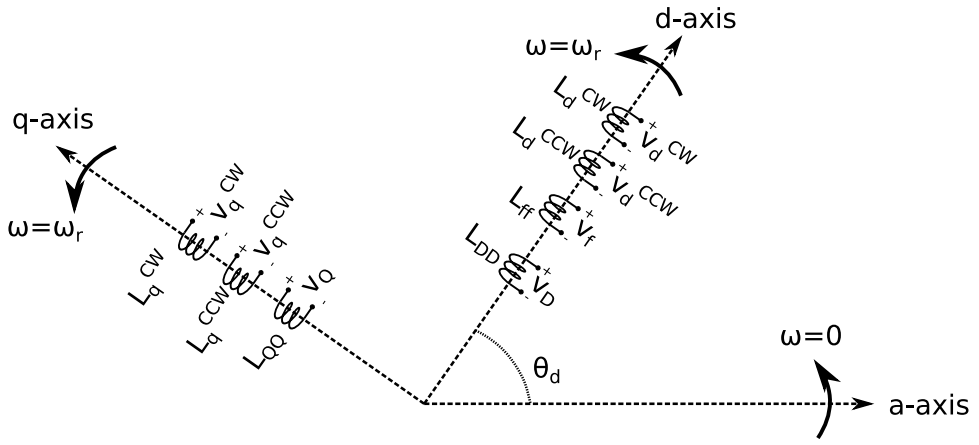

Figure 5.6: Counterclockwise rotating reference frame

5.2.5 Amplitude Size of MMF Distributions

The counterclockwise- and clockwise rotating MMF distributions combined enables the behavior of the pulsating MMF distribution to be observed. The trigonometric relation in which the theory of two rotating MMFs combined results in a pulsating MMF presented in (3.3). The MMF distribution of a single phase-winding are presented in (3.4), and is rewritten in (5.25).

$$\mathscr{F}_{S(1)} = \underbrace{\frac{1}{2}\mathscr{F}_{max}\cos(\alpha - \omega_e t)}_{\mathscr{F}_{S(1)}^{CCW}} + \underbrace{\frac{1}{2}\mathscr{F}_{max}\cos(\alpha + \omega_e t)}_{\mathscr{F}_{S(1)}^{CW}} \tag{5.25}$$

The amplitude of the MMF distribution from (5.25) is presented in (3.1), and is rewritten in (5.26).

$$\mathscr{F}_{max} = \frac{4}{\pi}\left(\frac{k_w N_S}{P}\right) I_S \tag{5.26}$$

The single-phase synchronous motor modeling method presented above applies two three-phase synchronous machines, each with a rotating MMF distribution, to simulate the pulsating MMF distribution occurring in the single phase-winding. The rotating MMF distribution from each machine has an amplitude of $\frac{3}{2}\mathscr{F}_{max}$, where $\mathscr{F}_{max}$ equals the peak MMF distribution of a single phase-winding. Adjustments are therefore necessary for enabling the two fictitious machines to together result in a pulsating MMF distribution with the correct peak value. The relationship between MMF distribution amplitudes for counterclockwise- and clockwise fictitious machines, three-phase "regular" machines and single phase-winding are presented in (5.27).

$$\mathscr{F}_{S(1)}^{CCW} = \mathscr{F}_{S(1)}^{CW} = \frac{1}{2}\mathscr{F}_{max} = \frac{1}{2}\frac{2}{3}\mathscr{F}_{3ph} = \frac{1}{3}\mathscr{F}_{3ph} \tag{5.27}$$

The number of turns for each armature winding in the two fictitious machines are therefore decreased by a factor of 3, enabling the two machines to induce a MMF distribution that in total results in a pulsating MMF distribution with a peak value equal to $\mathscr{F}_{max}$.

$$N_S^{CCW} = N_S^{CW} = \frac{1}{3}N_{S(3ph)} \tag{5.28}$$

Self- and mutual inductances for armature windings are the ratio between flux linkages and currents involved. These inductances are proportional to the product of the involved windings' number of turns. The self-inductance of a winding and the mutual inductance between two armature windings are therefore proportional to the square of the respective winding's number of turns. For the MMF distribution relationship presented in (5.27), the number of turns for the involved armature windings are as presented in (5.28). The stator inductance matrices $\boldsymbol{L_S^{CCW}}$ and $\boldsymbol{L_S^{CW}}$ presented in (5.16) and (5.19) are therefore decreased with a factor of $k_S = 3^2 = 9$.

$$\begin{aligned} \boldsymbol{L_{S(new)}^{CW}} &= \frac{1}{9}\boldsymbol{L_S^{CW}} \\ \boldsymbol{L_{S(new)}^{CCW}} &= \frac{1}{9}\boldsymbol{L_S^{CCW}} \end{aligned} \tag{5.29}$$

The mutual inductances between the stator and rotor windings are also proportional to the involved winding's number of turns. The rotor windings are not changed in any way when simulating the pulsating MMF distribution applying two fictitious machines. The mutual stator to rotor inductances matrices, $\boldsymbol{L_{SR}^{CCW}}$ and $\boldsymbol{L_{SR}^{CW}}$ presented in (5.17) and (5.20) are therefore decreased with a factor of $K_{SR} = 3$.

$$\begin{aligned} \boldsymbol{L_{SR(new)}^{CW}} &= \frac{1}{3}\boldsymbol{L_{SR}^{CW}} \\ \boldsymbol{L_{SR(new)}^{CCW}} &= \frac{1}{3}\boldsymbol{L_{SR}^{CCW}} \end{aligned} \tag{5.30}$$

5.2.6 Model Equations

5.2.6.1 Voltage Equations

The armature voltage balance equations for a three-phase synchronous machine with phase quantities are presented in (3.13) of Chapter 3. These equations are referenced to rotor by applying Park's matrix presented in (3.19). The calculations are presented in Appendix A. The same procedure is carried out for the two fictitious armature configurations presented above inducing the counterclockwise and clockwise rotating MMF distribution. The voltage balances for the counterclockwise rotating and clockwise rotating fictitious machines are presented in (5.31) and (5.32). The voltage balances for the rotor armature circuits are repeated in (5.33).

$$v_d^{CCW} = -R_s i_d^{CCW} + \frac{d}{dt}\psi_d^{CCW} - \omega_r \psi_q^{CCW} \tag{5.31a}$$

$$v_q^{CCW} = -R_s i_q^{CCW} + \frac{d}{dt}\psi_d^{CCW} + \omega_r \psi_d^{CCW} \tag{5.31b}$$

$$v_d^{CW} = -R_s i_d^{CW} + \frac{d}{dt}\psi_d^{CW} - \omega_r \psi_q^{CW} \tag{5.32a}$$

$$v_q^{CW} = -R_s i_q^{CW} + \frac{d}{dt}\psi_d^{CW} + \omega_r \psi_d^{CW} \tag{5.32b}$$

$$v_f = R_f i_f + \frac{d}{dt}\psi_f \tag{5.33a}$$

$$0 = R_D i_D + \frac{d}{dt}\psi_D \tag{5.33b}$$

$$0 = R_Q i_Q + \frac{d}{dt}\psi_Q \tag{5.33c}$$

5.2.6.2 Flux Linkages

The flux linkages applied for expressing the voltage balance for both fictitious machines in (5.31) and (5.32) are defined in (5.34) and (5.35). The flux linkages for the counterclockwise rotating machine are identical to the regular three-phase synchronous machine's. For the clockwise rotating machine,

it exists mutual magnetic coupling between the d- and q-axis. Chapter 3 presents these axes to be decoupled because they are located 90 electrical degrees apart. For the clockwise rotating machine, which induces a MMF distribution rotating at double rotor speed relative to the rotor, this decoupling doesn't occur.

$$\begin{bmatrix} \psi_d^{CCW} \\ \psi_q^{CCW} \\ \psi_0^{CCW} \end{bmatrix} = -\underbrace{\frac{1}{k_S}\begin{bmatrix} L_d^{CCW} & 0 & 0 \\ 0 & L_q^{CCW} & 0 \\ 0 & 0 & L_0^{CCW} \end{bmatrix}}_{\boldsymbol{L_{s,dq}^{CCW}}} \begin{bmatrix} i_d^{CCW} \\ i_q^{CCW} \\ i_0^{CCW} \end{bmatrix} + \underbrace{\frac{1}{k_{SR}}\begin{bmatrix} L_{sfP} & L_{sDP} & 0 \\ 0 & 0 & L_{sQP} \\ 0 & 0 & 0 \end{bmatrix}}_{\boldsymbol{L_{SR,dq}^{CCW}}} \begin{bmatrix} i_f \\ i_D \\ i_Q \end{bmatrix} \tag{5.34}$$

$$\begin{aligned} \begin{bmatrix} \psi_d^{CW} \\ \psi_q^{CW} \\ \psi_0^{CW} \end{bmatrix} = &-\underbrace{\frac{1}{k_S}\begin{bmatrix} L_{ls} + \frac{3}{2}(L_{ss0} + L_{ssP}\cos(4\theta_d)) & -\frac{3}{2}L_{ssP}\sin(4\theta_d) & 0 \\ -\frac{3}{2}L_{ssP}\sin(4\theta_d) & L_{ls} + \frac{3}{2}(L_{ss0} - L_{ssP}\cos(4\theta_d)) & 0 \\ 0 & 0 & L_{ls} \end{bmatrix}}_{\boldsymbol{L_{S,dq}^{CW}}} \begin{bmatrix} i_d^{CW} \\ i_q^{CW} \\ i_0^{CW} \end{bmatrix} \\ &+ \underbrace{\frac{1}{k_{SR}}\begin{bmatrix} L_{sfP}\cos(2\theta_d) & L_{sDP}\cos(2\theta_d) & -L_{sQP}\sin(2\theta_d) \\ -L_{sfP}\sin(2\theta_d) & -L_{sDP}\sin(2\theta_d) & -L_{sQP}\cos(2\theta_d) \\ 0 & 0 & 0 \end{bmatrix}}_{\boldsymbol{L_{SR}^{CW}}} \begin{bmatrix} i_f \\ i_D \\ i_Q \end{bmatrix} \end{aligned} \tag{5.35}$$

The flux linkages related to the rotor circuits are assumed to be the result of magnetic coupling between the armature of both fictitious machines and the rotor circuits. The result is presented in (5.36).

$$\begin{aligned} \begin{bmatrix} \psi_f \\ \psi_D \\ \psi_Q \end{bmatrix} = &-\underbrace{\frac{1}{k_{SR}}\frac{3}{2}\begin{bmatrix} L_{sfP} & 0 & 0 \\ L_{sDP} & 0 & 0 \\ 0 & L_{sQP} & 0 \end{bmatrix}}_{(\boldsymbol{L_{SR,dq}^{CCW}})^T} \begin{bmatrix} i_d^{CCW} \\ i_q^{CCW} \\ i_0^{CCW} \end{bmatrix} - \underbrace{\frac{1}{k_{SR}}\frac{3}{2}\begin{bmatrix} L_{sfP}\cos(2\theta_d) & -L_{sfP}\sin(2\theta_d) & 0 \\ L_{sDP}\cos(2\theta_d) & -L_{sDP}\sin(2\theta_d) & 0 \\ -L_{sQP}\sin(2\theta_d) & -L_{sQP}\cos(2\theta_d) & 0 \end{bmatrix}}_{(\boldsymbol{L_{SR,dq}^{CW}})^T} \begin{bmatrix} i_d^{CW} \\ i_q^{CW} \\ i_0^{CW} \end{bmatrix} \\ &+ \underbrace{\begin{bmatrix} L_{ff} & L_{fD} & 0 \\ L_{fD} & L_{DD} & 0 \\ 0 & 0 & L_{QQ} \end{bmatrix}}_{\boldsymbol{L_R}} \begin{bmatrix} i_f \\ i_D \\ i_Q \end{bmatrix} \end{aligned} \tag{5.36}$$

By applying the same base system when comparing stator and rotor quantities as presented in Chapter 3, the equations for flux linkages are rewritten and presented in (5.37).

$$\begin{bmatrix} \psi_d^{CCW} \\ \psi_q^{CCW} \\ \psi_0^{CCW} \\ \psi_d^{CW} \\ \psi_q^{CW} \\ \psi_0^{CW} \\ \psi_f \\ \psi_D \\ \psi_Q \end{bmatrix} = \underbrace{\begin{bmatrix} \boldsymbol{L_{S,dq}^{CCW}} & \boldsymbol{0} & \boldsymbol{L_{SR,dq}^{CCW}} \\ \boldsymbol{0} & \boldsymbol{L_{S,dq}^{CW}} & \boldsymbol{L_{SR,dq}^{CW}} \\ \boldsymbol{(L_{SR,dq}^{CCW})^T} & \boldsymbol{(L_{SR,dq}^{CW})^T} & \boldsymbol{L_R} \end{bmatrix}}_{\boldsymbol{L_{dq}}} \begin{bmatrix} i_d^{CCW} \\ i_q^{CCW} \\ i_0^{CCW} \\ i_d^{CW} \\ i_q^{CW} \\ i_0^{CW} \\ i_f \\ i_D \\ i_Q \end{bmatrix} \tag{5.37}$$

The inductance matrices in $\boldsymbol{L_{dq}}$, observed in (5.37), are presented in Appendix F.

5.2.6.3 Current Equations

The currents of the two fictitious machine systems are extracted by calculating the inverse inductance matrix of the system, $\boldsymbol{L_{dq}^{-1}}$. $\boldsymbol{L_{dq}^{-1}}$ is a singular matrix, and the inverse matrix cannot be calculated. The complete inductance matrix is therefore divided into two inductance matrices with $6x6$ elements each. These matrices inversed are presented in (5.38) and (5.39).

$$\begin{bmatrix} i_d^{CCW} \\ i_q^{CCW} \\ i_0^{CCW} \\ i_f^{CCW} \\ i_D^{CCW} \\ i_Q^{CCW} \end{bmatrix} = \underbrace{\begin{bmatrix} \boldsymbol{L_{S,dq}^{CCW}} & \boldsymbol{L_{SR,dq}^{CCW}} \\ \boldsymbol{(L_{SR,dq}^{CCW})^T} & \boldsymbol{L_R} \end{bmatrix}^{-1}}_{\boldsymbol{(L_{dq}^{CCW})^{-1}}} \begin{bmatrix} \psi_d^{CCW} \\ \psi_q^{CCW} \\ \psi_0^{CCW} \\ \psi_f \\ \psi_D \\ \psi_Q \end{bmatrix} \tag{5.38}$$

$$\begin{bmatrix} i_d^{CW} \\ i_q^{CW} \\ i_0^{CW} \\ i_f^{CW} \\ i_D^{CW} \\ i_Q^{CW} \end{bmatrix} = \underbrace{\begin{bmatrix} \boldsymbol{L_{S,dq}^{CW}} & \boldsymbol{L_{SR,dq}^{CW}} \\ \boldsymbol{(L_{SR,dq}^{CW})^T} & \boldsymbol{L_R} \end{bmatrix}^{-1}}_{\boldsymbol{(L_{dq}^{CW})^{-1}}} \begin{bmatrix} \psi_d^{CW} \\ \psi_q^{CW} \\ \psi_0^{CW} \\ \psi_f \\ \psi_D \\ \psi_Q \end{bmatrix} \tag{5.39}$$

The elements of $(\boldsymbol{L_{dq}^{CCW}})^{-1}$ and $(\boldsymbol{L_{dq}^{CW}})^{-1}$ are presented in Appendix G. It is here observed that $(\boldsymbol{L_{dq}^{CCW}})^{-1}$ contains only rotor angle invariant elements, while $(\boldsymbol{L_{dq}^{CW}})^{-1}$ contains several elements which varies in accordance with the position of the rotor.

It is noted that the rotor currents i_f, i_D and i_Q are derived by calculating (5.37). The calculations presented in (5.38) and (5.39) do not calculate the rotor currents directly, because both MMF distributions, counterclockwise- and clockwise rotating, interact with the rotor circuits. The rotor currents extracted by these equations are therefore the currents to the counterclockwise- and clockwise rotating MMF distribution, respectively. The rotor currents are obtained by appreciating the relationship between the rotor flux linkages, the armature currents from each fictitious machine and the rotor currents as presented in (5.36). The systems rotor currents are extracted by solving (5.36) with respect to the rotor currents. The result is presented in (5.40).

$$\begin{aligned}\begin{bmatrix} i_f \\ i_D \\ i_Q \end{bmatrix} = &\underbrace{\begin{bmatrix} L_{ff} & L_{fD} & 0 \\ L_{fD} & L_{DD} & 0 \\ 0 & 0 & L_{QQ} \end{bmatrix}^{-1}}_{\boldsymbol{L_R^{-1}}} \begin{bmatrix} \psi_f \\ \psi_D \\ \psi_Q \end{bmatrix} + \underbrace{\begin{bmatrix} L_{ff} & L_{fD} & 0 \\ L_{fD} & L_{DD} & 0 \\ 0 & 0 & L_{QQ} \end{bmatrix}^{-1}}_{\boldsymbol{L_R^{-1}}} \underbrace{\frac{1}{k_{SR}} \frac{3}{2} \begin{bmatrix} L_{sfP} & 0 & 0 \\ L_{sDP} & 0 & 0 \\ 0 & L_{sQP} & 0 \end{bmatrix}}_{(\boldsymbol{L_{SR,dq}^{CCW}})^T} \begin{bmatrix} i_d^{CCW} \\ i_q^{CCW} \\ i_0^{CCW} \end{bmatrix} \\ &+ \underbrace{\begin{bmatrix} L_{ff} & L_{fD} & 0 \\ L_{fD} & L_{DD} & 0 \\ 0 & 0 & L_{QQ} \end{bmatrix}^{-1}}_{\boldsymbol{L_R^{-1}}} \underbrace{\frac{1}{k_{SR}} \frac{3}{2} \begin{bmatrix} L_{sfP}\cos(2\theta_d) & -L_{sfP}\sin(2\theta_d) & 0 \\ L_{sDP}\cos(2\theta_d) & -L_{sDP}\sin(2\theta_d) & 0 \\ -L_{sQP}\sin(2\theta_d) & -L_{sQP}\cos(2\theta_d) & 0 \end{bmatrix}}_{(\boldsymbol{L_{SR,dq}^{CW}})^T} \begin{bmatrix} i_d^{CW} \\ i_q^{CW} \\ i_0^{CW} \end{bmatrix}\end{aligned} \tag{5.40}$$

5.2.6.4 Electromagnetic Power

The terminal power induced by a three-phase synchronous machine is presented in (3.32) and rewritten with respect to rotor referenced quantities in (3.33). The same procedure is carried out when obtaining an expression for the power output of the single-phase synchronous machine modeled with two rotating MMF distributions. The terminal power in rotor referenced quantities are presented in (5.41).

$$P_t = \frac{3}{2}(\underbrace{(i_d^{CCW}\frac{d}{dt}\psi_d^{CCW} + i_q^{CCW}\frac{d}{dt}\psi_q^{CCW} + 2i_0^{CCW}\frac{d}{dt}\psi_0^{CCW})}_{\textbf{Armature magnetic power for CCW MMF}} + \underbrace{\frac{2}{P}\omega_r(\psi_d^{CCW}i_q^{CCW} - \psi_q^{CCW}i_d^{CCW})}_{\textbf{Air-gap power for CCW MMF}} -$$
$$\underbrace{((i_d^{CCW})^2 + (i_q^{CCW})^2 + 2(i_0^{CCW})^2)R_s)}_{\textbf{Ohmic losses for CCW MMF}} +$$
$$\frac{3}{2}(\underbrace{(i_d^{CW}\frac{d}{dt}\psi_d^{CW} + i_q^{CW}\frac{d}{dt}\psi_q^{CW} + 2i_0^{CW}\frac{d}{dt}\psi_0^{CW})}_{\textbf{Armature magnetic power for CW MMF}} + \underbrace{\frac{2}{P}\omega_r(\psi_d^{CW}i_q^{CW} - \psi_q^{CW}i_d^{CW})}_{\textbf{Air-gap power for CW MMF}} -$$
$$\underbrace{((i_d^{CW})^2 + (i_q^{CW})^2 + 2(i_0^{CW})^2)R_s)}_{\textbf{Ohmic losses for CW MMF}} \tag{5.41}$$

Steady-state machine performance is assumed, and the electromagnetic power is defined as the air-gap power induced by the machine. Ohmic losses are therefore neglected, and the electromagnetic power is determined as presented in (5.42).

$$P_{em} = \frac{3}{2}\frac{2}{P}\omega_r(\psi_d^{CCW}i_q^{CCW} - \psi_q^{CCW}i_d^{CCW} + \psi_d^{CW}i_q^{CW} - \psi_q^{CW}i_d^{CW}) \tag{5.42}$$

5.2.7 Model 2 - Overview

A simplified overview of an implemented rotary frequency converter model is viewed in Fig. (5.7). The three-phase synchronous motor is applying the Park equations for a three-phase machine, while the single-phase synchronous machine applies the single-phase machine equations developed for two rotating armature MMF distributions.

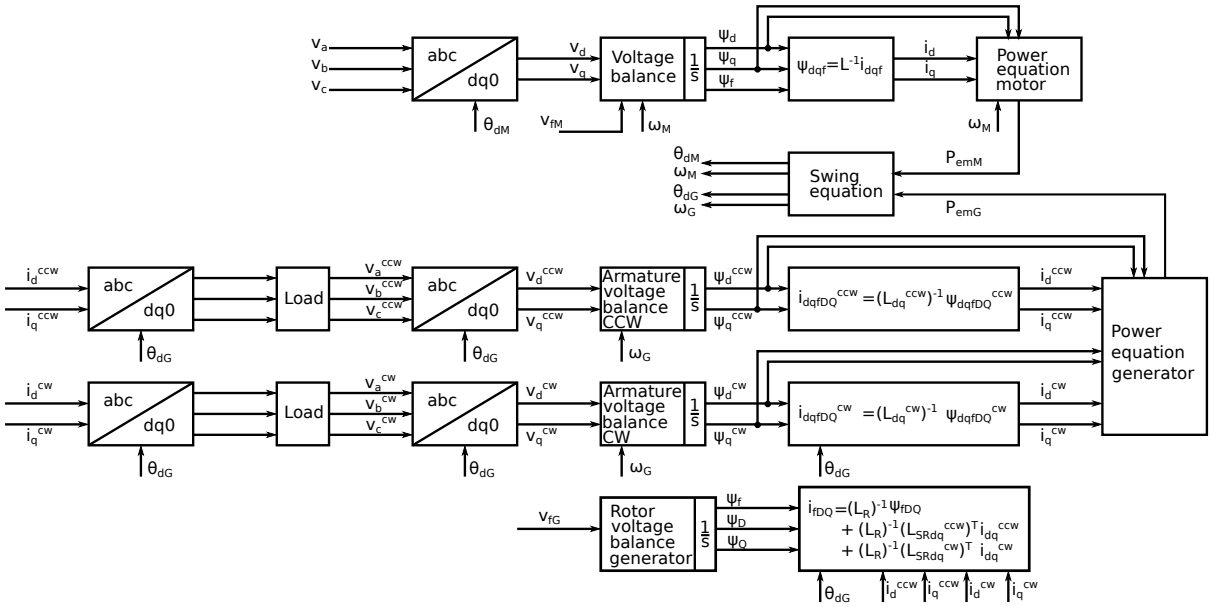

Figure 5.7: Rotary frequency converter with Model 2 of the single-phase synchronous machine implemented

The three-phase synchronous motor is identical to the one presented in Section 5.1 when observing the converter applying the Model 1 implementation of the single-phase synchronous generator in Fig. 5.3. The motor drives the generator, and electromagnetic power is induced. The dynamic interaction between the two machines, presented in Section 5.4, is applied for extracting the motor- and generator rotor speed, ω_M and ω_G, and rotor angle, θ_{dM} and θ_{dG}. The generator's rotor angle is applied to calculate the elements of the inverse clockwise inductance matrix, and to carry out the desired transformations of both armature currents and -voltages. The counterclockwise- and clockwise obtained flux linkages and currents for the single-phase machine are applied to calculate the electromagnetic power presented in (5.42). The generator's terminal voltages are calculated based on the connected load and the armature currents for each fictitious machine.

5.3 MODEL 3: THREE-PHASE MACHINE WITH ONE OPEN-CIRCUITED PHASE

The following section is based on single-phase synchronous machine modeling principles mentioned in [9], [10] and [12], and presented in detail in [7], [8] and [11]. The modeling method was applied with minor changes in [6] when a full rotary frequency converter where simulated. The following presentation of this method applies the equations obtained during work presented in [6].

A three-phase synchronous machine with three-phase currents flowing in their respective armature phase-windings induces a rotating armature MMF distribution. If one of these windings were to be open-circuited, no current would flow in that exact winding. If a load is connected between the two remaining phases, the two windings will induce one pulsating MMF distribution each. The windings are located 120 degrees apart in space, and the total MMF distribution of the three-phase machine is therefore pulsating. The following modeling method presents a system where machine parameters for a single-phase synchronous machine are adjusted so that a three-phase synchronous machine with one phase left idle and a load connected between the remaining two phases models the dynamic behavior of a single-phase machine. The idea is illustrated in Fig. 5.8.

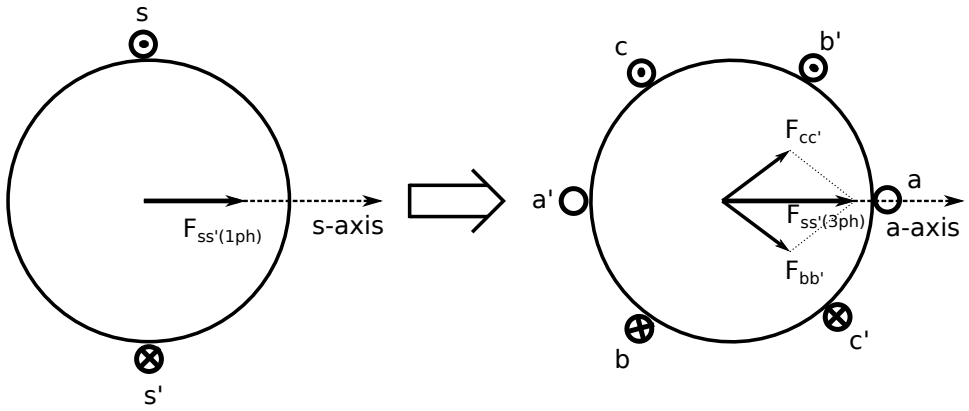

Figure 5.8: Single-phase machine viewed as three-phase machine with phase-a left idle[1]

The leftmost machine in Fig. 5.8 illustrates a conventional single-phase machine with one armature phase-winding. The MMF distribution $\mathscr{F}_{ss'(1ph)}$ is pulsating along the phase's magnetic s-axis. The rightmost machine presents the same situation, but the two armature windings now induce the pulsating MMF distribution $\mathscr{F}_{ss'(3ph)}$. For the following presentation, the conventional single-phase machine and the three-phased single-phase machine will be labeled (1) and (3), respectively.

[1] Based on [7]

5.3.1 The Equivalent Single-Phase Machine

The three-phased single-phase machine is from now on referred to as the equivalent single-phase machine. The armature windings of the equivalent machine are presented in Fig. 5.9. As observed, two phases are connected through a load. The windings share a common load current, referred to as i_s.

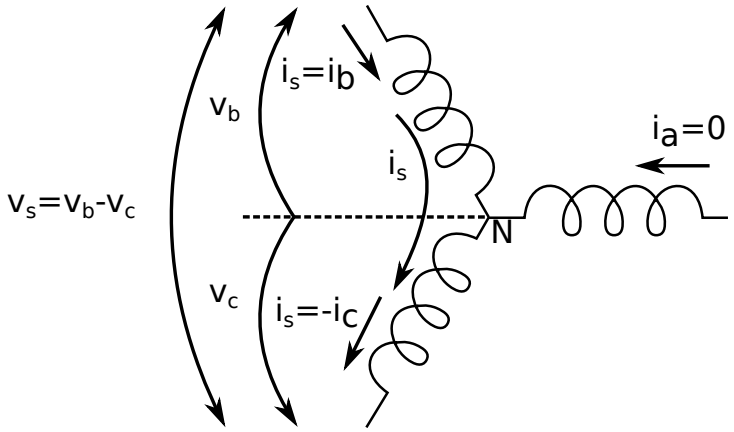

Figure 5.9: Unbalanced three-phase machine[2]

The three-phase currents for the equivalent single-phase machine are presented in (5.43). The load currents for phase-b and phase-c are shared, while the load current for phase-a is zero.

$$i_a = 0 \quad , \quad i_b = i_s \quad , \quad i_c = -i_s \tag{5.43}$$

The terminal voltage for the equivalent single-phase machine is referred to as v_s and is defined as the difference between the original voltages for phase-a and phase-b. The terminal voltage is presented in (5.44).

$$v_s = v_b - v_c \tag{5.44}$$

5.3.2 Model Equations

The following calculations present the model equations for the equivalent single-phase machine. The motivation for deriving these equations is to describe the instantaneous time-domain related

[2]Based on [7]

behavior of the single-phase synchronous machine by applying the model equations of the three-phase machine as presented in Chapter 3.

5.3.2.1 Rotor Referenced Equivalent Single-Phase Machine Currents

The armature- and rotor quantities of the equivalent single-phase machine are referenced to a stationary- and a rotating frame, respectively. It is preferred to transform all quantities to a rotor reference frame, as carried out for the three-phase synchronous machine in Chapter 3. The equivalent single-phase currents were presented in (5.43). The three-phase currents are described by applying the single-phase current i_s, and these currents are referenced to the rotor by applying (3.17). The resulting rotor referenced currents are presented in (5.45).

$$\begin{aligned}\begin{bmatrix} i_{d(3)} \\ i_{q(3)} \\ i_{0(3)} \end{bmatrix} &= \frac{2}{3}\begin{bmatrix} \cos(\theta_d) & \cos(\theta_d - \frac{2\pi}{3}) & \cos(\theta_d - \frac{4\pi}{3}) \\ -\sin(\theta_d) & -\sin(\theta_d - \frac{2\pi}{3}) & -\sin(\theta_d - \frac{4\pi}{3}) \\ \frac{1}{2} & \frac{1}{2} & \frac{1}{2} \end{bmatrix}\begin{bmatrix} i_a = 0 \\ i_b = i_s \\ i_c = -i_s \end{bmatrix} \\ &= \frac{2}{3} i_s \begin{bmatrix} \cos(\theta_d - \frac{2\pi}{3}) - \cos(\theta_d - \frac{4\pi}{3}) \\ -\sin(\theta_d - \frac{2\pi}{3}) + \sin(\theta_d - \frac{4\pi}{3}) \\ 0 \end{bmatrix}\end{aligned} \tag{5.45}$$

The d- and q-axis currents are rewritten by applying the Simpson´s theorem presented in (5.46).

$$\sin(\alpha \pm \beta) = \sin(\alpha)\cos(\beta) \pm \cos(\alpha)\sin(\beta) \tag{5.46a}$$

$$\cos(\alpha \pm \beta) = \cos(\alpha)\cos(\beta) \mp \sin(\alpha)\sin(\beta) \tag{5.46b}$$

The d- and q-axis currents for the equivalent single-phase machine are presented in (5.47).

$$\begin{bmatrix} i_{d(3)} \\ i_{q(3)} \\ i_{0(3)} \end{bmatrix} = \begin{bmatrix} \frac{2}{\sqrt{3}} i_s \sin(\theta_d) \\ \frac{2}{\sqrt{3}} i_s \cos(\theta_d) \\ 0 \end{bmatrix} \tag{5.47}$$

5.3.2.2 Voltage Balance

The armature voltage balance equations for the equivalent single-phase machine's applied phase-windings are presented in (5.48). Phase-a is here assumed non-active because the phase is open-circuited and no current is flowing through the phase-a winding.

$$v_b = -R_S i_b + \frac{d}{dt}\psi_b \tag{5.48a}$$

$$v_c = -R_S i_c + \frac{d}{dt}\psi_c \tag{5.48b}$$

The voltage balance for the equivalent single-phase machine is obtained by appreciating the defined terminal voltage for the equivalent single-phase machine presented in (5.44). The resulting voltage balance is presented in (5.49).

$$\begin{aligned} v_s = (v_b - v_c) &= -R_S(i_b - i_c) + \frac{d}{dt}(\psi_b - \psi_c) \\ &= -2R_S i_s + \frac{d}{dt}(\psi_b - \psi_c) \end{aligned} \tag{5.49}$$

5.3.2.3 MMF Distribution for the Equivalent Single-Phase Machine

The MMF distribution for a single phase-winding is presented in (3.1). The peak of the distribution is presented in (5.50).

$$\mathscr{F}_{S(1)} = \frac{4}{\pi}\left(\frac{k_w N_S}{P}\right) i_S \tag{5.50}$$

The peak MMF distribution can be resolved into two components with peak values along the d- and q-axis, respectively. This is viewed in Fig. 5.10. The armature MMF distribution is lagging the d-axis, which is aligned with the rotor field, with the rotor angle θ_d. The armature MMF distribution is pulsating aligned with the system's reference axis [32].

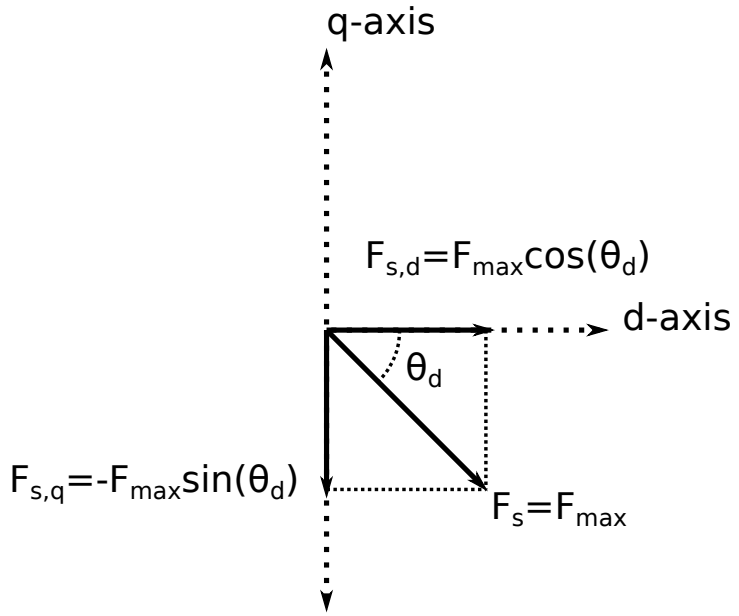

Figure 5.10: Components of the MMF distribution along the d- and q-axis[3]

The MMF distribution components for the single-phase synchronous machine are presented in (5.10) with respect to the single phase-current, i_s, and the single phase-winding's number of turns, $N_{(1)}$.

$$\begin{aligned} \mathscr{F}_{s,d(1)} &= \frac{4}{\pi}\frac{k_w N_{(1)}}{P} i_s \cos(\theta_d) \\ \mathscr{F}_{s,q(1)} &= -\frac{4}{\pi}\frac{k_w N_{(1)}}{P} i_s \sin(\theta_d) \end{aligned} \tag{5.51}$$

The resulting d- and q-axis MMF distribution for the equivalent single-phase machine when applying the single-phase machine's current, as shown in (5.45), are presented in (5.52) [7].

$$\begin{aligned} \mathscr{F}_{s,d(3)} &= \frac{4}{\pi}\frac{k_w N_{(3)}}{P}\frac{3}{2} i_{d(3)} = \frac{4}{\pi}\frac{k_w N_{(3)}}{P}\sqrt{3} i_s \cos(\theta_d - \frac{\pi}{2}) \\ \mathscr{F}_{s,q(3)} &= -\frac{4}{\pi}\frac{k_w N_{(3)}}{P}\frac{3}{2} i_{q(3)} = -\frac{4}{\pi}\frac{k_w N_{(3)}}{P}\sqrt{3} i_s \sin(\theta_d - \frac{\pi}{2}) \end{aligned} \tag{5.52}$$

Based on derivations presented in [7] and [8], the magnetic reference axis of the single-phase machine is located 90 electrical degrees ahead of the reference magnetic axis of the equivalent single-phase machine. A 90 electrical degrees rotation in space is therefore applied to the single-phase machine's

[3] Based on [32]

MMF distribution components presented in (5.51). The resulting MMF distributions for the single-phase machine and the equivalent single-phase machine with the same reference frames are presented in (5.53).

$$\begin{aligned} \mathscr{F}_{s,d(1)} &= \frac{4}{\pi}\frac{k_w N_{(1)}}{P} i_s \cos(\theta_d - \frac{\pi}{2}) \\ \mathscr{F}_{s,q(1)} &= -\frac{4}{\pi}\frac{k_w N_{(1)}}{P} i_s \sin(\theta_d - \frac{\pi}{2}) \end{aligned} \tag{5.53a}$$

$$\begin{aligned} \mathscr{F}_{s,d(3)} &= \frac{4}{\pi}\frac{k_w N_{(3)}}{P}\sqrt{3} i_s \cos(\theta_d - \frac{\pi}{2}) \\ \mathscr{F}_{s,q(3)} &= -\frac{4}{\pi}\frac{k_w N_{(3)}}{P}\sqrt{3} i_s \sin(\theta_d - \frac{\pi}{2}) \end{aligned} \tag{5.53b}$$

5.3.3 Parameter Adjustments for the Equivalent Single-Phase Machine

The equivalent single-phase machine, presented in Fig. 5.9, is applied for reflecting the time-domain related behavior of the single-phase machine. It is observed that the equivalent single-phase machine is a three-phase machine with unbalanced loading. Parameters for the single-phase machine are therefore necessarily adjusted when applying the equivalent single-phase machine. The rotor circuits for the single-phase are assumed to be equal to the rotor circuits used for the equivalent single-phase machine. Parameters describing rotor circuits quantities are therefore not adjusted.

5.3.3.1 Turns per Winding

The MMF distribution components of the single-phase machine and the equivalent single-phase machine are presented in (5.53). To receive the same dynamic behavior from both machines, the MMF distribution components have to be of the same magnitude. The equivalent single-phase machine's distributions are a factor $\sqrt{3}$ larger than those of the single-phase machine. The number of turns per winding for the equivalent single-phase machine is therefore assumed to be a factor of $\sqrt{3}$ smaller than that of the single-phase machine. The relationship between the number of turns per winding for the single-phase- and equivalent single-phase machine is presented (5.54).

$$N_{(3)} = \frac{1}{\sqrt{3}} N_{(1)} \tag{5.54}$$

5.3.3.2 Inductance

Self- and mutual inductances for windings, which is the ratio between flux linkages and currents involved, are proportional to the product of the involved windings' number of turns. The self-inductance of a winding and the mutual inductance between two armature windings are therefore proportional to the square of the respective armature winding's number of turns. The magnetizing inductance of the d- and q-axis windings are defined in (3.21a) and (3.21b). Since both L_{ss0} and L_{ssP} are proportional to the square of the number of turns per winding, the magnetizing inductances also depend on the squared of turns per winding. The resulting inductance relationship between the single-phase machine and the equivalent single-phase machine are presented in (5.55).

$$L_{md(3)} = \frac{1}{3} L_{md(1)} \tag{5.55a}$$

$$L_{mq(3)} = \frac{1}{3} L_{mq(1)} \tag{5.55b}$$

The leakage inductance is assumed the same for every winding in the equivalent single-phase machine. The equivalent single-phase machine, containing two current conducting windings, has a leakage inductance that is half of that of the single-phase winding. This is based on the fact that the same current is loaded for both the equivalent- and the single-phase machine. The leakage inductance relationship between the equivalent- and the single-phase machine are presented in (5.56).

$$L_{ls(3)} = \frac{1}{2} L_{ls(1)} \tag{5.56}$$

The synchronous d- and q-axis inductances for the equivalent single-phase machine are defined as presented in (5.57).

$$L_{d(3)} = \frac{1}{2} L_{ls(1)} + \frac{1}{3} L_{md(1)} \tag{5.57a}$$

$$L_{q(3)} = \frac{1}{2} L_{ls(1)} + \frac{1}{3} L_{aq(1)} \tag{5.57b}$$

The sub-transient- and transient inductances for the d- and q-axis are defined in (3.29). By appreciating the changes of (5.57) when applying parameters to the equivalent single-phase machine, subtransient- and transient inductances are obtained. These are presented in (5.58) and (5.59). The leakage

inductances for the rotor electrical circuits, L_{lf}, L_{lD} and L_{lQ}, are unchanged.

$$L'_{d(3)} = \frac{1}{2}L_{ls(1)} + \frac{\frac{1}{3}L_{md(1)}L_{lf}}{\frac{1}{3}L_{md(1)} + L_{lf}} \tag{5.58a}$$

$$L'_{q(3)} = \frac{1}{2}L_{ls(1)} + \frac{1}{3}L_{mq(1)} \tag{5.58b}$$

$$L''_{d(3)} = \frac{1}{2}L_{ls(1)} + \frac{\frac{1}{3}L_{md(1)}\frac{L_{lD}L_{lf}}{L_{lD}+L_{lf}}}{\frac{1}{3}L_{md(1)} + \frac{L_{lD}L_{lf}}{L_{lD}+L_{lf}}} \tag{5.59a}$$

$$L''_{q} = \frac{1}{2}L_{ls(1)} + \frac{\frac{1}{3}L_{mq(1)}L_{lQ}}{\frac{1}{3}L_{mq(1)} + L_{lQ}} \tag{5.59b}$$

5.3.3.3 Armature Resistance

The armature resistance is, as the leakage inductance, assumed equal for every winding. The load current for the equivalent single-phase machine is flowing through two windings. The armature resistance is therefore assumed to be half of that of the single-phase machine. The ohmic losses of the armature circuits are then equal for the equivalent- and single-phase machine. The relationship is presented in (5.60).

$$R_{S(3)} = \frac{1}{2}R_{S(1)} \tag{5.60}$$

The relationship between armature resistance for the single-phase- and the equivalent single-phase machine is also presented in (5.48). It is here observed that the armature resistance for the equivalent single-phase machine is twice the size of the armature resistance for the single-phase machine.

5.3.3.4 Time Constants

The time constants for a synchronous machine were presented in Chapter 3. When adjusting machine inductances and resistances for modeling the equivalent single-phase machine, the machines time constants will also change based on the time constant definitions presented in (3.31). The new time

constants for the equivalent single-phase machine are presented in (5.61).

$$T'_{d0(3)} = \frac{L_{lf} + \frac{1}{3}L_{md(1)}}{R_f} \tag{5.61a}$$

$$T''_{d0(3)} = \frac{L_{lD} + \frac{\frac{1}{3}L_{md(1)}L_{lf}}{l_{lf}+\frac{1}{3}L_{md(1)}}}{R_D} \tag{5.61b}$$

$$T''_{q0(3)} = \frac{L_{lQ} + \frac{1}{3}L_{mq(1)}}{R_Q} \tag{5.61c}$$

5.3.3.5 Adjusted Parameters

Parameters for the single-phase synchronous machine is presented in Appendix C Table C.1 and C.2. Parameters coinciding with the electrical circuits of the single-phase machine is calculated and presented in Appendix C, Table C.3.

Parameters for the single-phase synchronous machine are adjusted based on calculations carried out in Chapter 5 and presented in (5.57), (5.58), (5.59) and (5.61). The adjusted parameters are presented in Table 5.1. Label (1) and (3) denote the given single-phase machine's parameters and the calculated equivalent single-phase machine's parameters, respectively.

Table 5.1: Calculated Parameters for the Equivalent Single-Phase Synchronous Machine

Parameter	**Unit**	**SPSM**	**Value**	**Equivalent SPSM**	**Value**
Armature resistance	pu	$r_{S(1)}$	0.0018	$r_{S(3)}$	0.000875
Leakage inductance	pu	$L_{ls(1)}$	0.096	$L_{ls(3)}$	0.0480
d-axis synchronous inductance	pu	$L_{d(1)}$	1.02	$L_{d(3)}$	0.3560
d-axis transient inductance	pu	$L'_{d(1)}$	0.12	$L'_{d(3)}$	0.0708
d-axis sub-transient inductance	pu	$L''_{d(1)}$	0.1	$L''_{d(3)}$	0.052
q-axis synchronous inductance	pu	$L_{q(1)}$	0.47	$L_{q(3)}$	0.1727
q-axis sub-transient inductance	pu	$L''_{q(1)}$	0.11	$L''_{q(3)}$	0.061
d-axis transient open-circuit time constant	s	$T'_{d0(1)}$	8.6	$T'_{d0(3)}$	3.0156
d-axis sub-transient open-circuit time constant	s	$T''_{d0(1)}$	0.08	$T''_{d0(3)}$	0.0767
q-axis sub-transient open-circuit time constant	s	$T''_{q0(1)}$	3.4	$T''_{q0(3)}$	1.2182

5.4 Equation of Motion for a Synchronous-Synchronous Rotary Frequency Converter

The general equation of motion presents the dynamical characteristic of an electric machine and is given by (3.40). A synchronous-synchronous rotary frequency converter contains a three-phase synchronous motor fed by the three-phase 50 Hz public grid. The motor has a common shaft with a single-phase synchronous generator, supplying power to the $16^2/_3$ Hz traction power grid [44].

Since the rotary converter contains two machines, mechanically connected through a shaft, the equation of motion is rewritten for expressing the converter's dynamical characteristic. (5.62a) and (5.62b) are obtained for presenting each machine's instantaneous power balance [56].

$$\frac{2H_G}{\omega_{sG}}\frac{d^2}{dt^2}\delta_G + D_G\frac{d}{dt}\delta_G = p_{mG,pu} - p_{emG,pu} \tag{5.62a}$$

$$\frac{2H_M}{\omega_{sM}}\frac{d^2}{dt^2}\delta_M - D_M\frac{d}{dt}\delta_M = p_{emM,pu} - p_{mM,pu} \tag{5.62b}$$

(5.62a) presents the power balance for the generator. Positive power flow direction is defined as out from the generator and into the traction power grid. (5.62b) presents the power balance for the motor. Positive power flow is direction is here defined as into the motor from the three-phase public grid. The subscripts G and M denote generator and motor quantities, respectively. The positive direction of power flow is also observed from the direction of torques presented in Fig. 5.11. T_{emM} and T_{emG} are the electromagnetic torque of the motor and -generator, respectively. The electromagnetic power is obtained by multiplying the electromagnetic torque with its mechanical rotor velocity.

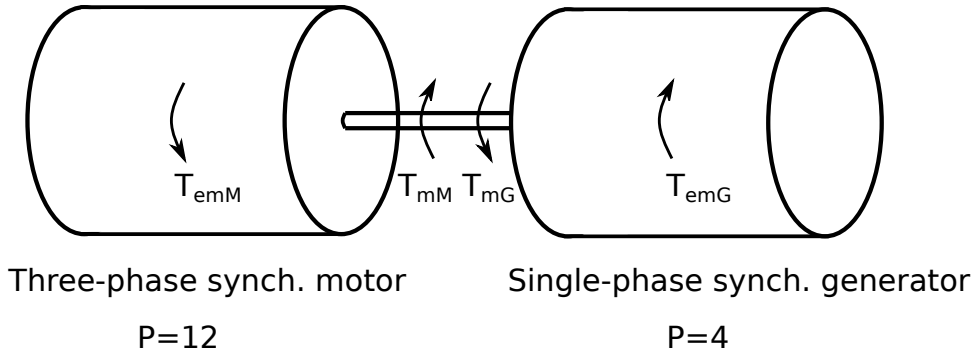

Figure 5.11: A 12-poled three-phase synchronous motor mechanically coupled to a 4-poled single-phase synchronous generator[4]

[4] Based on [32]

The shaft is rotating the same direction for both motor and generator. The positive rotational direction is chosen to follow the generator's rotation. This leads to the generator- and motor rotational velocities being defined as (5.63a) and (5.63b). The rotational deviation speed of the motor is therefore defined as having a negative sign compared to that of the generator.

$$\omega_{G,pu} \cdot \omega_{sG} = \omega_{sG} + \frac{d}{dt}\delta_G \tag{5.63a}$$

$$\omega_{M,pu} \cdot \omega_{sM} = \omega_{sM} - \frac{d}{dt}\delta_M \tag{5.63b}$$

The per unit rotational speed of the motor equals the per unit rotational speed of the generator when the sign convention for positive rotational direction is followed. The final equation of motion for the motor-generator set is obtained by combining (5.62a) and (5.62b). The result is presented in (5.64).

$$2\underbrace{(H_M + H_G)}_{H_{MG}}\frac{d^2}{dt^2}\delta_{pu} + (D_M\omega_{sM} + D_G\omega_{sG})\frac{d}{dt}\delta_{pu} = p_{emM,pu} - p_{emG,pu} \tag{5.64}$$

A block diagram describing (5.64) is given in Fig. 5.12. s is here given as the Laplace operator. Since both machines are modeled on a generator convention the sum of the two electromagnetic powers, p_{emM} and p_emG, is the generator's electromagnetic power extracted from the motors electromagnetic power.

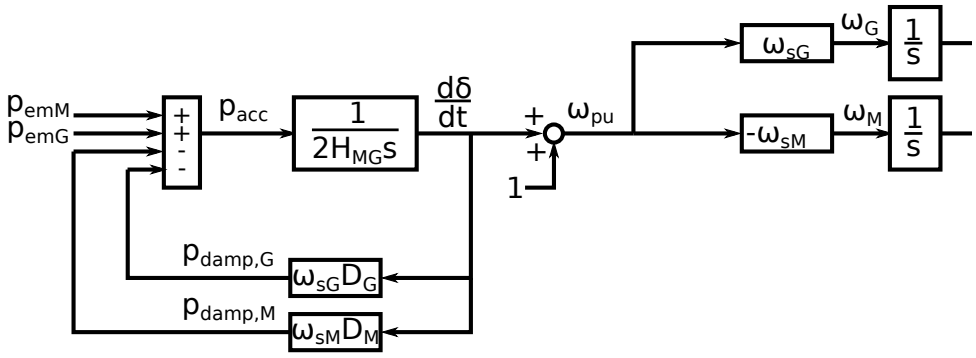

Figure 5.12: A block diagram for the rotary converter's equation of motion

Based on the equations presented above the behavior of the rotary converter is analyzed. If the rotor rotates at speed higher than it's synchronous speed, $\omega_{pu} > 1$, the rotary converter will decelerate until it reaches its synchronous speed. This is a result of the increase of delivered power to the traction power grid from the single-phase generator, the decrease of delivered power from the three-phase

public grid to the three-phase motor and the motor's- and generator's damping that is opposing the rotor's deviation from synchronous speed [56].

Chapter 6

Results and Discussion

The following chapter presents test results from three rotary converter models that have been implemented using MATLAB®/Simulink.

Each rotary converter model presented in the following sections apply a three-phase synchronous motor. Such a motor is implemented based on equations obtained in Chapter 3, and test results are presented in Section 6.1.

The three-phase synchronous motor is connected on a common shaft to a single-phase synchronous generator. The three different methods applied for implementing the single-phase machine model are summarized below, and main test results are presented:

- Applying a single phase-winding and obtaining equations based on the machine's phase quantities. The equations applied for the implemented model is presented in Section 5.1. The test results are presented in Section 6.2. The initial machine conditions cause the converter to display undesired behavior, and the results presented are unstable.
- Applying two rotating MMF distributions for presenting the behavior of the pulsating armature MMF distribution. Two separate three-phase synchronous machines have been implemented, magnetically coupled to common rotor circuits. The equations applied to the implemented model are presented in Section 5.2. The model's test results are presented in 6.3. The model has not presented successfully test results due to convergence issues during simulation.
- Applying a three-phase synchronous machine with one open-circuited armature phase and adjusting the applied single-phase machine parameters. The modeling method is presented in Section 5.3. The model's test results are presented in 6.4 for steady-state machine performance and during short-circuited single-phase terminals. The obtained short-circuit currents are

compared to rotary converter models applying the same modeling technique, but alternative parameter adjustments based on earlier sources dealing with the same modeling technique.

6.1 THREE-PHASE SYNCHRONOUS MACHINE

The three-phase synchronous machine presented below is modeled based on Park's equations presented in Chapter 3. The parameters are based on the three-phase synchronous machine applied in the rotary frequency converter and are presented in Appendix D.

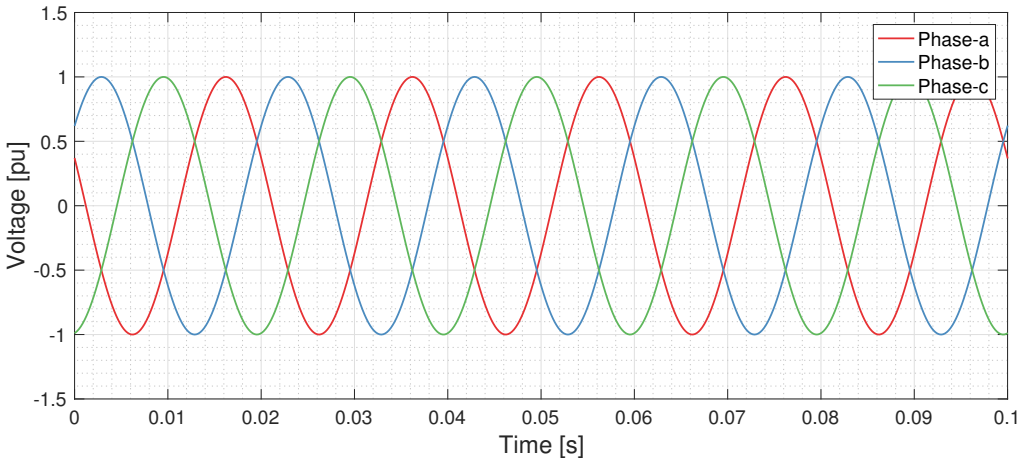

Figure 6.1: Three-phase terminal voltage

A stiff three-phase grid is feeding the machine, as presented in Fig. 6.1. A phase-shift is applied to the three-phase grid voltages due to the alignment of the rotor d-axis and the armature magnetic reference axis at 0 seconds.

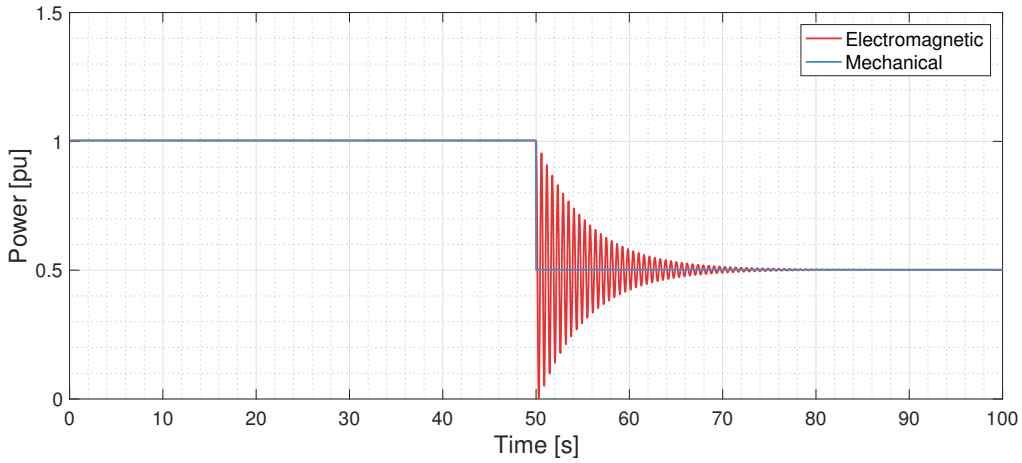

Figure 6.2: Three-phase synchronous machine power

The machine is driven by mechanical power, as presented in Fig. 6.2. A sudden change in this mechanical power is applied after 50 seconds, and the electromagnetic power induced by the machine is observed reacting to the changes. The electromagnetic power oscillates at 1.7 Hz and settles at a new steady-state value after 20 seconds. The damping of power is a result of the machine's electrical damping due to currents induced in the rotor circuits. These currents are presented in Fig. 6.3.

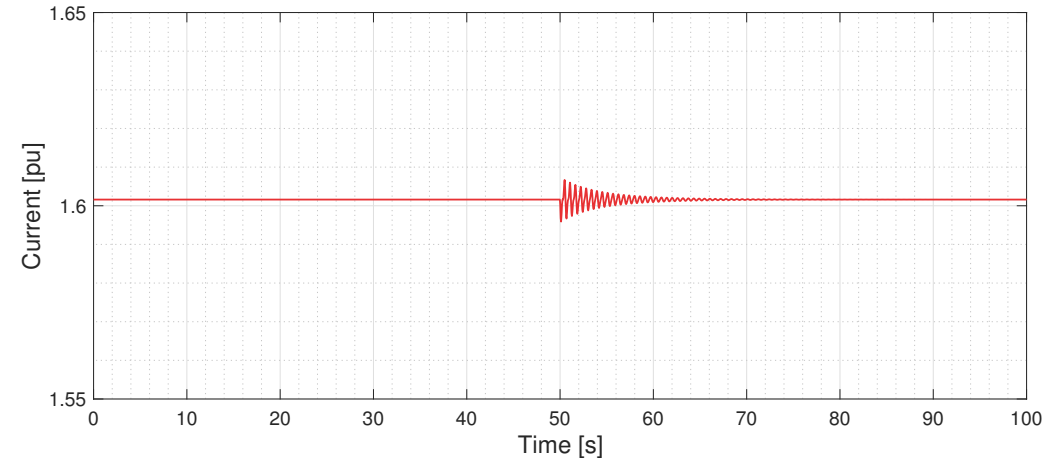

(a) Field current

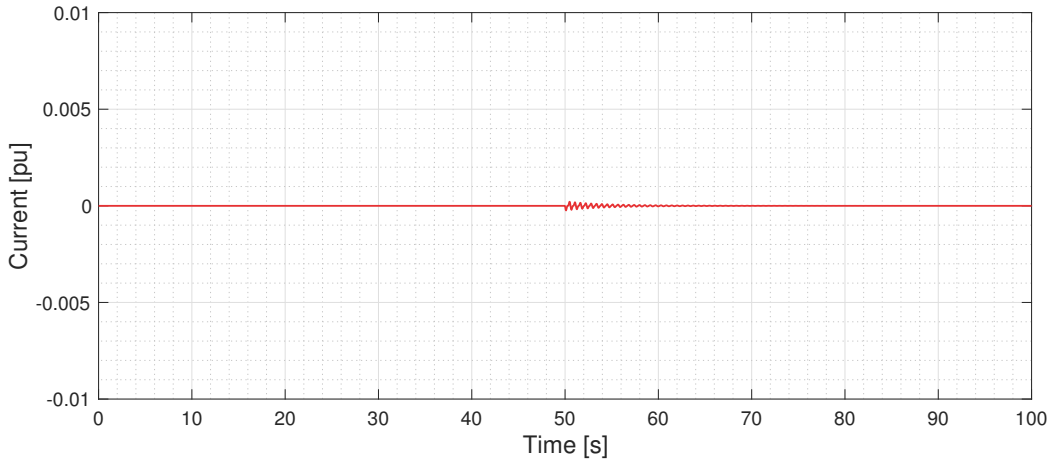

(b) d-axis damper current

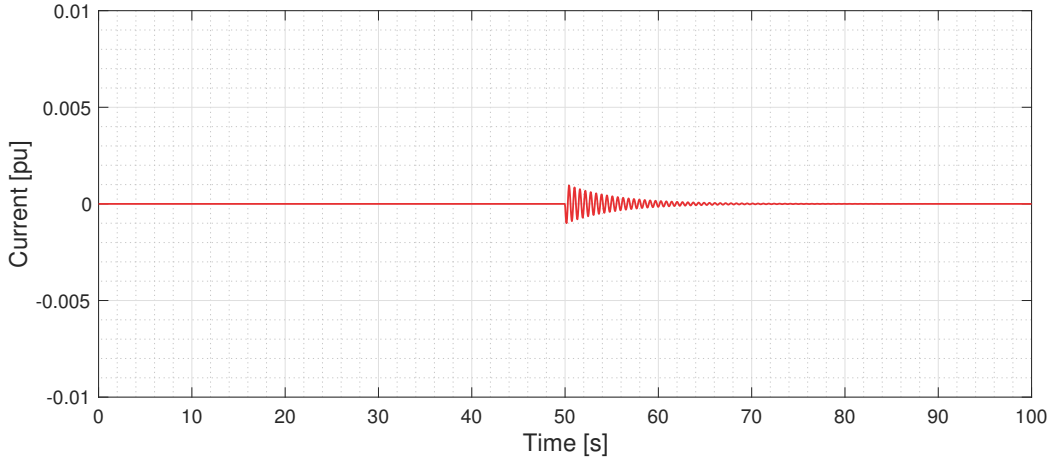

(c) q-axis damper current

Figure 6.3: Rotor currents for a three-phase synchronous machine

A constant field voltage is applied to the field circuit, causing a DC field current to induce a constant rotor field. The field current is observed in Fig. 6.3a. After the decrease of applied mechanical power to the machine, the rotor circuits experience induced currents. The currents induced in the damper bars of the rotor are here presented by a d- and q-axis current in Fig 6.3b and 6.3c, respectively. These currents, together with the additional induced current to the field circuit, have the same frequency as the oscillation of electromagnetic power, and they induce damping torque during the electromechanical transient. The damper currents and the additional current to the field circuit are damped out when the machine reaches its steady-state performance.

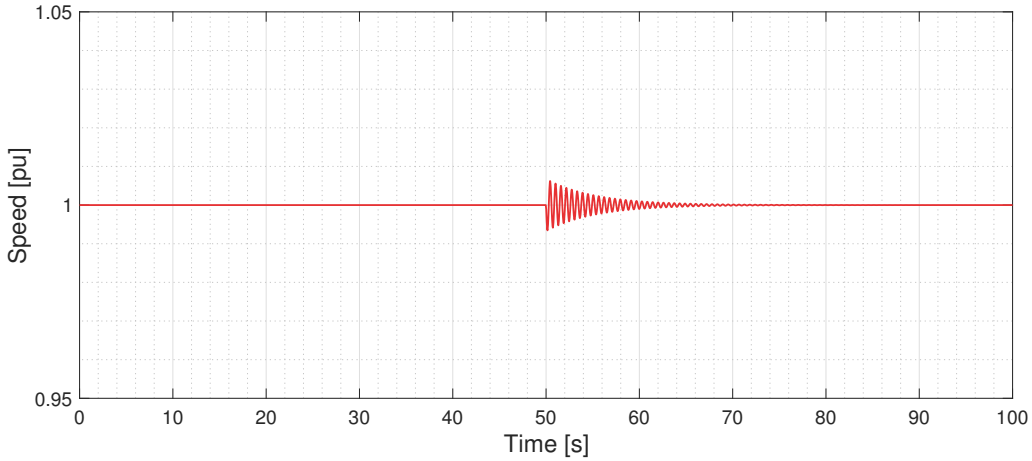

Figure 6.4: Three-phase machine rotor speed

The machine's rotor speed is observed in Fig. 6.4. After the electromechanical transient, the difference between applied mechanical power and induced electromagnetic power causes the rotor to accelerate and decelerate in an oscillating manner at frequency 1.7 Hz.

6.2 ROTARY FREQUENCY CONVERTER MODEL - APPLYING SPSG MODEL 1

The rotary converter model test results presented in the following section are a result of the three-phase synchronous machine presented in Chapter 3 and observed in Section 6.1, and a model based on the single-phase synchronous machine equations developed in Section 5.1. The mechanical interaction between the two synchronous machines are presented in Section 5.4.

The electromagnetic power induced by the two synchronous machines are observed in Fig. 6.5.

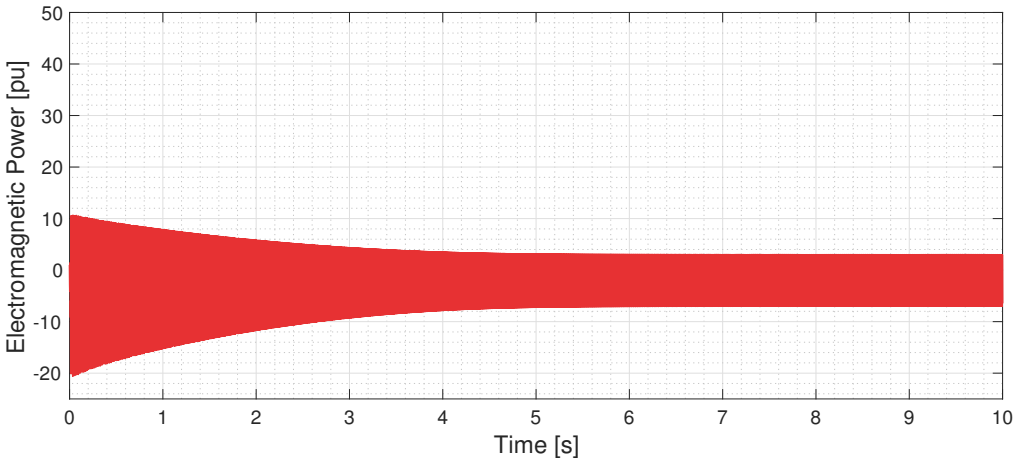

(a) Three-phase synchronous motor

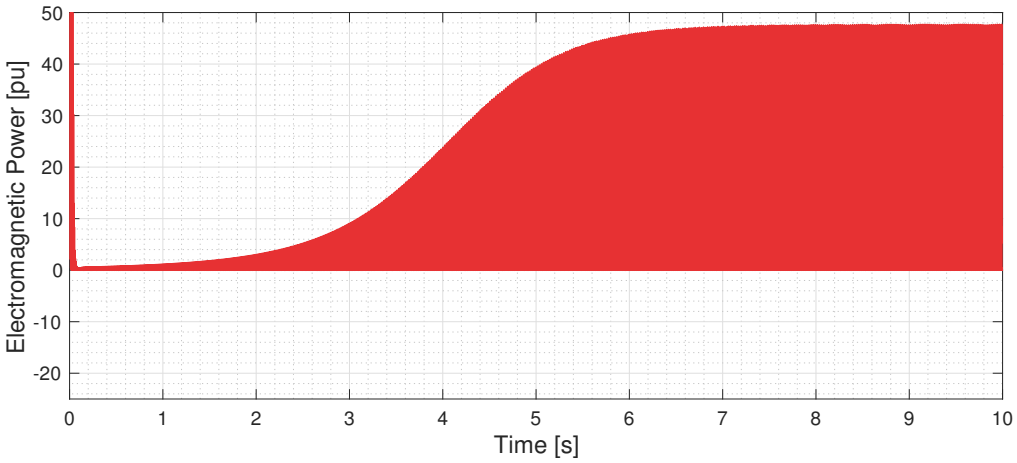

(b) Single-phase synchronous generator

Figure 6.5: Electromagnetic power induced by the synchronous machines in the rotary frequency converter

The system is unstable, as is observed in Fig. 6.5b. The single-phase generator experiences a massive step in power during the first milliseconds of simulation, and the large difference between induced motor- and generator power causes the rotor to accelerate. The rotor speed is presented in Fig.

6.6.

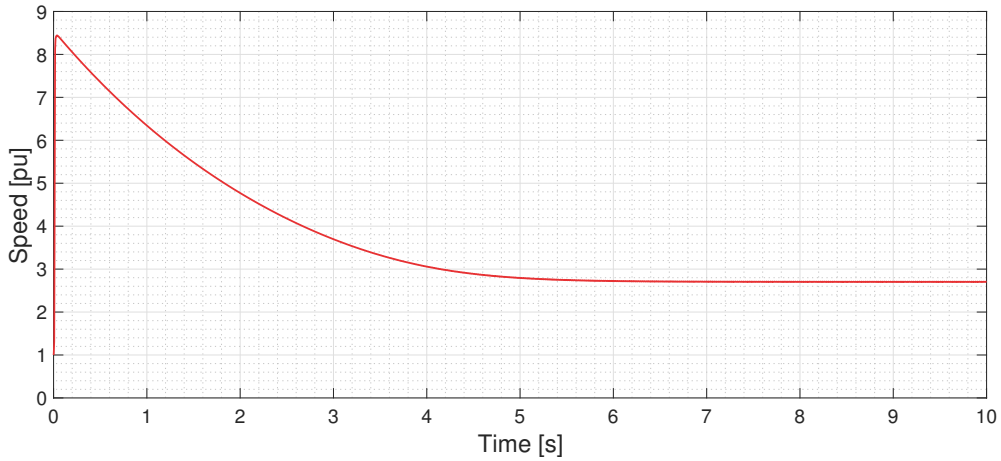

Figure 6.6: Rotary converter speed

It is observed in Fig. 6.6 that the rotor accelerates to 8.4 times rated mechanical rotor speed after 37 milliseconds of simulation. The rotor then decelerates until it reaches 2.7 pu speed, and the electromagnetic power induced by the motor and generator reaches a repeating steady-state performance. The electromagnetic powers, with their repetitive waveforms, are presented in Fig. 6.7 during the steady-state machine performance.

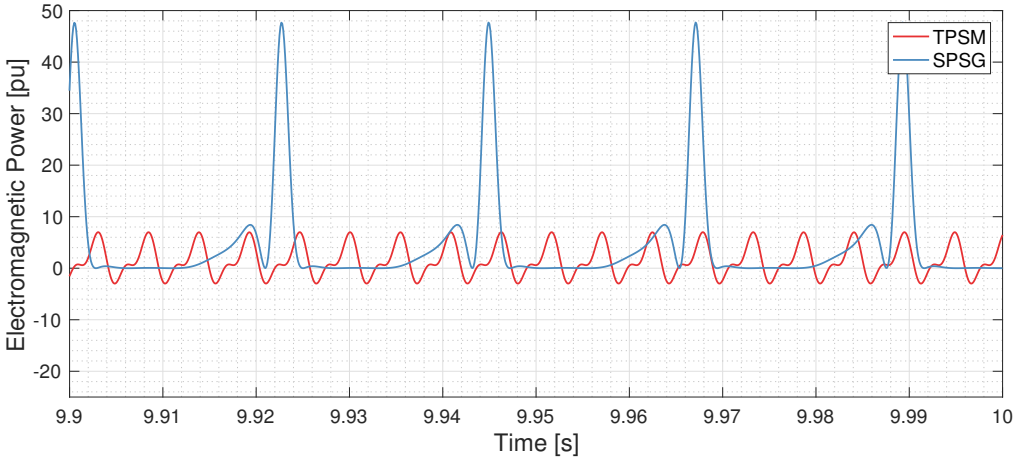

Figure 6.7: Electromagnetic power induced by the three-phase motor and the single-phase generator

It is observed in Fig. 6.7 that the three-phase synchronous motor's power, TPSM, is oscillating at 184 Hz. The single-phase synchronous generator's power, SPSG, is pulsating at 45 Hz. The rotor is, during the presented time frame in Fig. 6.7, rotating at 2.7 times synchronous speed. If assuming that the

rotor speed and frequency of single-phase power is dependent upon each other, the frequency at synchronous speed, 1 pu, would be $\frac{45}{2.7} = 16^2/_3$ Hz. An additional peak is observed for the single-phase induced power between each major peak pulsation. If assuming that this peak would be located midway between the larger pulsating peaks the induced power frequency would be $16^2/_3 \cdot 2 = 33^1/_3$ Hz.

The rotor circuit currents of the rotary frequency converter are presented in Fig. 6.8. TPSM and SPSG denote the three-phase synchronous motor- and the single-phase synchronous generator rotor currents, respectively. The frequency of the motor currents is 184 Hz, the same as the frequency for the electromagnetic power induced by the motor. The single-phase synchronous generator rotor currents pulsate in the same manner as the single-phase induced power, with a frequency of 45 Hz.

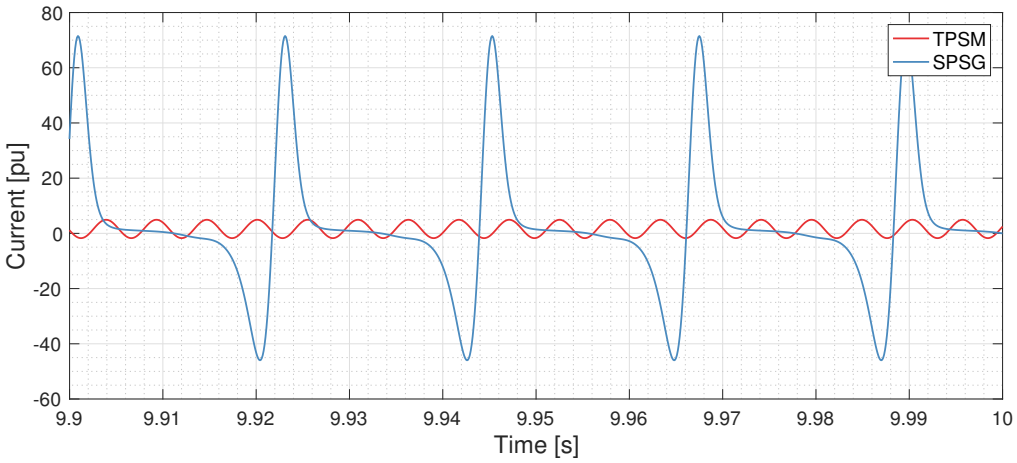

(a) Field currents

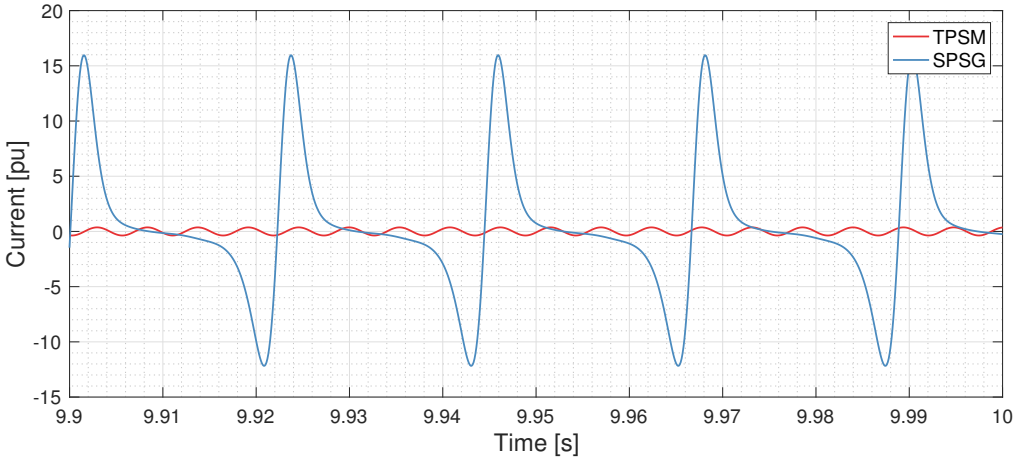

(b) d-axis damper currents

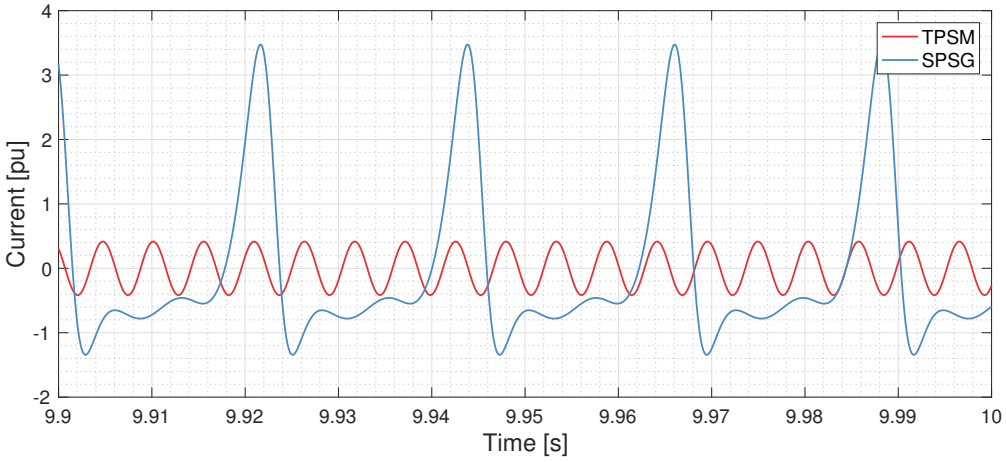

(c) q-axis damper currents

Figure 6.8: Rotor circuit currents for the rotary frequency converter

The terminal currents of the three-phase motor and single-phase generator are presented in Fig. 6.9 and 6.10, respectively. The three-phase currents contain harmonics components and have a frequency of 50 Hz. The single-phase current has a frequency of 45 Hz.

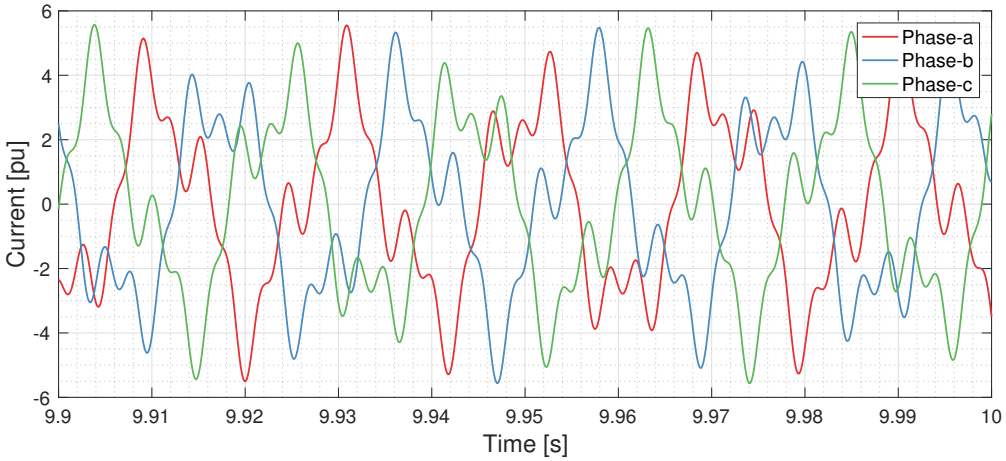

Figure 6.9: Three-phase motor armature currents

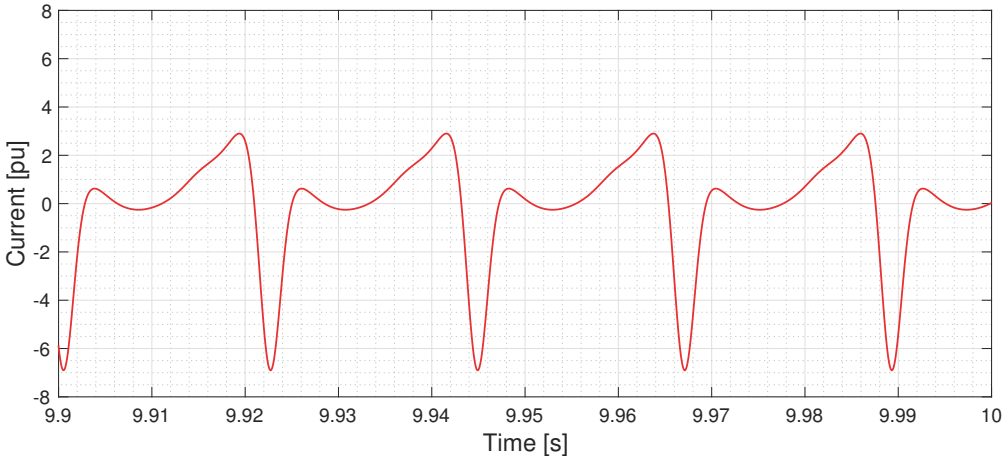

Figure 6.10: Single-phase generator armature current

The rotary converter voltages at three-phase and single-phase terminals are presented in Fig. 6.11 and 6.12. The three-phase voltage is applied at the three-phase motor terminals, while the single-phase voltage is generated at the single-phase terminals by the single-phase generator.

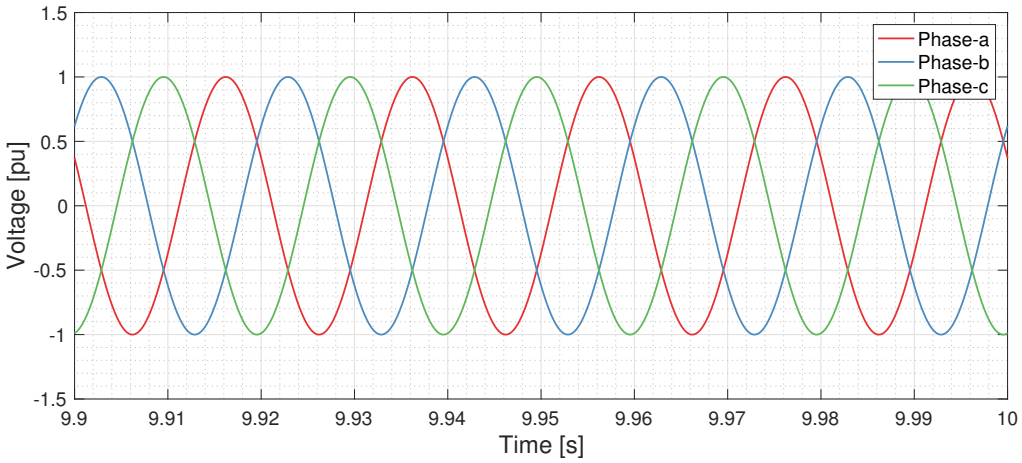

Figure 6.11: Three-phase motor terminal voltages

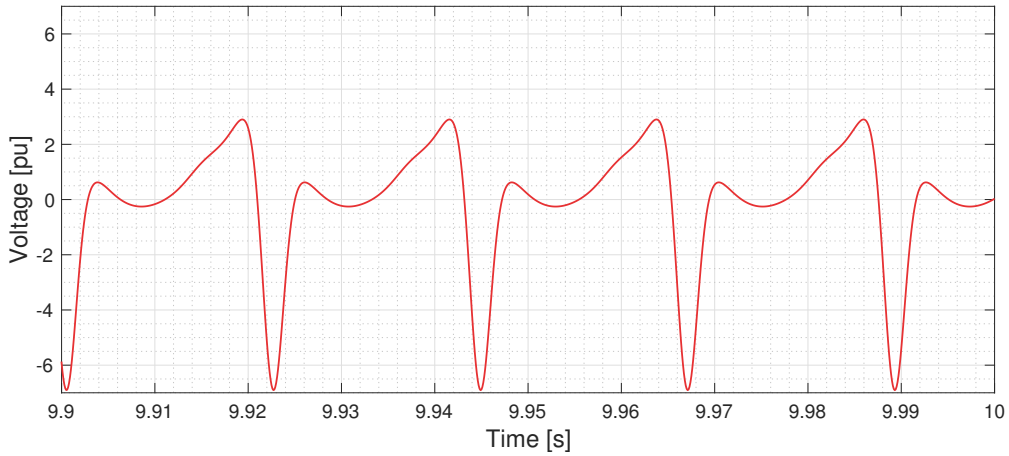

Figure 6.12: Single-phase generator terminal voltage

6.2.1 Evaluating Model 1

Simulation results for the rotary frequency converter model when applying Model 1, developed in Section 5.1, for the single-phase synchronous generator, is presented above. The system is unstable, causing the converter's rotor to accelerate significantly during the first milliseconds of simulation until it is damped by the electrical system and decelerates to 2.7 times nominal speed. The initial acceleration of the rotor is caused by initial conditions not satisfying the steady state behavior of the machine. Several unsuccessful attempts have been carried out for calculating such initial conditions.

The three-phase synchronous machine observed in Section 6.1 presents the time-domain related behavior of a synchronous machine during steady-state and transient electromechanical performance.

The simulation results for the three-phase machine of the rotary converter, introduced in Section 5.1 were expected to present similar behavior. The electromagnetic motor power shown in Fig. 6.5a should be constant during steady-state operation, not oscillating in the manner here presented. The oscillation of the single-phase generator induced power is on the other hand expected, but at $33^1/_3$ Hz, double the nominal single-phase frequency. It is expected that if acceptable initial conditions where to be obtained, the frequency of the single-phase power would become $33^1/_3$ Hz. This would further on maintain a stable motor induced power, and the rotor would not accelerate during the first milliseconds of simulation. Generated voltage and current at single-phase terminal would obtain their nominal electrical frequency. The voltage of the single-phase generator would be expected to resemble a sinusoidal waveform, but with an undecided third harmonic component content. The idea behind the additional single-phase voltage third harmonic component is presented in Chapter 4.

The frequency of oscillation for motor- and generator power in Fig. 6.7 is also observed in the rotor circuit currents presented in Fig. 6.8. This implies that the currents behave as expected, damping power pulsations from the motor- and generator electric system.

6.3 ROTARY FREQUENCY CONVERTER MODEL - APPLYING SPSG MODEL 2

The rotary converter model test results presented in the following section is a result of the three-phase synchronous machine presented in Chapter 3 and observed in Section 6.1, and a model based on the single-phase synchronous machine equations developed in Section 5.2.

The mechanical interaction between the two synchronous machines is presented by developed equations in Section 5.4.

The electromagnetic power induced by the three-phase- and single-phase synchronous machine are presented in Fig. 6.13a.

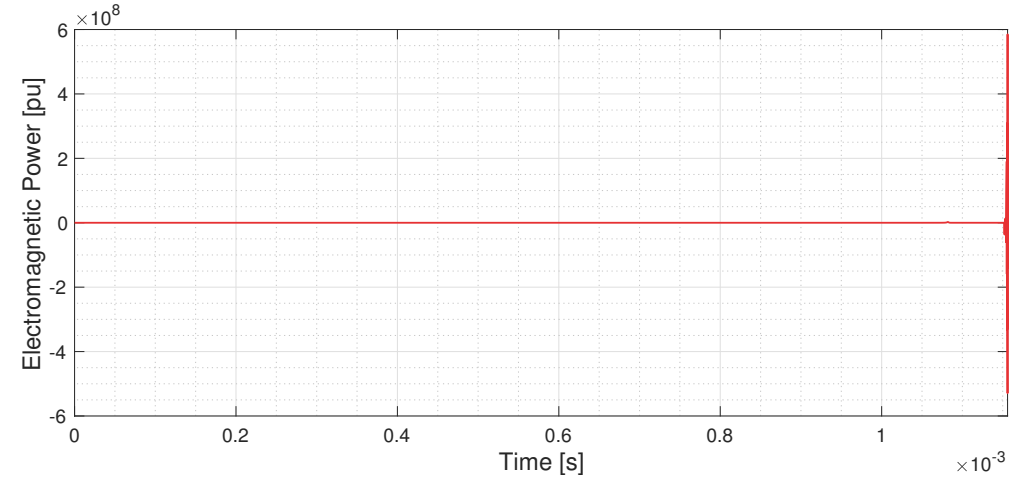

(a) Three-phase motor

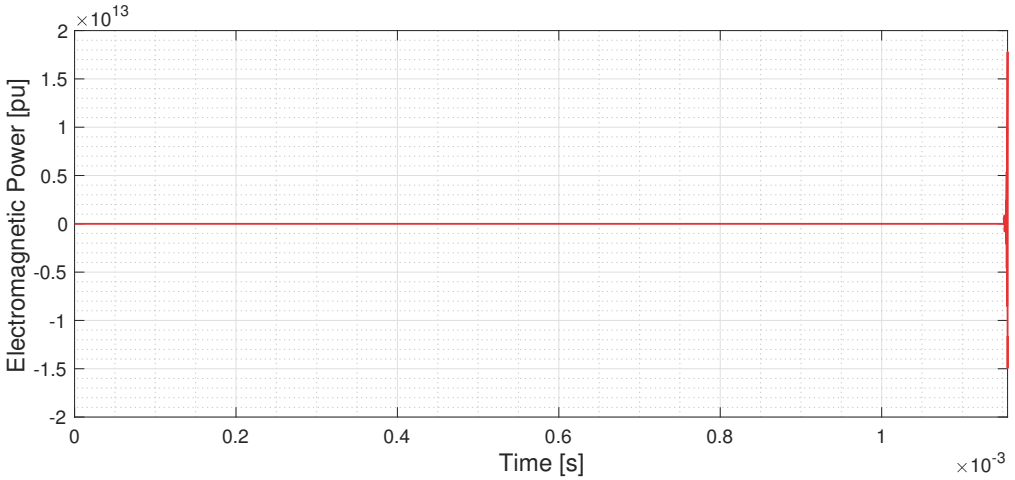

(b) Single-phase generator

Figure 6.13: Simulation results for electromagnetic power induced by the thee-phase synchronous motor and the single-phase synchronous generator respectively

The simulation is here carried out for 1.6 milliseconds. After this, the system is unable to converge to a final value, and the system solution becomes unstable. Unsuccessful attempts to stabilize the system has been carried out.

6.4 ROTARY FREQUENCY CONVERTER APPLYING EQUIVALENT SPSG

The rotary converter model test results presented in the following section are a result of applying physical systems in the Simscape language within the MATLAB® /Simulink environment. Two predefined three-phase synchronous machines are mechanically connected through a stiff shaft. The first machine is supplied by a three-phase stiff 50 Hz grid and applied parameters presented in Appendix D for the three-phase synchronous motor of the rotary frequency converter. The second machine has one open-circuited phase and a load connected between the remaining two phases. Parameters for the single-phase synchronous machine, presented in Appendix C, are adjusted based on developed equations obtained in Section 5.3. The parameter adjustments are shown in Tab. 5.1 as parameters for the equivalent single-phase synchronous machine. The rotary frequency converter system modeled are presented in Fig. 6.14.

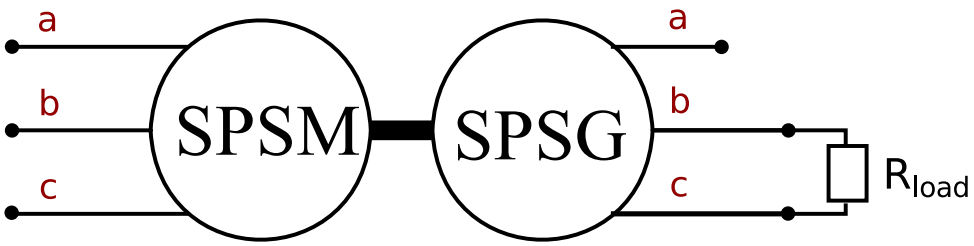

Figure 6.14: Two three-phase synchronous machines mechanically coupled

The rotary converter has been simulated during nominal steady state loaded conditions and short-circuited single-phase terminals. Both situations have been documented in the following sections.

6.4.1 Converter Behaviour during Loaded Conditions

The following section presents simulation results for the rotary frequency converter's time-domain related behavior during loaded conditions. The model configuration is observed in Fig. 6.14, with a load resistance of 100 Ω. A constant field voltage is applied to both motor and generator.

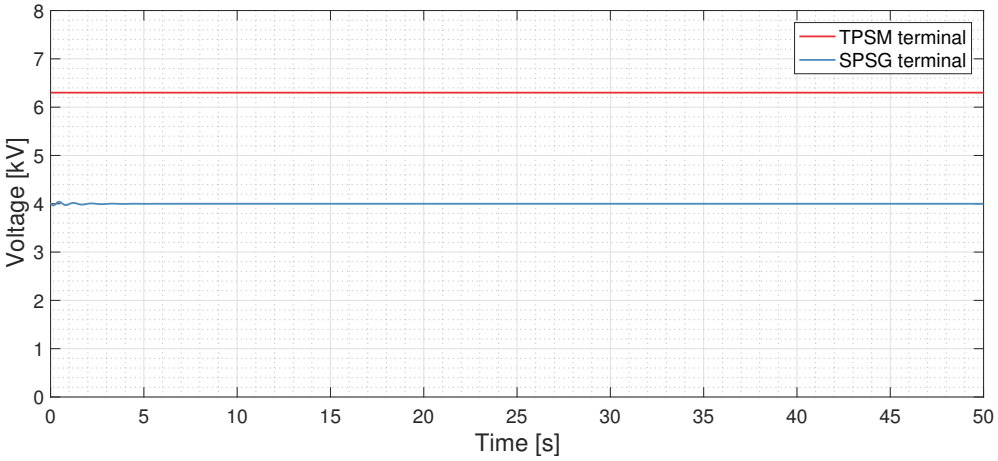

Figure 6.15: Terminal RMS voltage for the rotary frequency converter

A 6.3 kV RMS three-phase voltage is applied to the three-phase motor terminals, and a 4.0 kV RMS single-phase voltage is generated at the single-phase terminals. The RMS voltage levels are viewed in Fig. 6.15. Some initial transients are observed for the generated single-phase voltage during initialization of the simulation.

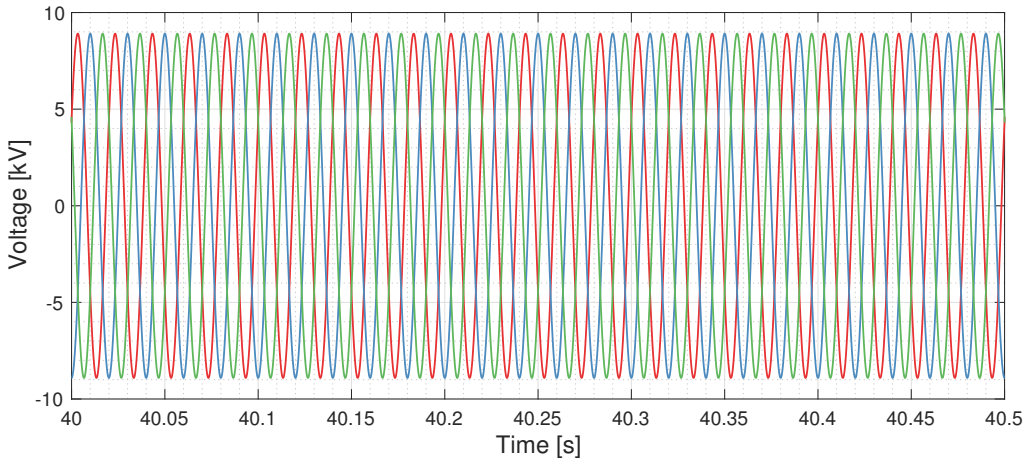

(a) Three-phase motor

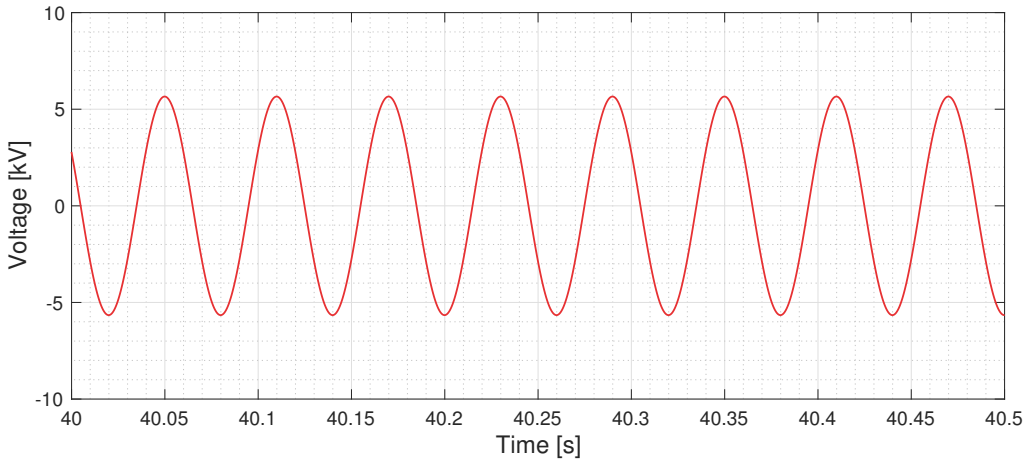

(b) Single-phase generator

Figure 6.16: Terminal voltages for the rotary frequency converter

The instantaneous voltages of the three-phase- and single-phase terminals are presented in Fig. 6.16. The frequency conversion from 50 Hz three-phase voltage in Fig. 6.16a to $16^2/_3$ Hz single-phase voltage in Fig. 6.16b is observed. These frequency levels are presented for clarity in Fig. 6.17.

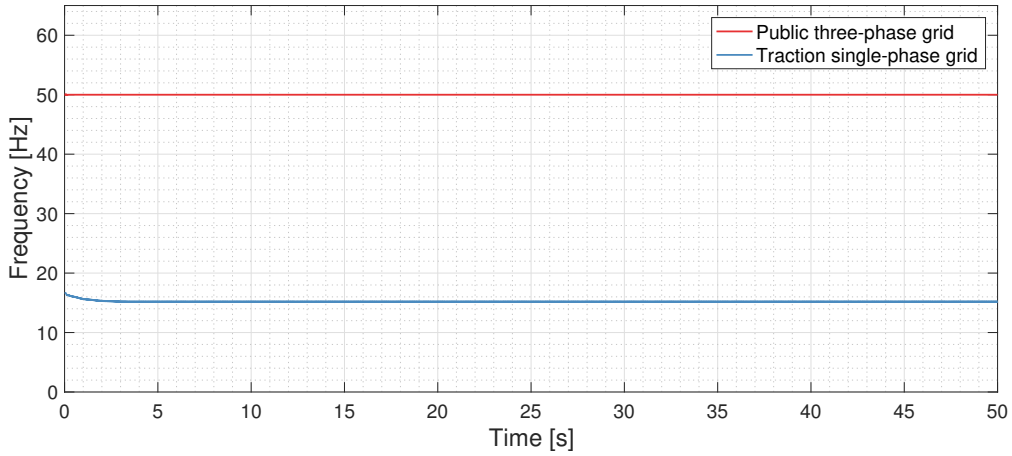

Figure 6.17: Frequency at the rotary converter terminals

The electromagnetic power induced by the three-phase synchronous motor, TPSM, and the equivalent single-phase synchronous generator, SPSG, is presented in Fig. 6.18.

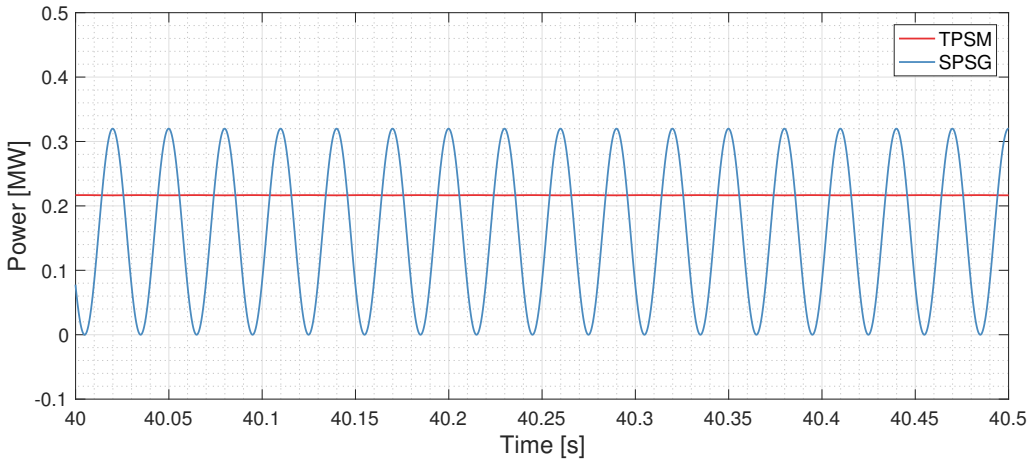

Figure 6.18: Active power at rotary converter terminals

The single-phase power in Fig. 6.18 is fed to a resistance of 100 Ω. The power is pulsating at frequency $33^1/_3$ Hz, twice single-phase voltage frequency. The pulsation of single-phase synchronous generator induced power is also observed in the field current of the generator's field circuit, observed in Fig. 6.19.

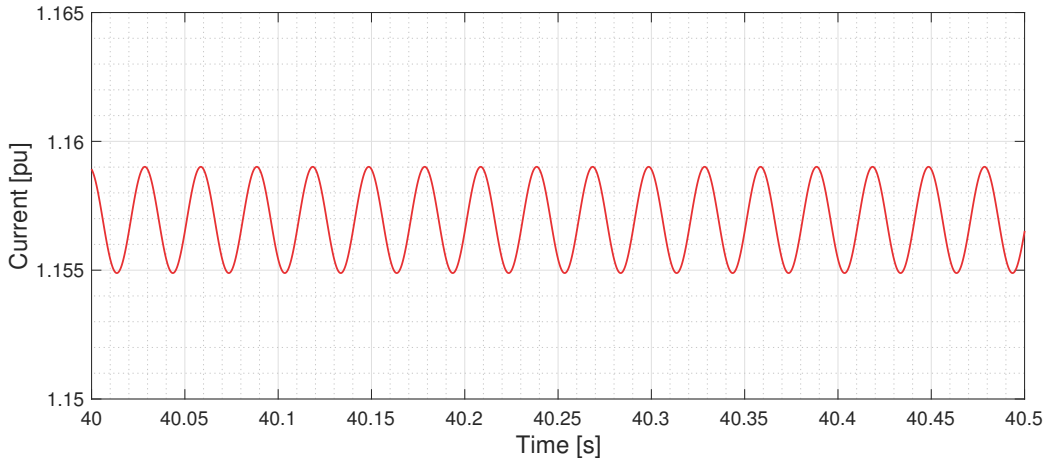

Figure 6.19: Field current for the single-phase synchronous generator

The field circuit is applied a constant terminal field voltage, and a DC field current induces the rotor field of the machine. The additional $33^1/_3$ Hz oscillation observed in Fig. 6.19 is a consequence of the pulsating power, inducing second harmonic currents in the rotor circuits. Since the machine's steady-state performance involves a pulsating power, the rotor circuits experience steady-state induced second harmonic currents. This causes the damper bars of the single-phase machine to be constructed larger than those of three-phase synchronous machines at same rated conditions. The effects of pulsating power of single-phase machines were presented in Chapter 4.

6.4.2 Converter Behaviour during Short-Circuited Terminals

The following section presents the rotary converter's performance during a short-circuit fault applied to the single-phase terminals at the traction grid side of the converter. The fault is carried out during zero terminal voltage crossing for obtaining the maximum DC-offset component to each asymmetrical short circuit fault current. The fault situation is presented in Fig. 6.20.

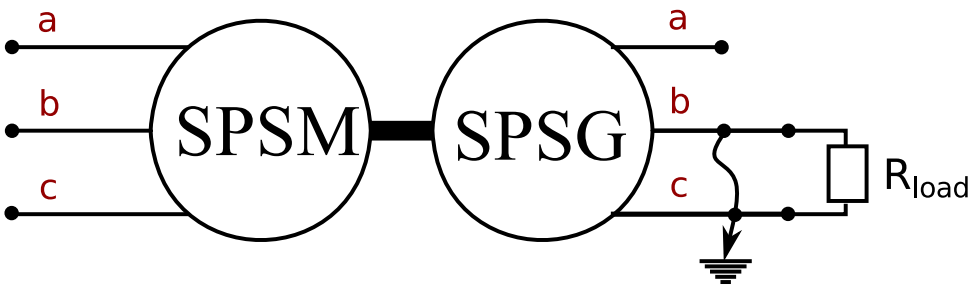

Figure 6.20: Rotary frequency converter with short-circuited single-phase terminals

Tab. 6.1 presents three different sets of parameters for the single-phase synchronous generator.

Table 6.1: Comparison of original-, old- and new obtained parameters for the single-phase synchronous machine

Parameter	**Unit**	**Original**	**Old**	**New**
r_S - Armature resistance	pu	0.0018	0.000875	0.000875
x_{ls} - Leakage inductance -	pu	0.096	0.0480	0.0480
x_d - d-axis synchronous inductance	pu	1.02	0.3560	0.3560
$x_d^{'}$ - d-axis transient inductance	pu	0.12	0.0708	0.0708
$x_d^{''}$ - d-axis sub-transient inductance	pu	0.1	0.052	0.052
x_q - q-axis synchronous inductance	pu	0.47	0.1727	0.1727
$x_d^{''}$ - q-axis sub-transient inductance	pu	0.11	0.061	0.061
$T_{d0}^{'}$ - d-axis transient open-circuit time constant	s	8.6	8.6	3.0156
$T_{d0}^{''}$ - d-axis sub-transient open-circuit time constant	s	0.08	0.08	0.0767
$T_{q0}^{''}$q-axis sub-transient open-circuit time constant	s	3.4	3.4	1.2182

The "original" parameters are obtained from [44] and presented in Appendix C. They are measured directly based on the single-phase synchronous generator's performance. The "old" parameters are presenting parameter adjustments carried out in [6], where modeling single-phase synchronous machines as three-phase synchronous machines with one open-circuited phase were studied. The "new" parameters are presenting parameter adjustment calculations carried out in Section 5.3. The adjusted parameters are presented in Tab. 5.1.

Fig. 6.21 present three short circuit currents for the fault situation observed in Fig. 6.20. Each fault current belongs to a set of parameters presented in Tab. 6.1 applied to the single-phase synchronous machine model in the rotary converter system. The resulting three short-circuit fault currents for the "new", "old" and "original parameter sets" are presented in Fig. 6.21a, 6.21b and 6.21c, respectively.

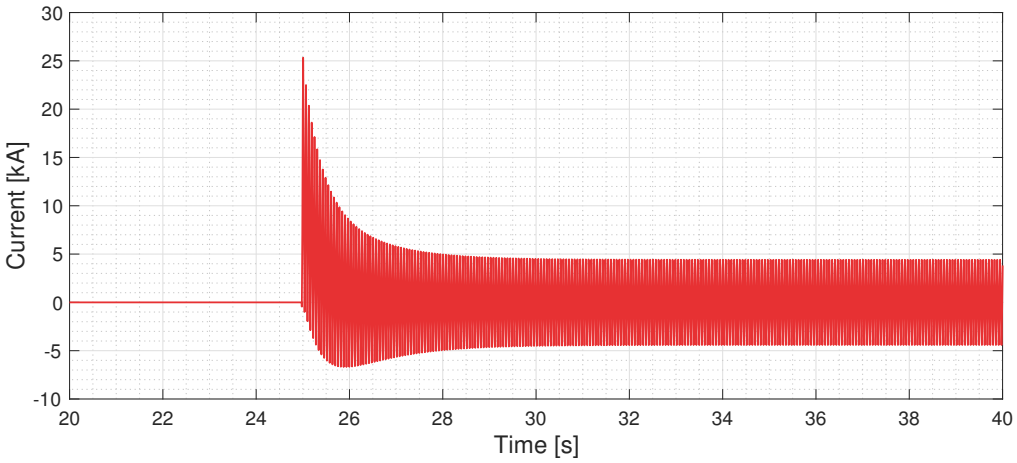

(a) New parameters

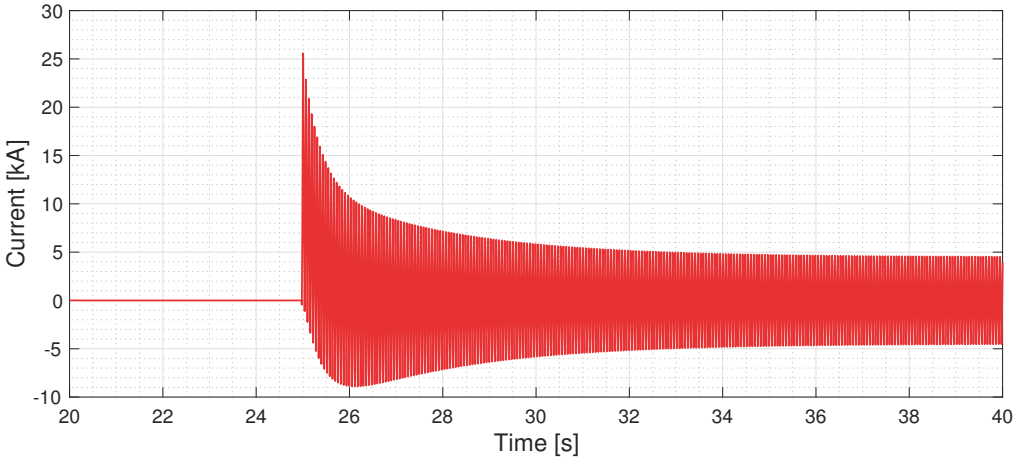

(b) Old parameters

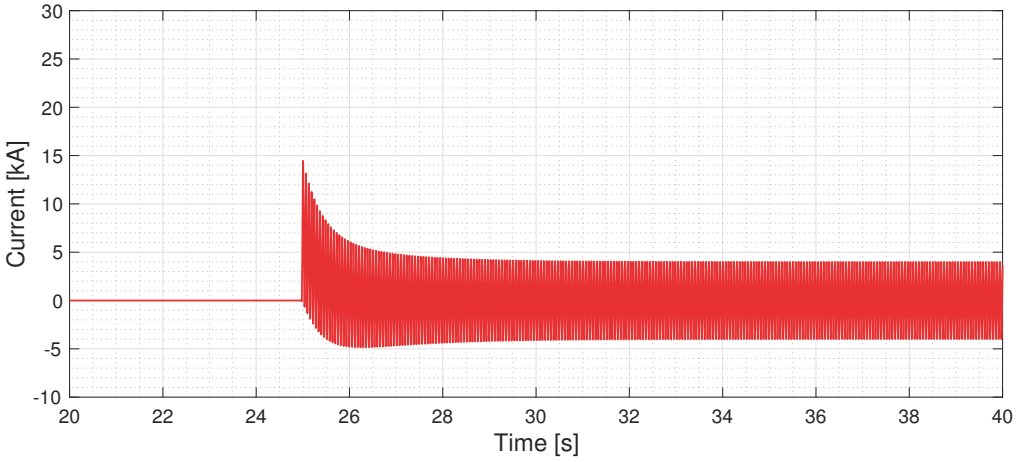

(c) Original parameters

Figure 6.21: Fault currents during short-circuited single-phase generator terminals

The asymmetrical short-circuit currents presented in Fig. 6.21 contains AC- and DC current components. The DC current components are obtained from the asymmetrical short-circuit currents by locating all local maximum- and minimum values and calculating the difference between the two sets of local extrema points.

$$i_{DC}(t) = |i_{max}(t)| - |i_{min}(t)|$$

The DC-offset components for the three short-circuit currents observed in Fig. 6.21 are presented in Fig. 6.22.

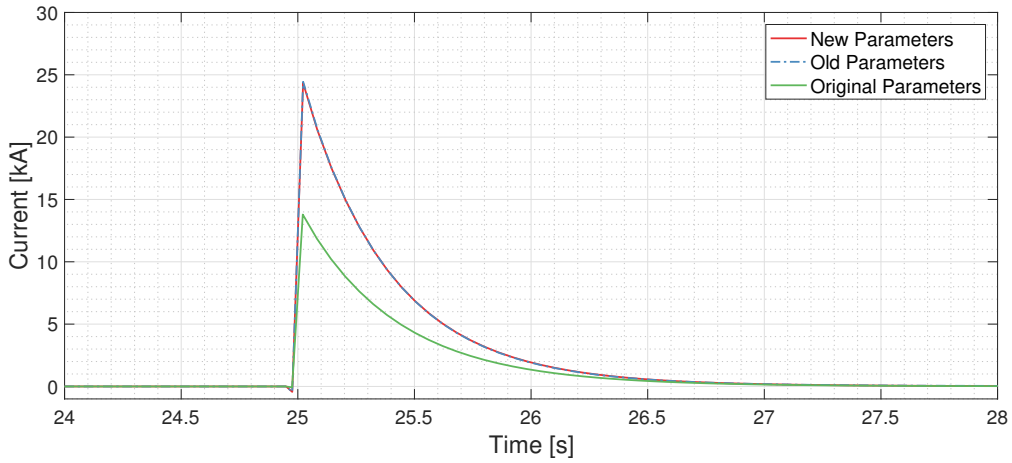

Figure 6.22: Fault currents DC-offset during short-circuited single-phase generator terminals

The new and old parameters include the same steady state-, transient and sub-transient reactances and armature resistance. The DC-offset fault current decays with the armature time constant, T_a, that is determined by the reactances and resistance of the armature phase-windings. The decay of DC-offset current for the models applying "new" and "old" parameters are therefore the same, while the model applying "old" parameters experiences a slower DC-offset decay.

The symmetrical fault currents are obtained by subtracting the DC-offset components of the short-circuit currents presented in Fig. 6.22 from the initial asymmetrical short-circuit currents presented in Fig. 6.21. The three symmetrical instantaneous short-circuit fault currents are presented in Fig. 6.23a. The local maxima values of these currents are extracted from the symmetrical current and presented in Fig. 6.23b for clarifying the peak values for each short-circuit fault current.

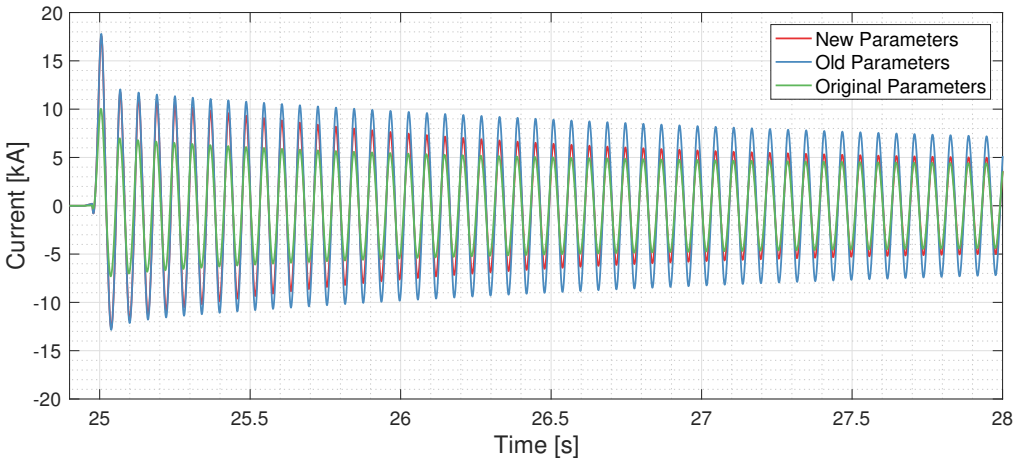

(a) Instantaneous symmetrical fault currents

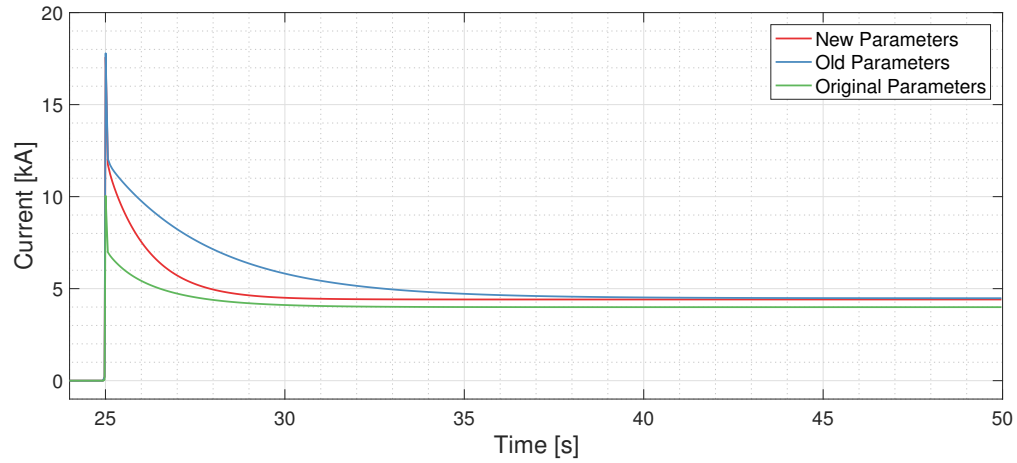

(b) Peak symmetrical fault currents

Figure 6.23: Symmetrical fault currents during short-circuited single-phase generator terminals

The transient- and sub-transient open-circuit time constants are different for the "new" and "old" sets of parameters. The decrement of current experienced during the sub-transient- and transient time regimes are therefore different for the models applying the two sets of parameters. This is observed in Fig. 6.23b, where the decay of symmetrical current is more rapid for the model applying the "new" set of parameters, compared to the one using the "old" set of parameters. This is a consequence of the "new" time constant being smaller than those presented in the "old" set of parameters.

6.5 Evaluation of Results for Three Rotary Frequency Converter Models

Simulation results for three rotary converter models are presented in Section 6.2, 6.3 and 6.4, respectively. Each model is applying different modeling techniques for presenting the time-domain related behavior of the single-phase synchronous generator. A direct comparison between results from the different converter models is not carried out due to the unstable test results obtained for Model 1 and the unsuccessful simulation of Model 2. Model 3 of the single-phase synchronous generator is the only model that returns rotary converter time-domain related behavior as expected.

The test results of Model 1 and Model 3 rotary converter are in the following compared. Only the fundamental behavior of both converters are viewed, as the Model 1 test results present an unstable steady state performance. Both converter model 1 and 3 experience a pulsating electromagnetic power on the single-phase converter side, as presented in Fig. 6.7 and 6.18, respectively. This is expected for the single-phase system and was presented in Chapter 4 as a pulsating single phase-winding's MMF distribution. It is noted that the frequency of the oscillations for Model 1 is larger than the converter's nominal frequency.

The rotor currents for the single-phase generators in both models present the pulsating power's effect on the field- and damper currents. The fact that second harmonic rotor currents are induced when a synchronous machine experiences power pulsating at twice fundamental frequency was presented in Chapter 4. The rotor currents oscillate at the same frequency as the induced powers in Model 1 and 3, as observed in Fig. 6.8 and 6.19.

The behavior presented by model 3 is as expected for single-phase synchronous machines. The fault current obtained by applying the three parameters sets presented for the short-circuit case study in Section 6.4 are presented in Fig. 6.23. The parameter adjustments presented in Section 5.3 results in a faster rate of decay for symmetrical fault current than the ones based on parameters obtained in previous work.

Chapter 7

Conclusion

7.1 Summary and Concluding Remarks

The work presented in this Master's Thesis contributes to describing approaches for modeling the single-phase synchronous machine for rotary frequency converters in the Norwegian traction power system.

Three different model approaches related to instantaneous time-domain simulations of synchronous-synchronous rotary frequency converters are suggested. In all three models, a three-phase synchronous machine is applied based on the classical Park's equation for three-phase machines.

Model 1 presents a single-phase synchronous machine described by developed sets of equations dealing with the machine's phase quantities. Two reference frames are applied when dealing with the machine equations, the armature reference frame that is stationary and the rotor reference frame rotating aligned with the rotor. No attempts are made to transform the quantities related to two reference frames to one common reference frame. Equations describing the voltage balance in armature- and rotor circuits, and equations describing the machine's magnetic coupling are developed. A consideration when developing the machine's magnetic coupling is the rotor angle dependent inductance matrix. The dependency causes large rotor angle dependent expressions when calculating the machine currents. Machine power is calculated based on terminal armature voltage and current.

Model 2 presents a single-phase synchronous machine described by sets of equations for two fictitious three-phase synchronous machines. Each fictitious machine induces one resultant armature MMF distribution, rotating at synchronous speed in counterclockwise- and clockwise direction. The two machines are presented individually, and no magnetic coupling occurs between the two machines' armature windings. The two sets of equations, describing voltage balance and armature magnetic

coupling for each fictitious machine, are transformed to a common rotor reference frame. The armature magnetic coupling equations are decreased by factors for representing each rotating MMF distribution's magnitude. The armature magnetic coupling equations for both fictitious machines are combined when developing the rotor magnetic coupling of the single-phase machine. The armature magnetic coupling of the clockwise rotating fictitious machine of model 2 will experience rotor angle dependency. Large rotor angle dependent expressions are therefore obtained when calculating the single-phase machine's currents. Machine power is calculated based on the air-gap power obtained for both fictitious machines.

Model 3 presents a single-phase synchronous machine as a three-phase synchronous machine with one open-circuited phase. Load is connected between the remaining two phases. The single-phase synchronous machine's reactances and time constants are adjusted by comparing single-phase machine behavior to the behavior of the three-phase synchronous machine with one open-circuited phase.

Test results when implementing the three rotary converter models have given varying results. Model 1 presents an unstable converter performance. The converter experiences large initial disturbances, and are unable to obtain synchronous behavior.

Model 2 has not been successfully simulated, and the converging simulation solutions have not been obtained.

Model 3 presents test results as expected for a rotary converter. Three-phase 50 Hz voltage is applied at the synchronous motor terminals, and single-phase voltage at $16^2/_3$ Hz are generated at generator terminals. Parameters obtained in Section 5.3 for the equivalent single-phase machine represents a faster rate of decay in the sub-transient- and transient time regimes compared to parameters obtained in previous work.

7.2 RECOMMENDATION FOR FURTHER WORK

The work presented in this Master's Thesis has not been able to conclude in any way regarding instantaneous time-domain related modeling of single-phase synchronous machines. Recommendations for further work are presented below:

- Model 1 has not been initialized correctly, and stable conditions have not been obtained. Work regarding initializing the three-phase motor and single-phase generator is necessary for obtaining synchronous operation for the converter.
- Converging simulation solutions for Model 2 have not been obtained. Work regarding the

implementation of equations for Model 2, presented in this Master's Thesis, should be continued for obtaining possible simulation results.

- Rotary converter measurements should be obtained for enabling a comparison between obtained results for Model 3 and real-life measurements. An analysis based on the expected current decay during short-circuited terminals is then possible to carry out.
- Models should be obtained taking the effect of machine saturation into account. This has been neglected for all three modeling methods implemented in this Master's Thesis.

References

[1] The Voice of European Railways and The International Union of Railways. “Rail Transport and Environment - Facts and Figures”. Oct. 2015.

[2] L. Abrahamsson, T. Schütte, and S. Östlund. “Use of Converters for Feeding of AC Railways for all Frequencies”. In: *Energy for Sustainable Development* (Aug. 2012).

[3] Jernbaneverket. *Slik fungerer jernbanen - En presentasjon av trafikksystements infrastruktur*. 1st ed. Jernbaneverket, 2011.

[4] Bane NOR. *Generell beskrivelse av kontaktledningsannlegg*. 2012. URL: `http://www.jernbanekompetanse.no/wiki/Generell_beskrivelse_av_kontaktledningsanlegg` (visited on 02/06/2018).

[5] A. Steimel. *Electric Traction - Motive Power and Energy Supply - Basics and Practical Experience*. 1st ed. Oldenbourg Industrieverlag, 2008.

[6] G. M. Solberg. “Model of Single-Phase Synchronous Machine for Rotary Frequency Converter”. Project Thesis. NTNU, Dec. 2017.

[7] T. Stoltze. “Dynamiches Verhalten von Synchron-Synchron-Umformern”. PhD thesis. Hochschule für Verkehrswesen Dresden, July 1992.

[8] E. J. Jenssen. “Model of Single-Phase Synchronous Machine for Rotary Frequency Converter”. Master’s Thesis. NTNU, June 2016.

[9] B. L. Robertson and T. A. Rogers. “Performance of the Single-Phase Synchronous Machine”. In: *Transactions of the American Institute of Electrical Engineers* 67.1 (Jan. 1948), pp. 194–196.

[10] W. L. Waters. “Modern Development in Single-Phase Generators”. In: *Proceedings of the American Institute of Electrical Engineers* 27.5 (May 1908), pp. 579–586.

[11] G. Mûller and B. Ponick. *Theorie Elektrischer Machinen*. 6th ed. Wiley-VCH Verlag, 2009.

[12] I. A. Terry and B. L. Robertson. “Single-Phase Synchronous Machine”. In: *Transactions of the American Institute of Electrical Engineers* 67.1 (Jan. 1948), pp. 186–193.

[13] D. P. Kothari and I. J. Nagrath. *Electric Machines*. 4th ed. McGraw-Hill, 2010.

[14] G. McPhereson and R. Laramore. *An Introduction to Electrical Machines and Transformers*. 2nd ed. John Wiley and Sons, 1990.

[15] D. Mohammadi. “Dynamic Modeling of Single-Phase Induction Motor Loads”. Master’s Thesis. Boise State University, Aug. 2012.

[16] E. Sorrentino and S. Fernandez. “Comparison of Six Steady-State Models for Single-Phase Induction Motors”. In: *IET Electric Power Applications* 5.8 (Oct. 2011), pp. 611–617.

[17] F. W. Suhr. “Symmetrical Components as Applied to the Single-Phase Induction Motor”. In: *Electrical Engineering* 64.12 (Dec. 1945), pp. 958–958.

[18] B. Lesieutre, D. Kosterev, and J. Undrill. “Phasor Modeling Approach for Single Phase A/C Motors”. In: *2008 IEEE Power and Energy Society General Meeting - Conversion and Delivery of Electrical Energy in the 21st Century*. Aug. 2008, pp. 1–7.

[19] A. M. Stankovic, B. C. Lesieutre, and T. Aydin. “Modeling and Analysis of Single-Phase Induction Machines with Dynamic Phasors”. In: *IEEE Transactions on Power Systems* 14.1 (Feb. 1999), pp. 9–14.

[20] P. L. Alger. “The Dilemma of Single-Phase Induction Motor Theory”. In: *Transactions of the American Institute of Electrical Engineers. Part III: Power Apparatus and Systems* 77.3 (Apr. 1958), pp. 1045–1053.

[21] S. Singla, J. Srivastava, and D. Blandina. “Obtaining Maximum Torque Operation of Single Phase Induction Motor using Simulation Technique of MATLAB”. In: *2014 Innovative Applications of Computational Intelligence on Power, Energy and Controls with their impact on Humanity (CIPECH)*. Nov. 2014, pp. 304–309.

[22] N. Mohan. *Advanced electric drives - Analysis, Control and Modeling using MATLAB and Simulink*. 1st ed. John Wiley and Sons, 2014.

[23] P. S. Bimbhra. *Generalized Theory of Electrical Machines*. 5th ed. Khanna Publishers, 2015.

[24] S. D. Umans. *Fitzgerald and Kingsley’s Electric Machinery*. 7th ed. McGraw-Hill, 2014.

[25] A. E. Fitzgerald, C. Kingsley, and S. D. Umans. *Fitzgerald and Kingsley’s Electric Machinery*. 5th ed. McGraw-Hill, 1990.

[26] S. J. Chapman. *Electric Machinery Fundamentals*. 5th ed. McGraw-Hill, 2012.

[27] P. C. Sen. *Principles of Electric Machines and Power Electronics*. 3rd ed. John Wiley and Sons, 2014.

[28] P. S. Bimbhra. *Electrical Machinery*. 7th ed. Khanna Publishers, 2014.

[29] C. M. Ong. *Dynamic Simulation of Electric Machinery - Using MATLAB/Simulink*. 1st ed. Prentice Hall PTR, 1998.

[30] P. C. Krause, O. Wasynczuk, and S. D. Sudhoff. *Analysis of Electric Machinery and Drive Systems*. 7th ed. Wiley Inter-science, 2002.

[31] B. K. Kumar. *Power System Stability and Control*. 1st ed. Department of Electrical Engineering, Indian Institute of Technology Madras, Chennai, India, 2012.

[32] P. Kundur. *Power System Stability and Control*. 1st ed. McGraw-Hill, 1994.

[33] A. Fransua and R. Mâgureanu. *Electrical Machines and Drive Systems*. 1st ed. The Technical Press, 1984.

[34] J. Machowski, J. W. Bialek, and J. R. Bumby. *Power System Dynamics - Stability and Control*. 2nd ed. John Wiley and Sons, 2008.

[35] D. P. Sen Gupta and J. W. Lynn. *Electrical Machine Dynamics*. 1st ed. The Macmillan Press, 1980.

[36] B. Adkins. *The General Theory of Electrical Machines*. 1st ed. Chapman and Hall, 1957.

[37] M. Pavella and P. G. Murthy. *Transient Stability of Power Systems - Theory and Practice*. 1st ed. John Wiley and Sons, 1994.

[38] J. D. Glover and M. S. Sarma ans T. J. Overbye. *Power System Analysis and Design*. 5th ed. Cengage Learning, 2012.

[39] G. Andersson. *Dynamica adn Control of Electric Power Systems*. 1tst ed. EEH - Power Systems Laboratory - EEH Zürich, 2012.

[40] D. W. Novotny and T. A. Lipo. *Vector Control and Dynamics of AC Drives*. 3rd ed. Oxford Science Publication, 2000.

[41] Z. Chen, F. Blaabjerg, and F. Iov. "A study of Synchronous Machine Model Implementations in Matlab/Simulink Simulations for New and Renewable Energy Systems". In: *2005 International Conference on Electrical Machines and Systems*. Sept. 2005, pp. 1960–1965.

[42] R. H. Park. "Abridgment of Two-Reaction Theory of Synchronous Machines Generalized Method of Analysis; Part I". In: *Journal of the A.I.E.E.* (1929).

[43] Jernbanedirektoratet. "Jernbanestatistikk 2016". In: *Jernbanestatistikk* (Aug. 2017).

[44] S. Danielsen. "Electric Traction Power System Stability - Low-Frequency Interaction between Advanced Rail Vehicles and a Rotary Frequency Converter". PhD thesis. NTNU, Apr. 2010.

[45] F. H. M. Torgersen. "Kraftsystemutredning". In: *Hovedrapport Bane NOR* (2017).

[46] T. Toftevaag and T. Gjengedal. "Banestrømforsyning - også et aktuelt tema for forskning og utvikling". In: *Seminar om Elektrisk Banestrømforsyning* (1994).

[47] F. Schmid and C. J. Goodman. "Electric Railway Systems in Common Use". In: *6th IET Professional Development Course on Railway Electrification Infrastructure and Systems (REIS 2013)*. June 2013, pp. 1–15.

[48] R. J. Hill. "Electric railway traction. Part 3. Traction power supplies". In: *Power Engineering Journal* (Dec. 1994), pp. 275–286.

[49] C. Heising et al. "Modelling of Rotary Converter in Electrical Railway Traction Power-Systems for Stability Analysis". In: *Electrical Systems for Aircraft, Railway and Ship Propulsion*. Oct. 2010, pp. 1–6.

[50] A. Steimel. "Power-Electronic Grid Supply of AC Railway Rystems". In: *2012 13th International Conference on Optimization of Electrical and Electronic Equipment (OPTIM)*. May 2012, pp. 16–25.

[51] J. Laury and L. Abrahamsson. “Transient Stability Analysis of Low Frequency Railway Grids”. In: *15th International Conference on Railway Engineering Design and Operation (CR 2016)*. Vol. 162. Nov. 2016, pp. 16–25.

[52] Banverket. “Tekniska Data för Roterande Omformare”. Dec. 2007.

[53] T. Toftevaag and M. T. Palsson. “Low-Frequency Oscillations in the Norwegian Electric Traction Power Supply System by Interaction Between the Supply System and Propulsion Machinery . Analysis and Consequences”. In: *7t International Conference "Modern Electric Traction in Integrated XXI st Century Europe"*. Oct. 2005.

[54] O. M. Hanssen. *Referat av Prof. K. Faye-Hansens forelesninger over Synkronmaskiner*. Tapirs Forlag, 1932.

[55] A. Pfeiffer et al. “Modern Rotary Converters for Railway Applications”. In: *Proceedings of the 1997 IEEE/ASME Joint Railroad Conference*. Mar. 1997, pp. 29–33.

[56] S. Danielsen, O. B. Fosso, and T. Toftevaag. “Extended Swing Equation for a Synchronous-Synchronous Rotary Frequency Converter”. Dec. 2008.

Appendix A

Voltage Equations in the Rotating Reference Frame

The set of equations for the armature voltages are presented in (A.1).

$$\begin{bmatrix} v_a \\ v_b \\ v_c \end{bmatrix} = - \begin{bmatrix} R_S & 0 & 0 \\ 0 & R_S & 0 \\ 0 & 0 & R_S \end{bmatrix} \begin{bmatrix} i_a \\ i_b \\ i_c \end{bmatrix} + \frac{d}{dt} \begin{bmatrix} \psi_a \\ \psi_b \\ \psi_c \end{bmatrix} \tag{A.1}$$

The voltages, current and flux linkages are referenced to the rotor by applying the transformation presented in (3.17).

$$\boldsymbol{P^{-1}} \begin{bmatrix} v_d \\ v_q \\ v_0 \end{bmatrix} = - \begin{bmatrix} R_S & 0 & 0 \\ 0 & R_S & 0 \\ 0 & 0 & R_S \end{bmatrix} \boldsymbol{P^{-1}} \begin{bmatrix} i_d \\ i_q \\ i_0 \end{bmatrix} + \frac{d}{dt} (\boldsymbol{P^{-1}} \begin{bmatrix} \psi_d \\ \psi_q \\ \psi_0 \end{bmatrix}) \tag{A.2}$$

The equations are rewritten with an extra term due to the product derivation of $\frac{d}{dt}(\boldsymbol{P^{-1}\psi_{dq0}})$, as presented in (A.3)

$$\boldsymbol{P^{-1}} \begin{bmatrix} v_d \\ v_q \\ v_0 \end{bmatrix} = - \begin{bmatrix} R_S & 0 & 0 \\ 0 & R_S & 0 \\ 0 & 0 & R_S \end{bmatrix} \boldsymbol{P^{-1}} \begin{bmatrix} i_d \\ i_q \\ i_0 \end{bmatrix} + \frac{d}{dt} (\boldsymbol{P^{-1}}) \begin{bmatrix} \psi_d \\ \psi_q \\ \psi_0 \end{bmatrix} + \boldsymbol{P^{-1}} \frac{d}{dt} (\begin{bmatrix} \psi_d \\ \psi_q \\ \psi_0 \end{bmatrix}) \tag{A.3}$$

(A.3) is multiplied with $\boldsymbol{P}$ and presented in (A.4).

$$\boldsymbol{P}\boldsymbol{P}^{-1}\begin{bmatrix} v_d \\ v_q \\ v_0 \end{bmatrix} = -\boldsymbol{P}\begin{bmatrix} R_S & 0 & 0 \\ 0 & R_S & 0 \\ 0 & 0 & R_S \end{bmatrix}\boldsymbol{P}^{-1}\begin{bmatrix} i_d \\ i_q \\ i_0 \end{bmatrix} + \boldsymbol{P}\frac{d}{dt}(\boldsymbol{P}^{-1})\begin{bmatrix} \psi_d \\ \psi_q \\ \psi_0 \end{bmatrix} + \boldsymbol{P}\boldsymbol{P}^{-1}\frac{d}{dt}(\begin{bmatrix} \psi_d \\ \psi_q \\ \psi_0 \end{bmatrix}) \tag{A.4}$$

The time derivative of the inverse Park's matrix are presented in (A.5).

$$\begin{aligned} \frac{d}{dt}(\boldsymbol{P}^{-1}) &= \frac{d}{dt}(\theta_d)\begin{bmatrix} -\sin(\theta_d) & -\cos(\theta_d) & 0 \\ -\sin(\theta_d - \frac{2\pi}{3}) & -\cos(\theta_d - \frac{2\pi}{3}) & 0 \\ -\sin(\theta_d - \frac{4\pi}{3}) & -\cos(\theta_d - \frac{4\pi}{3}) & 0 \end{bmatrix} \\ &= \omega_r \begin{bmatrix} -\sin(\theta_d) & -\cos(\theta_d) & 0 \\ -\sin(\theta_d - \frac{2\pi}{3}) & -\cos(\theta_d - \frac{2\pi}{3}) & 0 \\ -\sin(\theta_d - \frac{4\pi}{3}) & -\cos(\theta_d - \frac{4\pi}{3}) & 0 \end{bmatrix} \end{aligned} \tag{A.5}$$

The resulting set of voltage equations are presented in (A.6).

$$\begin{bmatrix} v_d \\ v_q \\ v_0 \end{bmatrix} = -\begin{bmatrix} R_s & 0 & 0 \\ 0 & R_s & 0 \\ 0 & 0 & R_s \end{bmatrix}\begin{bmatrix} i_d \\ i_q \\ i_0 \end{bmatrix} + \frac{d}{dt}\begin{bmatrix} \psi_d \\ \psi_q \\ \psi_0 \end{bmatrix} + \omega_r \begin{bmatrix} 0 & -1 & 0 \\ 1 & 0 & 0 \\ 0 & 0 & 0 \end{bmatrix}\begin{bmatrix} \psi_d \\ \psi_q \\ \psi_0 \end{bmatrix} \tag{A.6}$$

Appendix B

Flux Linkages in the Rotating Reference Frame

The magnetic coupling of a three-phase synchronous machine are described by appreciating the relationship between machine currents and inductances. By applying (3.10) the total magnetic coupling of the machine can be presented as shown in (B.1).

$$\begin{bmatrix} \psi_a \\ \psi_b \\ \psi_c \\ \psi_f \\ \psi_D \\ \psi_Q \end{bmatrix} = \begin{bmatrix} \boldsymbol{L_S} & \boldsymbol{L_{SR}} \\ \boldsymbol{L_{SR}^T} & \boldsymbol{L_R} \end{bmatrix} \cdot \begin{bmatrix} -i_a \\ -i_b \\ -i_c \\ i_f \\ i_D \\ i_Q \end{bmatrix} \tag{B.1}$$

The armature flux linkages presented in (B.1), ψ_a, ψ_b and ψ_c, are referenced to the stationary armature windings. The rotor flux linkages, ψ_f, ψ_D and ψ_Q, are referenced to the rotor. The armature flux linkages are transformed to rotor reference by applying Park's matrix (3.15)

$$\begin{bmatrix}\psi_a\\ \psi_b\\ \psi_c\end{bmatrix} = -\underbrace{\begin{bmatrix} L_{ls}+L_{ss0}-L_{ssP}\cos(2\theta_d) & -L_{s1s2}-L_{ssP}\cos(2(\theta_d+\frac{\pi}{6})) & -L_{s1s2}-L_{ssP}\cos(2(\theta_d+\frac{5\pi}{6}))\\ -L_{s1s2}-L_{ssP}\cos(2(\theta_d+\frac{\pi}{6})) & L_{ls}+L_{ss0}-L_{ssP}\cos(2(\theta_d-\frac{2\pi}{3})) & -L_{s1s2}-L_{ssP}\cos(2(\theta_d-\frac{\pi}{2}))\\ -L_{s1s2}-L_{ssP}\cos(2(\theta_d+\frac{5\pi}{6})) & -L_{s1s2}-L_{ssP}\cos(2(\theta_d-\frac{\pi}{2})) & L_{ls}+L_{ss0}-L_{ssP}\cos(2(\theta_d-\frac{4\pi}{3}))\end{bmatrix}}_{\boldsymbol{L_S}} \cdot \begin{bmatrix}i_a\\ i_b\\ i_c\end{bmatrix}$$
$$+\underbrace{\begin{bmatrix} L_{sfP}\cos(\theta_d) & M_{sDP}\cos(\theta_d) & -L_{sQP}\sin(\theta_d)\\ L_{sfP}\cos(\theta_d-\frac{2\pi}{3}) & L_{sDP}\cos(\theta_d-\frac{2\pi}{3}) & -L_{sQP}\sin(\theta_d-\frac{2\pi}{3})\\ M_{sfP}\cos(\theta_d-\frac{4\pi}{3}) & L_{sDP}\cos(\theta_d-\frac{4\pi}{3}) & -L_{sQP}\sin(\theta_d-\frac{4\pi}{3})\end{bmatrix}}_{\boldsymbol{L_{SR}}} \cdot \begin{bmatrix}i_f\\ i_D\\ i_Q\end{bmatrix} \tag{B.2}$$

The flux linkages and current are all referenced to rotor by applying the transformation presented in (3.17).

$$\boldsymbol{P^{-1}}\begin{bmatrix}\psi_d\\ \psi_q\\ \psi_0\end{bmatrix} = -\boldsymbol{L_S P^{-1}}\begin{bmatrix}i_d\\ i_q\\ i_0\end{bmatrix} + \boldsymbol{L_{SR}}\begin{bmatrix}i_f\\ i_D\\ i_Q\end{bmatrix} \tag{B.3}$$

(B.3) is further on multiplied with $\boldsymbol{P}$, and the resulting equation is presented in (B.4).

$$\boldsymbol{PP^{-1}}\begin{bmatrix}\psi_d\\ \psi_q\\ \psi_0\end{bmatrix} = -\boldsymbol{PL_S P^{-1}}\begin{bmatrix}i_d\\ i_q\\ i_0\end{bmatrix} + \boldsymbol{PL_{SR}}\begin{bmatrix}i_f\\ i_D\\ i_Q\end{bmatrix} \tag{B.4}$$

The new inductance matrices are presented in (B.5) and (B.8).

$$\boldsymbol{PL_S P^{-1}} = -\begin{bmatrix} L_{ls}+L_{ss0}+L_{s1s2}+\frac{3}{2}L_{ssP} & 0 & 0\\ 0 & L_{ls}+L_{ss0}+L_{s1s2}-\frac{3}{2}L_{ssP} & 0\\ 0 & 0 & L_{ls}+L_{ss0}-2L_{s1s2}\end{bmatrix} \tag{B.5}$$

The magnetizing inductances are defined as (B.6a) and (B.6b) and the rotor referenced stator inductance matrix is therefore equal to (B.7).

$$L_{md} = \frac{3}{2}(L_{ss0}+L_{ssP}) \tag{B.6a}$$

$$L_{mq} = \frac{3}{2}(L_{ss0} - L_{ssP}) \tag{B.6b}$$

$$\begin{bmatrix} L_d & 0 & 0 \\ 0 & L_q & 0 \\ 0 & 0 & L_0 \end{bmatrix} = \begin{bmatrix} L_{ls} + L_{md} & 0 & 0 \\ 0 & L_{ls} + L_{mq} & 0 \\ 0 & 0 & L_0 \end{bmatrix} \tag{B.7}$$

$$\boldsymbol{PL_{SR}} = \begin{bmatrix} L_{SfP} & L_{SDP} & 0 \\ 0 & 0 & L_{SQP} \\ 0 & 0 & 0 \end{bmatrix} \tag{B.8}$$

The rotor flux linkages are given as (B.9).

$$\begin{aligned} \begin{bmatrix} \psi_f \\ \psi_D \\ \psi_Q \end{bmatrix} = &- \underbrace{\begin{bmatrix} L_{sfP}\cos(\theta_d) & M_{sDP}\cos(\theta_d) & -L_{sQP}\sin(\theta_d) \\ L_{sfP}\cos(\theta_d - \frac{2\pi}{3}) & L_{sDP}\cos(\theta_d - \frac{2\pi}{3}) & -L_{sQP}\sin(\theta_d - \frac{2\pi}{3}) \\ M_{sfP}\cos(\theta_d - \frac{4\pi}{3}) & L_{sDP}\cos(\theta_d - \frac{4\pi}{3}) & -L_{sQP}\sin(\theta_d - \frac{4\pi}{3}) \end{bmatrix}^T}_{\boldsymbol{L_{SR}^T}} \begin{bmatrix} i_a \\ i_b \\ i_c \end{bmatrix} \\ &+ \underbrace{\begin{bmatrix} L_{ff} & L_{fD} & 0 \\ L_{fD} & L_{DD} & 0 \\ 0 & 0 & L_{QQ} \end{bmatrix}}_{\boldsymbol{L_R}} \begin{bmatrix} i_f \\ i_D \\ i_Q \end{bmatrix} \end{aligned} \tag{B.9}$$

The armature currents are transformed to rotor reference by applying (3.17).

$$\begin{bmatrix} \psi_f \\ \psi_D \\ \psi_Q \end{bmatrix} = -\boldsymbol{L_{SR}^T P^{-1}} \begin{bmatrix} i_d \\ i_q \\ i_0 \end{bmatrix} + \boldsymbol{L_R} \begin{bmatrix} i_f \\ i_D \\ i_Q \end{bmatrix} \tag{B.10}$$

The new inductance matrix $\boldsymbol{L_{SR}^T P^{-1}}$ is presented in (B.11).

$$\begin{bmatrix} \frac{3}{2}L_{sfP} & 0 & 0 \\ \frac{3}{2}L_{sDP} & 0 & 0 \\ 0 & \frac{3}{2}L_{sQP} & 0 \end{bmatrix} \tag{B.11}$$

The final flux linkage transformed to rotor reference are presented in (B.12).

$$\begin{bmatrix} \psi_d \\ \psi_q \\ \psi_0 \\ \psi_f \\ \psi_D \\ \psi_Q \end{bmatrix} = \begin{bmatrix} \boldsymbol{PL_S P^{-1}} & \boldsymbol{PL_{SR}} \\ \boldsymbol{L_{SR}^T P^{-1}} & \boldsymbol{L_R} \end{bmatrix} \cdot \begin{bmatrix} i_d \\ i_q \\ i_0 \\ i_f \\ i_D \\ i_Q \end{bmatrix} \tag{B.12}$$

The final inductance matrix is presented in (B.13), applying a common per unit base for both stator- and rotor referenced currents.

$$\begin{bmatrix} \boldsymbol{PL_S P^{-1}} & \boldsymbol{PL_{SR}} \\ \boldsymbol{L_{SR}^T P^{-1}} & \boldsymbol{L_R} \end{bmatrix} = \begin{bmatrix} L_d & 0 & 0 & L_{md} & L_{md} & 0 \\ 0 & L_q & 0 & 0 & 0 & L_{mq} \\ 0 & 0 & L_0 & 0 & 0 & 0 \\ L_{md} & 0 & 0 & L_{ff} & L_{md} & 0 \\ L_{md} & 0 & 0 & L_{md} & L_{DD} & 0 \\ 0 & L_{mq} & 0 & 0 & 0 & L_{QQ} \end{bmatrix} \tag{B.13}$$

Appendix C

Calculating Parameters for the Single-Phase Synchronous Generator

Table C.1: Single-phase synchronous generator's rated conditions [44]

Parameter	**Unit**	**Value**
S_N - Rated power	MVA	4.0
V_N - Rated voltage	kV	4.0
f_N - Nominal frequency	Hz	$16^2/_3$
H - Inertia constant	MWs/MVA	1.87

Table C.2: Single-phase synchronous generator's parameters [44]

Parameter	**Unit**	**Value**
r_S - Armature resistance	pu	0.0018
x_{ls} - Armature leakage reactance	pu	0.0960
x_d - d-axis synchronous reactance	pu	1.0200
$x_d^{'}$ - d-axis transient reactance	pu	0.1200
$x_d^{''}$ - d-axis subtransient reactance	pu	0.1000
x_q - q-axis synchronous reactance	pu	0.4700
$x_q^{'}$ - q-axis transient reactance (=x_q)	pu	0.4700
$x_q^{''}$ - q-axis subtransient reactance	pu	0.1100
$T_{d0}^{'}$ - d-axis transient open-circuit time constant	s	8.6000
$T_{d0}^{''}$ - d-axis subtransient open-circuit time constant	s	0.0800
$T_{q0}^{''}$ - q-axis subtransient open-circuit time constant	s	3.4000

The following calculations are based on Chapter 3, and are carried out as for a three-phase synchronous machine.

Per unit reactances are defined as the the reactance divided by a base impedance value as presented in (C.1).

$$x_{pu} = \frac{X}{Z_{base}} \tag{C.1}$$

By appreciating that a purely inductive system contains a base impedance equal to $2\pi f_{base} L_{base}$ and that if f_{base} equals the frequency, then the per unit value of the reactance equals the per unit value of the inductance. This is presented in (C.2) [32].

$$x_{pu} = \frac{2\pi f L}{2\pi f_{base} L_{base}} = \frac{L}{L_{base}} = L_{pu} \tag{C.2}$$

The per unit reactances presented in Table C.2 are therefore equal to their respective per unit inductances.

The magnetizing inductance for the d- and q-axis are

$$L_{md} = L_d - L_{ls} = 1.020 - 0.096 = 0.924$$
$$L_{mq} = L_q - L_{ls} = 0.470 - 0.096 = 0.374$$

The constant term of the self inductance of an armature winding and the peak of the self inductance's second harmonic term is assumed to be

$$L_{ss0} = \frac{L_d + L_q}{2} = \frac{1.020 + 0.470}{2} = 0.745$$

$$L_{ssP} = \frac{L_d - L_q}{2} = \frac{1.020 - 0.470}{2} = 0.2750$$

The assumption here is based on the fact that $L_d > L_q$. When the rotor rotates, the maximum self inductance of the winding occurs when the rotor field is aligned with the magnetic axis of the armature winding. The d-axis synchronous inductance is defined as the inductance for this situation. The minimum self inductance of the winding occurs when the rotor field is 90 electrical degrees away from the winding's magnetic axis. The q-axis synchronous inductance is defined as the inductance for this

situation.

The self inductance of the field winding is calculated based on (3.29)

$$L_{ff} = \frac{L_{md}^2}{L_d - L_d^{'}} = \frac{0.924^2}{1.020 - 0.135} = 0.9486$$

The leakage inductance of the field winding is calculated by extracting the magnetizing inductance from the winding's self inductance

$$L_{lf} = L_{ff} - L_{md} = 0.9486 - 0.9240 = 0.0246$$

The leakage inductance of the d-axis damper winding is calculated based on (3.29)

$$\begin{aligned} L_{lD} &= \frac{L_{md}L_{lf}(L_d^{''} - L_{ls})}{L_{ls}(L_{md} + L_{lf}) + L_{md}L_{lf} - L_d^{''}(L_{md} + L_{lf})} \\ &= \frac{0.924 \cdot 0.0246(0.096 - 0.12)}{0.12(0.9240 + 0.0246) - 0.096(0.9240 + 0.0246) - 0.924 \cdot 0.0246} \\ &= 0.0048 \end{aligned}$$

The self inductance of the d-axis damper winding equals

$$L_{DD} = L_{lD} + L_{md} = 0.0048 + 0.924 = 0.9288$$

The self inductance of the q-axis damper winding is calculated based on (3.29).

$$L_{QQ} = \frac{L_{mq}^2}{L_q - L_q^{'}} = \frac{0.374^2}{0.47 - 0.11} = 0.3885$$

The leakage inductance of the q-axis damper winding is calculated by extracting the magnetizing inductance from the winding's self inductance

$$L_{lQ} = L_{QQ} - L_{mq} = 0.3885 - 0.374 = 0.0145$$

The field winding resistance, d-axis damper winding resistance and q-axis damper winding resistance are calculated based on (3.31).

$$r_f = \frac{L_{ff}}{T'_{d0}} = \frac{0.9486}{8.6000} = 0.1103$$

$$r_D = \frac{L_{lD} + \frac{L_{md}L_{lf}}{L_{md}+L_{lf}}}{T''_{d0}} = \frac{0.0048 + \frac{0.924 \cdot 0.0246}{0.924+0.0246}}{0.08s} = 0.3600$$

$$r_Q = \frac{L_{QQ}}{T''_{q0}} = \frac{0.3885}{3.4s} = 0.1143$$

Table C.3: Single-phase synchronous generator's calculated parameters

Parameter	**Unit**	**Value**
L_{md} - d-axis magnetizing inductance	pu	0.9240
L_{mq} - q-axis magnetizing inductance	pu	0.3740
L_{lf} - Leakage inductance for field winding	pu	0.0246
L_{lD} - Leakage inductance for d-axis damper winding	pu	0.0048
L_{lQ} - Leakage inductance for q-axis damper winding	pu	0.0145
L_{ss0} - Constant term of armature self inductance	pu	0.7450
L_{ssP} - Amplitude of second harmonic armature self inductance	pu	0.2750
L_{ff} - Self inductance for field winding	pu	0.9486
L_{DD} - Self inductance for d-axis damper winding	pu	0.9288
L_{QQ} - Self inductance for q-axis damper winding	pu	0.3885
r_f - Field winding resistance	pu	0.1103
r_D - d-axis damper winding resistance	pu	0.3600
r_Q - q-axis damper winding resistance	pu	0.1143

Appendix D

Calculating Parameters for the Three-Phase Synchronous Motor

Table D.1: Three-phase synchronous motor's rated conditions [44]

Parameter	Unit	Value
S_N - Rated power	MVA	4.4
V_N - Rated voltage	kV	6.3
f_N - Nominal frequency	Hz	50
H - Inertia constant	MWs/MVA	1.7

Table D.2: Three-phase synchronous motor's parameters [44]

Parameter	Unit	Value
r_S - Armature resistance	pu	0.0033
x_{ls} - Armature leakage reactance	pu	0.1100
x_d - d-axis synchronous reactance	pu	0.9000
$x_d^{'}$ - d-axis transient reactance	pu	0.2400
$x_d^{''}$ - d-axis subtransient reactance	pu	0.1650
x_q - q-axis synchronous reactance	pu	0.4000
$x_q^{'}$ - q-axis transient reactance (=X_q)	pu	0.4000
$x_q^{''}$ - q-axis subtransient reactance	pu	0.3400
$T_{d0}^{'}$ - d-axis transient open-circuit time constant	s	4.000
$T_{d0}^{''}$ - d-axis subtransient open-circuit time constant	s	0.04
$T_{q0}^{''}$ - q-axis subtransient open-circuit time constant	s	0.1

The following calculations are based on Chapter 3, and are carried out as for a three-phase synchronous machine. The calculations are similar as those presented for the single-phase generator in Appendix C.

The magnetizing inductance for the d- and q-axis are

$$L_{md} = L_d - L_{ls} = 0.9000 - 0.1100 = 0.7900$$
$$L_{mq} = L_q - L_{ls} = 0.4000 - 0.1100 = 0.2900$$

The self inductance of the field winding is calculated based on (3.29)

$$L_{ff} = \frac{L_{md}^2}{L_d - L_d^{'}} = \frac{0.7900^2}{0.9000 - 0.2400} = 0.9456$$

The leakage inductance of the field winding is calculated by extracting the magnetizing inductance from the winding's self inductance

$$L_{lf} = L_{ff} - L_{md} = 0.9456 - 0.7900 = 0.1556$$

The field winding resistance is calculated based on (3.31).

$$r_f = \frac{L_{ff}}{T_{d0}^{'}} = \frac{0.9456}{4.0000s} = 0.2364$$

Table D.3: Three-phase synchronous motor's calculated parameters

Parameter	**Unit**	**Value**
L_{md} - d-axis magnetizing inductance	pu	0.7900
L_{mq} - q-axis magnetizing inductance	pu	0.2900
L_{lf} - Leakage inductance for field winding	pu	0.1556
L_{ff} - Self inductance for field winding	pu	0.9456
r_f - Field winding resistance	pu	0.2364

Appendix E

Model 1 - Inverse Inductance Matrix

The following calculation presents the inverse inductance matrix of the single-phase synchronous generator when modeled applying one armature winding together with one field., one d-axis- and one q-axis damper winding. The inverse inductance matrix is presented in (E.1).

$$\boldsymbol{L}^{-1} = \begin{bmatrix} -L_{ss} & L_{sf} & L_{sD} & L_{sQ} \\ -L_{sf} & L_{ff} & L_{fD} & 0 \\ -L_{sD} & L_{fD} & L_{DD} & 0 \\ -L_{sQ} & 0 & 0 & L_{QQ} \end{bmatrix}^{-1} = \begin{bmatrix} a_{11} & a_{12} & a_{13} & a_{14} \\ a_{21} & a_{22} & a_{23} & a_{24} \\ a_{31} & a_{32} & a_{33} & a_{34} \\ a_{41} & a_{42} & a_{43} & a_{44} \end{bmatrix} \tag{E.1}$$

The inverse inductance matrix' elements are presented in (E.2), with their common denominator given by (E.3).

$$
\begin{aligned}
a_{11} &= -\frac{L_{QQ}(L_{DD}L_{ff} - L_{fD}^2)}{A} \\
a_{12} &= \frac{L_{QQ}(L_{DD}L_{sf} - L_{fD}L_{sD})}{A} \\
a_{13} &= -\frac{L_{QQ}(L_{fD}L_{sf} - L_{ff}L_{sD})}{A} \\
a_{14} &= \frac{L_{sQ}(L_{DD}L_{ff} - L_{fD}^2)}{A} \\
a_{21} &= -\frac{L_{QQ}(L_{DD}L_{sf} - L_{fD}L_{sD})}{A} = -a_{12} \\
a_{22} &= \frac{L_{DD}L_{QQ}L_{ss} - L_{DD}L_{sQ}^2 - L_{QQ}L_{sD}^2}{A} \\
a_{23} &= -\frac{L_{QQ}L_{fD}L_{ss} - L_{QQ}L_{sD}L_{sf} - L_{fD}L_{sQ}^2}{A} \\
a_{24} &= \frac{L_{sQ}(L_{DD}L_{sf} - L_{fD}L_{sD})}{A} \\
a_{31} &= \frac{L_{QQ}(L_{fD}L_{sf} - L_{ff}L_{sD})}{A} = -a_{13} \\
a_{32} &= -\frac{L_{QQ}L_{fD}L_{ss} - L_{QQ}L_{sD}L_{sf} - L_{fD}L_{sQ}^2}{A} = a_{23} \\
a_{33} &= \frac{L_{QQ}L_{ff}L_{ss} - L_{QQ}L_{sf}^2 - L_{ff}L_{sQ}^2}{A} \\
a_{34} &= -\frac{L_{sQ}(L_{fD}L_{sf} - L_{ff}L_{sD})}{A} \\
a_{41} &= -\frac{L_{sQ}(L_{DD}L_{ff} - L_{fD}^2)}{A} = -a_{14} \\
a_{42} &= \frac{L_{sQ}(L_{DD}L_{sf} - L_{fD}L_{sD})}{A} = a_{24} \\
a_{43} &= -\frac{L_{sQ}(L_{fD}L_{sf} - L_{ff}L_{sD})}{A} = a_{34} \\
a_{44} &= \frac{L_{DD}L_{ff}L_{ss} - L_{DD}L_{sf}^2 - L_{fD}^2L_{ss} + 2L_{fD}L_{sD}L_{sf} - L_{ff}L_{sD}^2}{A}
\end{aligned}
\tag{E.2}
$$

$$
\begin{aligned}
A = {} & L_{DD}L_{QQ}L_{ff}L_{ss} - L_{DD}L_{QQ}L_{sf}^2 - L_{DD}L_{ff}L_{sQ}^2 - L_{QQ}L_{fD}^2L_{ss} \\
& + 2L_{QQ}L_{fD}L_{sD}L_{sf} - L_{QQ}L_{ff}L_{sD}^2 + L_{fD}^2L_{sQ}^2
\end{aligned}
\tag{E.3}
$$

Appendix F

Model 2 - Inductance Matrix

The inductance matrix $\boldsymbol{L_{dq}}$ presented in the flux linkage equations of (5.37) contains nine 3x3 inductance matrices. These matrices are presented in the following Appendix. (F.1) and (F.2) presents the stator and stator to rotor inductances for the counterclockwise rotating fictitious machine. (F.3) and (F.4) presents the stator and stator to rotor inductances for the clockwise rotating fictitious machine.

$$\boldsymbol{L_{S,dq}^{CCW}} = \begin{bmatrix} L_{ls} + L_{md} & 0 & 0 \\ 0 & L_{ls} + L_{mq} & 0 \\ 0 & 0 & L_0^{CCW} \end{bmatrix} \tag{F.1}$$

$$\boldsymbol{L_{SR,dq}^{CCW}} = \begin{bmatrix} L_{md} & L_{md} & 0 \\ 0 & 0 & L_{mq} \\ 0 & 0 & 0 \end{bmatrix} \tag{F.2}$$

$$\boldsymbol{L_{S,dq}^{CW}} = \begin{bmatrix} L_{ls} + \frac{3}{2}(L_{ss0} + L_{ssP}\cos(4\theta_d)) & -\frac{3}{2}L_{ssP}\sin(4\theta_d) & 0 \\ -\frac{3}{2}L_{ssP}\sin(4\theta_d) & L_{ls} + \frac{3}{2}(L_{ss0} - L_{ssP}\cos(4\theta_d)) & 0 \\ 0 & 0 & L_{ls} \end{bmatrix} \tag{F.3}$$

$$\boldsymbol{L_{SR,dq}^{CW}} = \begin{bmatrix} L_{md}\cos(2\theta_d) & -L_{md}\sin(2\theta_d) & 0 \\ -L_{md}\sin(2\theta_d) & -L_{mq}\cos(2\theta_d) & \\ 0 & 0 & 0 \end{bmatrix} \tag{F.4}$$

Appendix G

Model 2 - Inverse Inductance Matrix

$$\begin{bmatrix} \boldsymbol{L_{S,dq}^{CCW}} & \boldsymbol{L_{SR,dq}^{CCW}} \\ \boldsymbol{(L_{SR,dq}^{CCW})^T} & \boldsymbol{L_R} \end{bmatrix}^{-1} = \begin{bmatrix} a_{11} & a_{12} & a_{13} & a_{14} & a_{15} & a_{16} \\ a_{21} & a_{22} & a_{23} & a_{24} & a_{25} & a_{26} \\ a_{31} & a_{32} & a_{33} & a_{34} & a_{35} & a_{36} \\ a_{41} & a_{42} & a_{43} & a_{44} & a_{45} & a_{46} \\ a_{51} & a_{52} & a_{53} & a_{54} & a_{55} & a_{56} \\ a_{61} & a_{62} & a_{63} & a_{64} & a_{65} & a_{66} \end{bmatrix} \tag{G.1}$$

$$
\begin{aligned}
a_{11} &= -\frac{9(L_{DD}L_{ff} - L_{md}^2)}{L_{DD}L_dL_{ff} - L_{DD}L_{md}^2 - L_dL_{md}^2 - L_{ff}L_{md}^2 + 2L_{md}^3} \\
a_{12} &= 0 \\
a_{13} &= 0 \\
a_{14} &= \frac{3L_{md}(L_{DD} - L_{md})}{L_{DD}L_dL_{ff} - L_{DD}L_{md}^2 - L_dL_{md}^2 - L_{ff}L_{md}^2 + 2L_{md}^3} \\
a_{15} &= \frac{3L_{md}(L_{ff} - L_{md})}{L_{DD}L_dL_{ff} - L_{DD}L_{md}^2 - L_dL_{md}^2 - L_{ff}L_{md}^2 + 2L_{md}^3} \\
a_{16} &= 0 \\
a_{21} &= 0 \\
a_{22} &= -\frac{9L_{QQ}}{L_{QQ}L_q - L_{mq}^2} \\
a_{23} &= 0 \\
a_{24} &= 0 \\
a_{25} &= 0 \\
a_{26} &= \frac{3L_{mq}}{L_{QQ}L_q - L_{mq}^2}
\end{aligned}
\tag{G.2}
$$

$$
\begin{aligned}
a_{31} &= 0 \\
a_{32} &= 0 \\
a_{33} &= -\frac{9}{L_0} \\
a_{34} &= 0 \\
a_{35} &= 0 \\
a_{36} &= 0 \\
a_{41} &= -a_{14} \\
a_{42} &= 0 \\
a_{43} &= 0 \\
a_{44} &= \frac{L_{DD}L_d - L_{md}^2}{L_{DD}L_dL_{ff} - L_{DD}L_{md}^2 - L_dL_{md}^2 - L_{ff}L_{md}^2 + 2L_{md}^3} \\
a_{45} &= \frac{L_{md}(L_d - L_{md})}{L_{DD}L_dL_{ff} - L_{DD}L_{md}^2 - L_dL_{md}^2 - L_{ff}L_{md}^2 + 2L_{md}^3} \\
a_{46} &= 0 \\
a_{51} &= -a_{15} \\
a_{61} &= 0 \\
a_{62} &= -a_{26} \\
a_{63} &= 0 \\
a_{64} &= 0 \\
a_{65} &= 0 \\
a_{66} &= \frac{L_q}{L_{QQ}L_q - L_{mg}^2}
\end{aligned}
\tag{G.3}
$$

$$
\begin{bmatrix} \boldsymbol{L_{S,dq}^{CW}} & \boldsymbol{L_{SR,dq}^{CW}} \\ (\boldsymbol{L_{SR,dq}^{CW}})^{\boldsymbol{T}} & \boldsymbol{L_R} \end{bmatrix}^{-1} = \begin{bmatrix} b_{11} & b_{12} & b_{13} & b_{14} & b_{15} & b_{16} \\ b_{21} & b_{22} & b_{23} & b_{24} & b_{25} & b_{26} \\ b_{31} & b_{32} & b_{33} & b_{34} & b_{35} & b_{36} \\ b_{41} & b_{42} & b_{43} & b_{44} & b_{45} & b_{46} \\ b_{51} & b_{52} & b_{53} & b_{54} & b_{55} & b_{56} \\ b_{61} & b_{62} & b_{63} & b_{64} & b_{65} & b_{66} \end{bmatrix} \tag{G.4}
$$

$$
\begin{aligned}
b_{11} =& \frac{((72L_{md}^3 + (-36L_{DD} - 36L_{ff} - 108L_{ssP})L_{md}^2 + 108L_{DD}L_{ff}L_{ssP})L_{QQ} + ...}{...} \\
& \frac{36L_{mq}^2(L_{DD}L_{ff} - L_{md}^2))\cos(2\theta_d)^2 - (36(2L_{md}^3 + (-L_{DD} - L_{ff} - L_d)L_{md}^2 + L_{DD}L_{ff}L_d))L_{QQ}}{...4(2L_{md}^3 + (-L_{DD} - L_{ff} - L_d)L_{md}^2 + L_{DD}L_{ff}L_d)(L_qL_{QQ} - L_{mq}^2))} \\
b_{12} =& \frac{-\frac{27}{2}\sin(4\theta_d)(2L_{QQ}\frac{L_{md}^3}{3} + ((-\frac{L_{DD}}{3} - \frac{L_{ff}}{3} - L_{ssP})L_{QQ} - \frac{L_{mq}^2}{3})L_{md}^2 + L_{DD}L_{ff}(L_{QQ}L_{ssP} + \frac{L_{mq}^2}{3}))}{2L_{md}^3 + (-L_{DD} - L_{ff} - L_d)L_{md}^2 + L_{DD}L_{ff}L_d)(L_qL_{QQ} - L_{mq}^2)} \\
b_{13} =& 0 \\
b_{14} =& \frac{6(L_{DD} - L_{md}))L_{md}\cos(2\theta_d)}{2(2L_{md}^3 + (-L_{DD} - L_{ff} - L_d)L_{md}^2 + L_{DD}L_{ff}L_d)} \\
b_{15} =& \frac{6(L_{ff} - L_{md}))L_{md}\cos(2\theta_d)}{2(2L_{md}^3 + (-L_{DD} - L_{ff} - L_d)L_{md}^2 + L_{DD}L_{ff}L_d)} \\
b_{16} =& \frac{-6L_{mq}\sin(2\theta_d)}{(2L_qL_{QQ} - 2L_{mq}^2} \\
b_{21} =& a_{12} \\
b_{22} =& \frac{(-72L_{QQ}L_{md}^3 + ((36L_{DD} + 36L_{ff} + 108L_{ssP})L_{QQ} + 36L_{mq}^2)L_{md}^2 - ...}{...} \\
& \frac{108L_{DD}L_{ff}(L_{QQ}L_{ssP} + \frac{L_{mq}^2}{3}))\cos(2\theta_d)^2 - (36((L_q)L_{QQ} - L_{mq}^2))(L_{DD}L_{ff} - L_{md}^2)}{4(2L_{md}^3 + (-L_{DD} - L_{ff} - L_d)L_{md}^2 + L_{DD}L_{ff}L_d)(L_qL_{QQ} - L_{mq}^2))} \\
b_{23} =& 0 \\
b_{24} =& \frac{6(L_{DD} - L_{md})L_{md}\sin(2\theta_d)}{2(2L_{md}^3 + (-L_{DD} - L_{ff} - L_d)L_{md}^2 + L_{DD}L_{ff}L_d)} \\
b_{25} =& \frac{-6(L_{ff} - L_{md})L_{md}\sin(2\theta_d)}{2(2L_{md}^3 + (-L_{DD} - L_{ff} - L_d)L_{md}^2 + L_{DD}L_{ff}L_d)} \\
b_{26} =& \frac{-6L_{mq}\cos(2\theta_d)}{(2L_qL_{QQ} - 2L_{mq}^2}
\end{aligned}
\tag{G.5}
$$

$$
\begin{aligned}
b_{31} &= 0 \\
b_{32} &= 0 \\
b_{33} &= \frac{-9}{L_{ls}} \\
b_{34} &= 0 \\
b_{35} &= 0 \\
b_{36} &= 0 \\
b_{41} &= -a_{14} \\
b_{42} &= -a_{24} \\
b_{43} &= 0 \\
b_{44} &= \frac{(2L_dL_{DD} - 2L_{md}^2}{(-2L_{md}^2 + (2L_dL_{ff})L_{DD} - (2(L_{ff} - 2 * Lmd + L_d))L_{md}^2} \\
b_{45} &= \frac{-(2L_d - 2L_{md})L_{md}}{2(2L_{md}^3 + (-L_{DD} - L_{ff} - L_d)L_{md}^2 + L_{DD}L_{ff}L_d)} \\
b_{46} &= 0
\end{aligned}
\tag{G.6}
$$

$$
\begin{aligned}
b_{51} &= -a_{15} \\
b_{52} &= -a_{25} \\
b_{53} &= 0 \\
b_{54} &= a_{45} \\
b_{55} &= \frac{2L_{ff}L_d - 2L_{md}^2}{(-2L_{md}^2 + 2L_dL_{DD})L_{ff} - 2L_{md}^2(L_{DD} + L_d - 2L_{md})} \\
b_{56} &= 0 \\
b_{61} &= -a_{16} \\
b_{62} &= -a_{26} \\
b_{63} &= 0 \\
b_{64} &= 0 \\
b_{65} &= 0 \\
b_{66} &= \frac{2L_q}{2L_qL_{QQ} - 2L_{mq}^2}
\end{aligned}
\tag{G.7}
$$